DIST: A

REPORT DOCUMENTATION PAGE

Form Approved
OMB No. 0704-0188

1. AGENCY USE ONLY (Leave blank)	2. REPORT DATE	3. REPORT TYPE AND DATES COVERED
	6/20/94	Annual Report, 4/15/93 - 4/14/94

4. TITLE AND SUBTITLE
(U) Studies on High Pressure and Unsteady Flame Phenomena

5. FUNDING NUMBERS
PE - 61102F
PR - 2308
SA - BS
G - F49620-92-J-0227

6. AUTHOR(S)
C. K. Law

7. PERFORMING ORGANIZATION NAME(S) AND ADDRESS(ES)
Princeton University
Department of Mechanical and Aerospace Engineering
Princeton, NJ 08544

8. PERFORMING ORGANIZATION REPORT NUMBER
AFOSR-TR- 94 0501

9. SPONSORING/MONITORING AGENCY NAME(S) AND ADDRESS(ES)
AFOSR/NA
110 Duncan Avenue, Suite B115
Bolling AFB, DC 20332-0001

10. SPONSORING/MONITORING AGENCY REPORT NUMBER

11. SUPPLEMENTARY NOTES

55pg

12a. DISTRIBUTION/AVAILABILITY STATEMENT
Approved for public release; distribution is unlimited

A

13. ABSTRACT (Maximum 200 words)

The objective of the present program is to study the structure and response of steady and unsteady laminar premixed and nonpremixed flames in reduced and elevated pressure environments through (a) non-intrusive experimentation, (b) computational simulation using detailed flame and kinetic codes, and (c) asymptotic analysis with reduced kinetic mechanisms. During the reporting period progress has been made in the following projects: (1) a theoretical and experimental study of unsteady diffusion flames; (2) a computational and experimental study of hydroge /air diffusion flames at sub- and super-atmospheric pressures; (3) an asymptotic analysis of the structure of premixed flames with volumetric heat loss; (4) asymptotic analyses of ignition in the supersonic hydrogen/air mixing layer with reduced mechanisms; (5) a new numerical algorithm for generating the ignition-extinction S-curves. A total of three reprints are appended.

14. SUBJECT TERMS
Flames, extinction, high pressure combustion, unsteady combustion, H2-O2 Combustion, Supersonic Combustion

15. NUMBER OF PAGES
54

16. PRICE CODE

17. SECURITY CLASSIFICATION OF REPORT	18. SECURITY CLASSIFICATION OF THIS PAGE	19. SECURITY CLASSIFICATION OF ABSTRACT	20. LIMITATION OF ABSTRACT
Unclassified	Unclassified	Unclassified	UL

1. Introduction

The objective of the present program is to study the structure and response of steady and unsteady laminar premixed and nonpremixed flames in reduced and elevated pressure environments through (a) non-intrusive experimentation, (b) computational simulation using detailed flame and kinetic codes, and (c) asymptotic analysis with reduced kinetic mechanisms. During the reporting period progress has been made in the following projects: (1) a theoretical and experimental study of unsteady diffusion flames; (2) a computational and experimental study of hydrogen/air diffusion flames at sub- and super-atmospheric pressures; (3) an asymptotic analysis of the structure of premixed flames with volumetric heat loss; (4) asymptotic analyses of ignition in the supersonic hydrogen/air mixing layer with reduced mechanisms; (5) a new numerical algorithm for generating the ignition-extinction S-curves. These accomplishements are briefly discused in the following.

2. Studies on Unsteady Diffusion Flames

A crucial influence on the flame behavior which so far has not been adequately addressed is the effect of unsteadiness of the environment on the flame behavior. This issue is of particular relevance to the modeling of turbulent flames through the concept of laminar flamelets. These flamelets are subjected to fluctuating flows with various intensities of straining, and it is reasonable to expect that the flame would respond differently in an oscillating strained flow field than in a steady strained flow field.

During the reporting period we have analyzed the response of a counterflow diffusion flame subjected to an oscillating strain rate, using large activation energy asymptotics. The characteristic oscillation time of practical interest is found to be of the same order as the characteristic diffusion time of the flame, so that the flame structure consists of a quasi-steady reactive-diffusive layer embedded in the outer unsteady-convective-diffusive zones. A linear analysis is conducted by

assuming that the amplitude of the strain rate oscillation is small relative to the mean strain rate.

Figure 1 shows the real parts of the fluctuations in heat release as a function of the frequency of oscillation, when the mean flame is either near equilibrium or near extinction. It has been found that the flame response is controlled mainly by two effects: (a) the response of the convective mass flux into the reaction sheet, which is directly related to the flow-field variation applied at the boundary, and (b) the response of the reaction sheet to adjust the reduced residence time due to finite-rate chemistry. For flames near equilibrium, the former effect tends to be dominant, so that the response of the net heat release is in phase (i.e. positive real) with the strain rate oscillation. For flames near extinction, however, the finite-rate chemistry effect overtakes the fluid-dynamic effect such that increasing strain rate leads to a reduction of the reactivity of the flame during the oscillatory cycle. As such, the net heat release response of the near-extinction flame becomes out of phase with the strain rate oscillation in the sense of the Rayleigh's criterion. Results of the present study suggest the possibility that the unsteady characteristics of the near-extinction diffusion flame can be significantly different from those in the Burke-Schumann limit.

A parallel experimental study is also in progress. Figure 2 shows the schematic of the experimental setup. To achieve the instantaneous measurement of the unsteady counterflow flame, the laser beam is modulated by an optical chopper at the applied perturbation frequency. Then the signal is delayed and sent to the loudspeakers, which generate the acoustic perturbation of the flow in the nozzle. By comparing the signal sent to the loudspeakers with the chopped laser signal detected by the photodiode, the entire applied sine wave can be mapped out. We shall measure the instantaneous snapshots of the strain rate field and flame responses in order to provide more deterministic information of the unsteady flame phenomena.

The theoretical part of this work is reported in Publication No. 1.

3. Pressure Effects on Extinction of Hydrogen-Air Diffusion Flames

Recent interests in high-speed aero-propulsion have led to considerable research on hydrogen/oxygen chemistry, as well as its coupling to fluid flows. Because of the high-speed nature of the flow, the available residence time for mixing and chemical reaction is significantly reduced. Furthermore, the combustion chamber within aero-engines not only operates at higher pressures, but the chamber pressure can also undergo strong fluctuations such that chemical kinetics and the flame behavior can be significantly modified from those at the atmospheric condition. Consequently, it is of importance to understand the ignition and extinction phenomena involving hydrogen/oxygen mixtures under variable pressures.

We have conducted LDV measurements of local extinction strain rates of nonpremixed counterflow flames of diluted hydrogen against air, at pressures of 0.5 to 1.0 atmosphere. The measured data compare well with results obtained from computational simulation with detailed chemistry and transport. We have subsequently performed additional computational studies of the pressure effect on flame extinction. Figure 3 shows extinction flame temperatures calculated for a 13% hydrogen mixture as a function of the system pressure. The relationship of extinction temperatures with pressure for this system exhibits the familiar non-monotonic "Z" shaped dependency as observed for the homogeneous hydrogen/oxygen explosion limits. This implies that an increase in pressure could render a mixture to change from an extinguished state, to a burning state, and back to an extinguished state. This behavior is explained on the basis of the intrinsic chain branching-termination kinetics of hydrogen oxidation.

This work is reported in Publication No. 2.

4. Asymptotic Analysis of Premixed Flames with Volumetric Heat Loss

A classical model problem for the study of premixed flame extinction is that of Spalding, who analyzed a one-dimensional freely-propagating flame with a temperature-sensitive one-step overall reaction and radiative heat loss. More sophisticated analyses have since been performed using one-step chemistry and activation energy asymptotics. These studies predict that extinction occurs when the ratio of the burning rate to its adiabatic value is reduced to $e^{-1/2} \approx 0.61$, a result that is insensitive to the nature of the heat loss. Subsequent numerical computations that consider detailed transport and chemistry also predict extinction when the burning rate is reduced to roughly 60% of its adiabatic value, suggesting that this value may represent a universal constant, independent of reaction and loss mechanisms.

In order to gain a better understanding of the role of dominant kinetic parameters, we have revisited this classical problem and have performed asymptotic analyses with multi-step reaction mechanisms. We first employed the two-step Zel'dovich-Liñán mechanism which consists of a branching reaction and a competing recombination reaction, thus capturing the chain nature of real flames. The analysis again predicts the normalized burning rate at extinction to be $e^{-1/2}$. This work is reported in Publication No. 3.

We have also made considerable progress in understanding the extinction characteristics of nonadiabatic methane/air flames by considering a reduced reaction mechanism that has been systematically derived from larger detailed mechanisms. Thus the reduced mechanism contains many important chemical parameters that are dominant in the chemistry of "real" flames. Extinction conditions were found explicitly in terms of these parameters. Results show that the critical value of the burning rate at extinction, though not a universal constant, varies only slightly, in the range between 0.61 and 0.64. In figure 4 we have plotted the nondimensional burning rate as a function of the loss parameter. At the (extinction) turning point, the burning rate is

nearly the same for all curves, but the critical value of the heat loss parameter is seen to be less than that for one-step models. The corresponding reduction in flame temperature needed for extinction is therefore substantially less than that predicted by one-step models.

This work is reported in Publication Nos. 4 and 5.

5. Ignition in the Supersonic Hydrogen/Air Mixing Layer

The development of the scramjet engine for supersonic propulsion and the scramaccelerator for hypervelocity projectile launching has renewed interest in supersonic combustion. Fundamental studies such as ignition within chemically-reactive supersonic boundary layer flows can provide better understanding of the key factors in developing supersonic combustors. In our previous study (Publication No. 6) with one-step reaction chemistry model, several distinct ignition situations were identified, and it was shown that ignition can be greatly facilitated by use of the kinetic energy of the high-speed flow through viscous heating. In the present study we take one step further and consider the more realistic hydrogen/air mixing layer using reduced mechanisms. In particular, two distinct reduced mechanisms are identified depending on the maximum characteristic ignition temperature (T^*) relative to the crossover temperature (T_c), at which the rates of the crucial H-O2 chain branching and termination reactions are equal. Each regime is further subdivided into two distinct cases, namely the hot stream ($\beta > \mu$) case and the viscous heating ($\beta < \mu$) case, depending on the relative dominance of the external and internal ignition sources, where β and μ are parameters respectively representing the extent of external heating to internal viscous heating. These four cases are analyzed separately using asymptotic technique, and the analysis properly captures the ignition process in a well-defined manner.

Figure 5 shows the minimum ignition distance as a function of the flow Mach number. Although the gross trend is similar to that of the one-step analysis, it is clearly shown that the system response is significantly enriched when realistic chemistry is

properly taken into account. For example, ignition in the low temperature regime (I, II) is controlled by a large activation energy process, so that the ignition distance is more sensitive to its characteristic temperature than that in the high temperature regime (III, IV). In Fig. 6, it is shown that the ignition distance varies non-monotonically with the system pressure in the manner of the well-known hydrogen/oxygen explosion limits, thereby further substantiating the importance of chemical chain mechanisms in this class of chemically-reacting boundary layer flows.

This work is reported in Publication No. 7.

6. Numerical Algorithm for Generating S-Curves

Most combustion phenomena are intrinsically nonlinear because of the associated chain mechanisms and Arrhenius kinetics. Consequently, theoretical studies of their steady-state behavior frequently yield multiple solutions connected by turning points when a system response is plotted versus an imposed system parameter. A prominent example is the S-curve representation of quasi-one-dimensional strained flames which results when a flame response such as its maximum temperature is plotted versus the system strain rate. Specifically, the lower branch of the S-curve represents weakly-reactive states, the middle branch unstable solutions, and the upper branch vigorously-burning states. As such, the lower and upper turning points can be respectively defined as the ignition and extinction states of the system. Identification and description of these critical states of transition therefore commands both fundamental and practical interest.

When numerical solution is sought for the S-curve response, especially with detailed chemistry, difficulty is encounters as one attempts to continue the calculation from, say, the upper branch to the middle branch by negotiating the extinction turning point because the Jacobian matrix used in the Newton method becomes singular at the turning point. Consequently, the arclength continuation method has been applied to trace through

the ignition and extinction turning points in a number of studies on strained flames.

While the arclength continuation method is clearly a valuable approach in generating the S-curve, special skill apparently is still needed in its implementation and as a result its use has not been wide spread. In this study we have developed a new, flame-controlling continuation method. Using the counterflow premixed and diffusion flames as examples, the method capitalizes on the distinct nature of the profile and location of the scalars of the flame properties, such as the temperature and species concentrations, in response to changes in the flow strain rate. Thus instead of using the strain rate as an imposed parameter and the scalars as the flame responses, the values of a flame scalar at a give location is used as an internal boundary condition while the strain rate becomes the flame response. The method appears to be fairly simple in implementation and efficient and robust in execution, especially in negotiating the turning points.

This work is reported in Phblication No. 8.

7. Journal Publications

1. "Response of counterflow diffusion flames to oscillating strain rates," by H. G. Im, C. K. Law, J. S. Kim and F. A. Williams, to appear in *Combustion and Flame* as part of the *Twenty-Fifth Symposium (International) on Combustion* (1994).

2. "Effects of pressure and dilution on the extinction of counterflow nonpremixed hydrogen-air flames," by P. Papas, I. Glassman and C. K. Law, to appear in the *Proceedings of the Twenty-Fifth Symposium (International) on Combustion*, the Combustion Institute, Pittsburgh, PA (1994).

3. "Laminar flame propagation with volumetric heat loss and chain branching-termination reactions," by B. H. Chao and C. K. Law, *International Journal of Heat and Mass Transfer*, Vol. 37, pp. 673-680 (1994). **Appendix A**

4. "The structure of premixed methane-air flames with large activation energy," J.K. Bechtold and C.K. Law, *Combustion and Flame*, Vol. 97, pp. 317-338 (1994) **Appendix B**.

5. "Extinction of premixed methane-air flames with volumetric heat loss," by J. K. Bechtold and C. K. Law, accepted for publication in *Combustion Science and Technology*.

6. "Analysis of thermal ignition in the supersonic mixing layer," by H. G. Im, B. H. Chao, J. K. Bechtold and C. K. Law, *AIAA Journal*, Vol. 32, No. 2, pp. 341-349 (1994). **Appendix C**

7. "Ignition in the supersonic hydrogen/air mixing layer with reduced reaction mechanisms," by H. G. Im, S. R. Lee and C. K. Law, submitted to *Journal of Fluid Mechanics*.

8. "A flame-controlling continuation method for generating S-curve responses with detailed chemistry," M. Nishioka, C.K. Law and T. Takeno, submitted to *Combustion and Flame*.

8. Preprints and Presentations

1. "Experimental and numerical investigation of strained-induced extinction of dilute nonpremixed hydrogen-air flames," by P. Papas, I. Glassman and C.K. Law, Paper No. 96, Tech. Meeting of the Eastern States Section of the Combustion Institute, Princeton, NJ, Oct. 25-27, 1993.

2. "Response of counterflow diffusion flame with oscillating strain rates," by H.G. Im and C.K. Law, Paper No. 99, Tech. Meeting of the Eastern States Section of the Combustion Institute, Princeton, NJ, Oct. 25-27, 1993.

3. "Ignition analysis of the supersonic hydrogen/air mixing layer," by H.G. Im, S.R. Lee and C.K. Law, AIAA Paper No. 94-0548, 32nd Aerospace Sciences Meeting, Reno, NV, Jan. 10-13, 1994.

9. Personnel

1. J.K. Bechtold (Research Staff)

2. B.H. Chao (Research Staff)

3. H.G. Im (Graduate Student)

4. J.S. Kistler (Graduate Student)

5. S.R. Lee (Post-Doctoral Fellow)

6. M. Nishioka (Post-Doctoral Fellow)

7. P. Papas (Graduate Student)

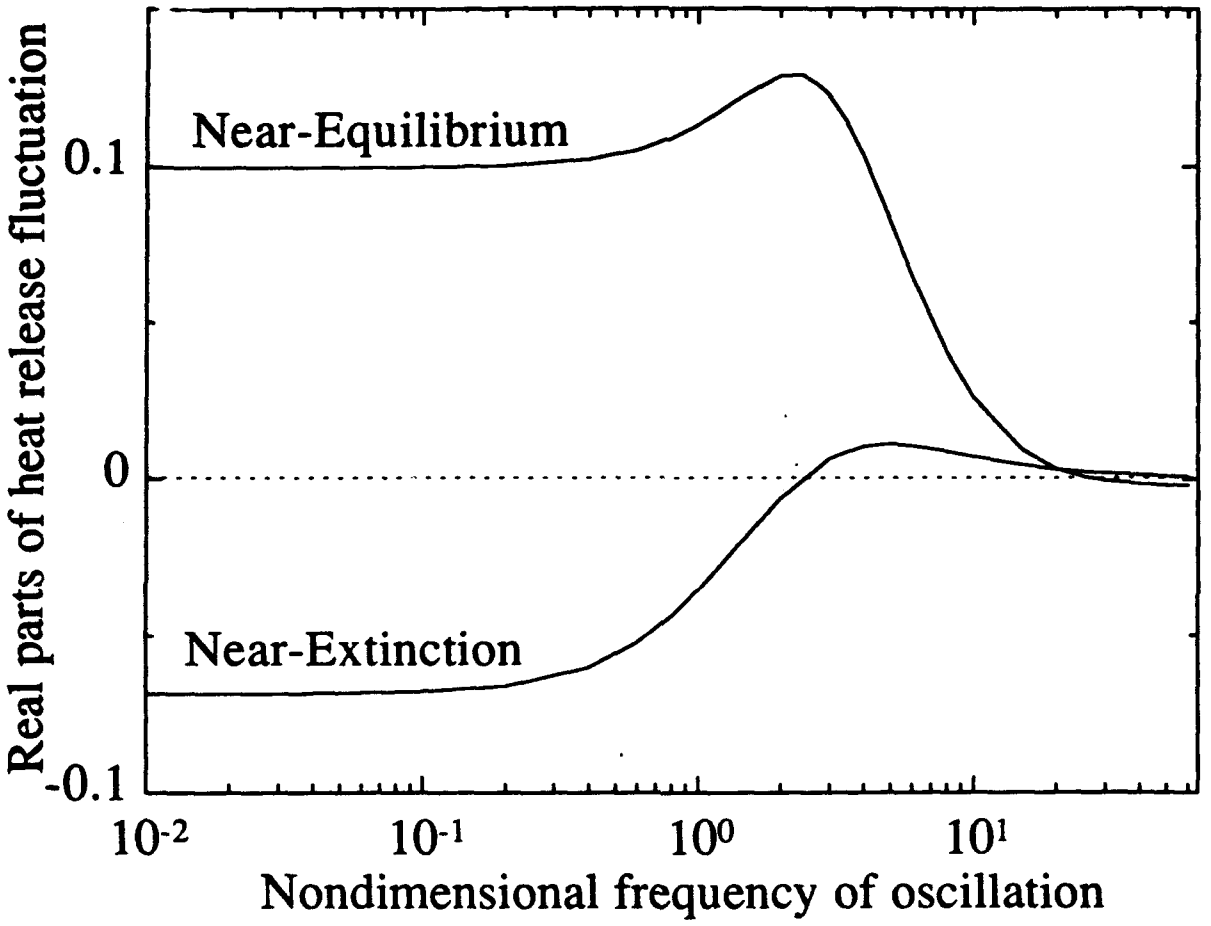
Near-Equilibrium
Near-Extinction
0.1
0
-0.1
Real parts of heat release fluctuation
10-2
10-1
100
101
Nondimensional frequency of oscillation

Figure 1

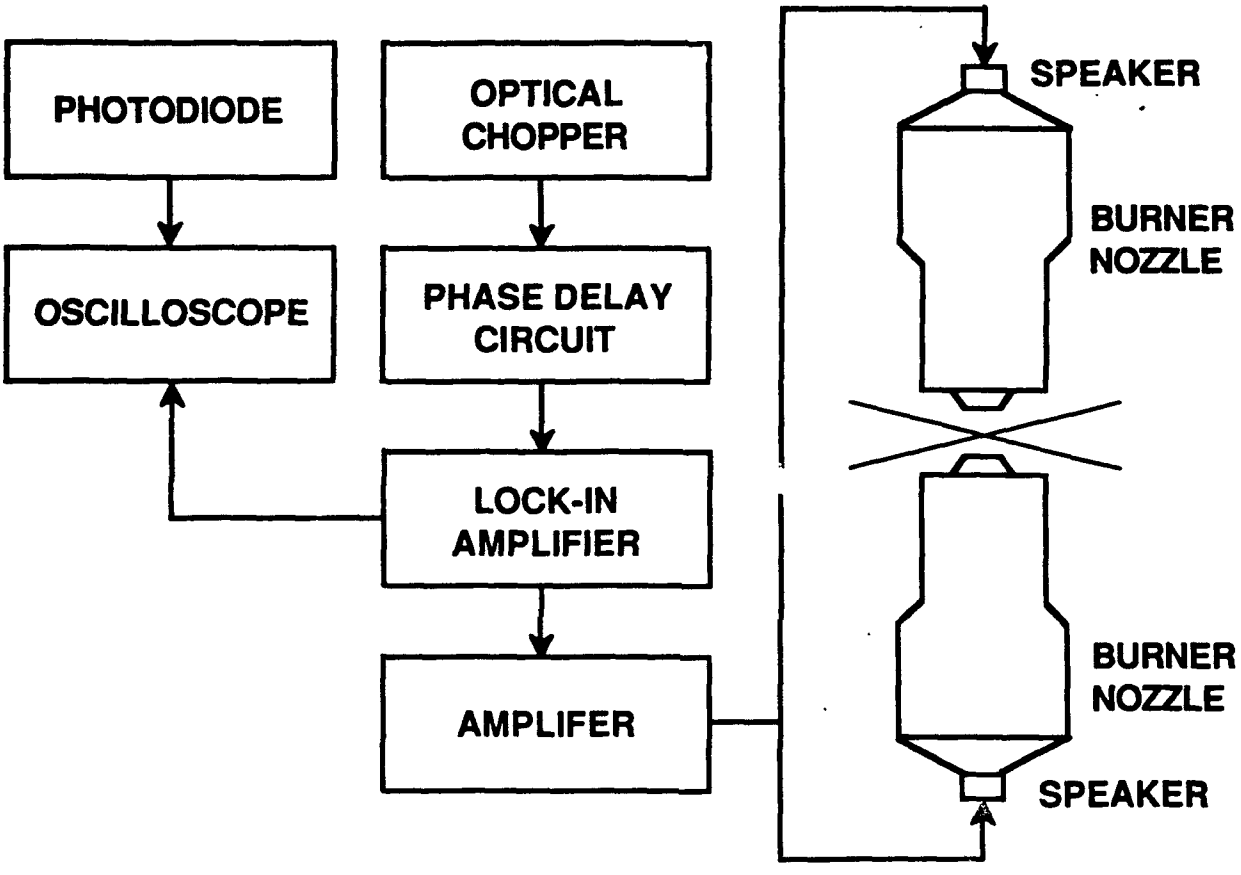

EXPERIMENTAL SET-UP

Figure 2

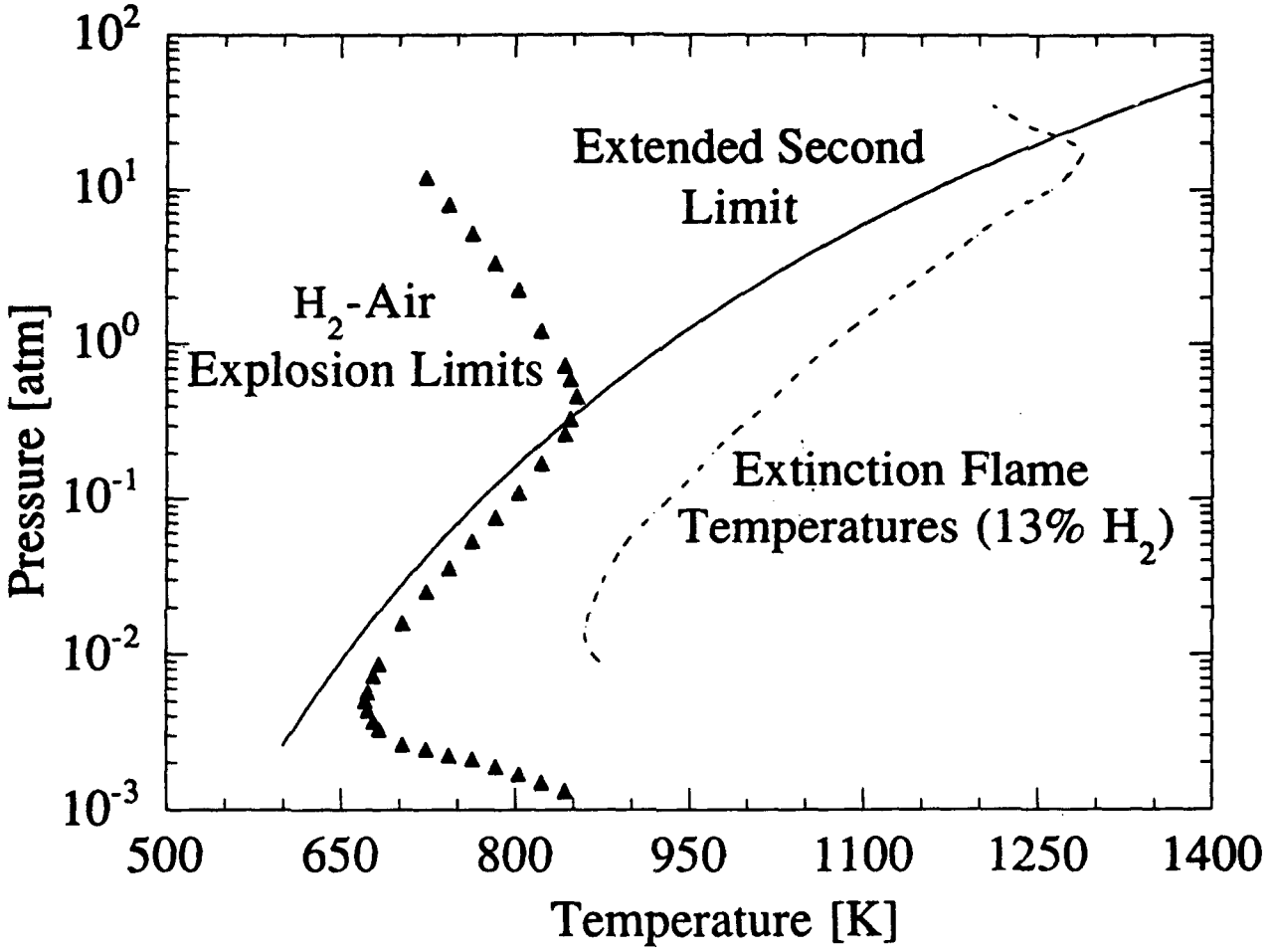
Extended Second Limit
H2-Air Explosion Limits
Extinction Flame Temperatures (13% H2)
Pressure [atm]
Temperature [K]
10^2
10^1
10^0
10^-1
10^-2
10^-3
500
650
800
950
1100
1250
1400

Figure 3

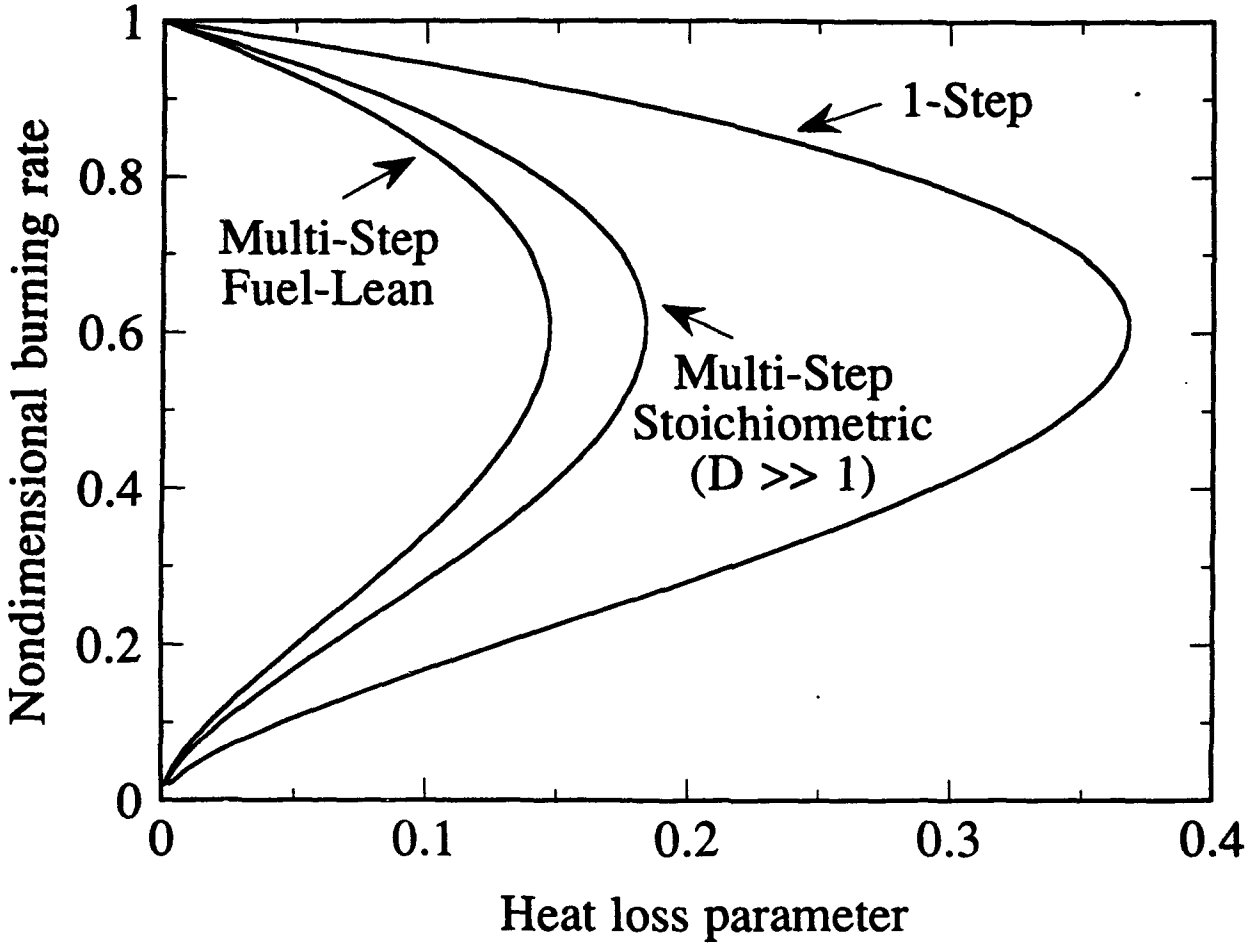
1
0.8
0.6
0.4
0.2
0
0
0.1
0.2
0.3
0.4
Nondimensional burning rate
Heat loss parameter
1-Step
Multi-Step
Fuel-Lean
Multi-Step
Stoichiometric
(D >> 1)

Figure 4

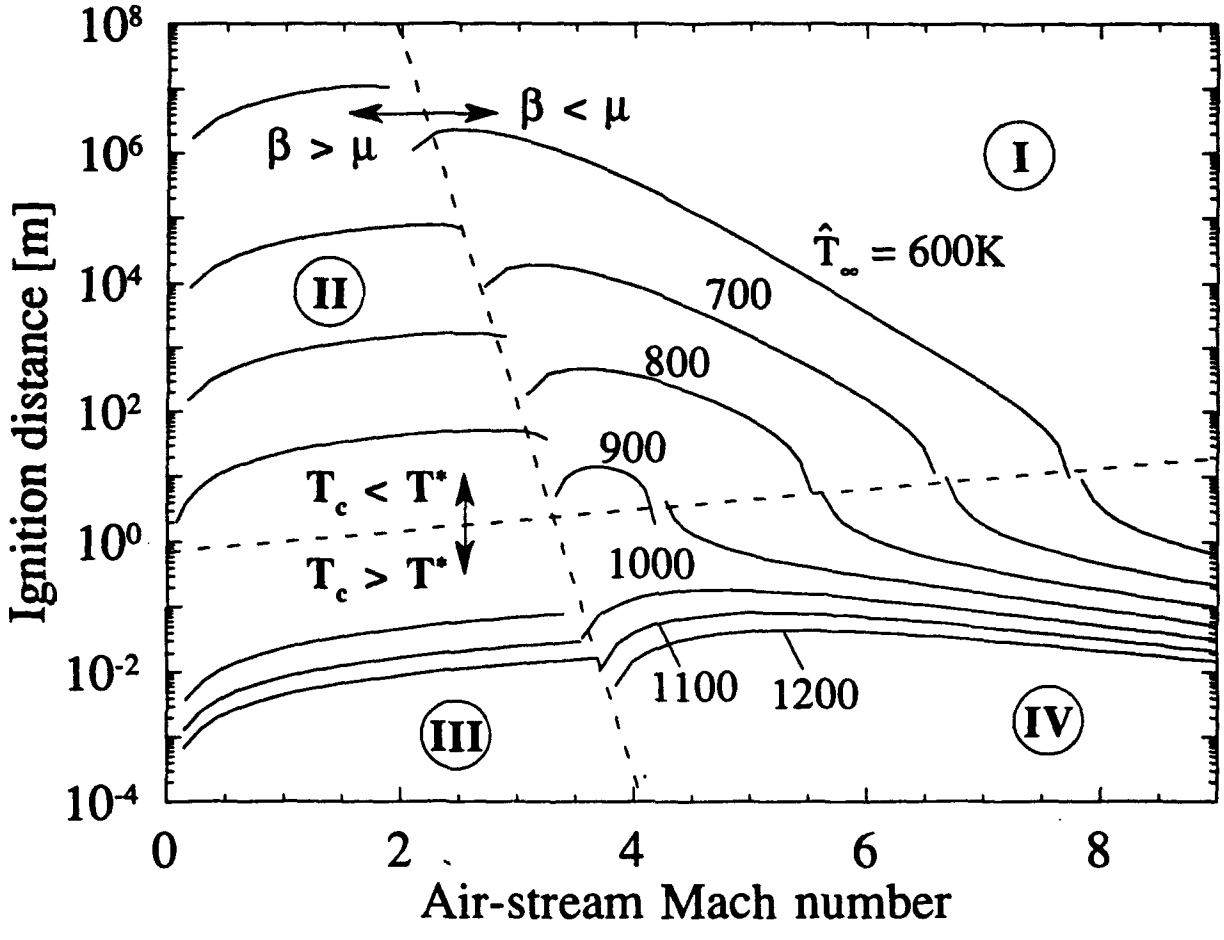
Ignition distance [m]
10^8
10^6
10^4
10^2
10^0
10^{-2}
10^{-4}
0
2
4
6
8
Air-stream Mach number
β > μ
β < μ
I
II
III
IV
$\hat{T}_\infty$ = 600K
700
800
900
1000
1100
1200
$T_c < T^*$
$T_c > T^*$

Figure 5

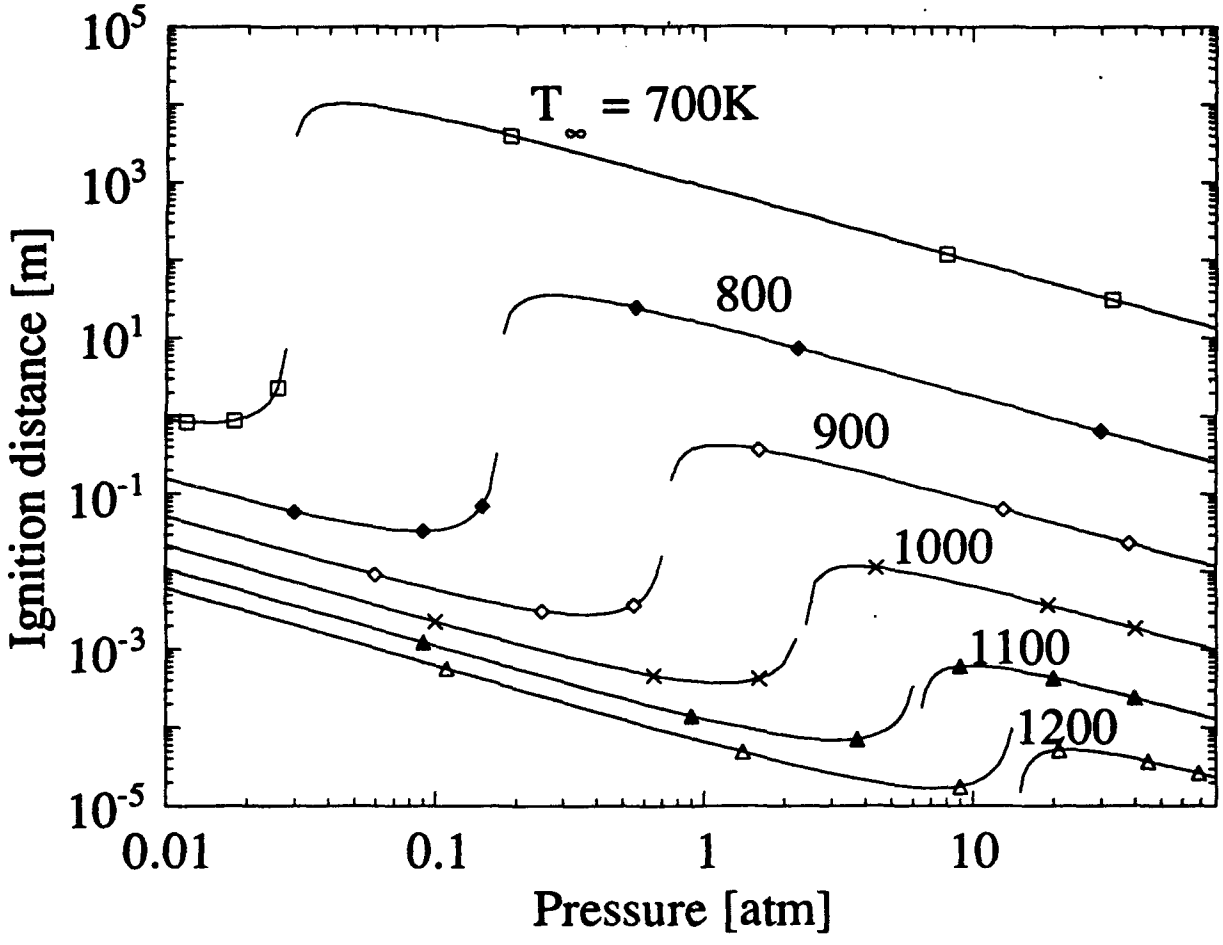
10^5
10^3
10^1
10^{-1}
10^{-3}
10^{-5}
Ignition distance [m]
T_∞ = 700K
800
900
1000
1100
1200
0.01
0.1
1
10
Pressure [atm]

Figure 6

Appendix A

Pergamon

Int. J. Heat Mass Transfer Vol. 37, No. 4, pp. 673–680, 1994

0017-9310/94 $6.00 + 0.00

Laminar flame propagation with volumetric heat loss and chain branching–termination reactions

B. H. CHAO
Department of Mechanical Engineering, University of Hawaii, Honolulu, HI 96822, U.S.A.

and

C. K. LAW
Department of Mechanical and Aerospace Engineering, Princeton University, Princeton, NJ 08544, U.S.A.

(*Received* 23 *December* 1992 *and in final form* 13 *April* 1993)

Abstract—The steady propagation of the planar laminar premixed flame in the doubly-infinite domain, with chain branching-termination reactions and weak volumetric heat loss, is studied using activation energy asymptotics. Two flame propagation regimes are identified and analyzed: a fast recombination regime in which the recombination reaction occurs in a steady-state manner with the high-activation-energy branching reaction in an overall reaction region which is much thinner than that of diffusion, and an intermediate recombination regime in which the recombination region is much thicker than the branching region but much thinner than the diffusion region. The analysis yields the characteristic dual solution, extinction turning point flame response, and shows that the flame propagation speed is reduced to $e^{-1/2}$ of the adiabatic value for both reaction mechanisms. The generality of this limit flame speed is noted.

1. INTRODUCTION

A CLASSICAL model problem for the study of premixed flame extinction is that of Spalding [1], who analyzed the one-dimensional freely-propagating flame with temperature sensitive one-step overall reaction and radiative heat loss. By letting these processes assume power-law temperature variations, with the exponents being 11 and 4 for the reaction rate and heat loss rate such that the former is more temperature sensitive than the latter, the analysis yields an extinction turning point, at which the normalized flame speed $\tilde{s}_{f,ex} = s_{f,ex}/s_f^0$ is 0.504, where s_f is the flame speed and s_f^0 the adiabatic, laminar flame speed, and the subscript 'ex' designates the extinction state. A more rigorous analysis [2] of the Spalding problem by using activation energy asymptotics and for weak, $O(\varepsilon)$ conductive heat loss subsequently yielded $\tilde{s}_{f,ex} = e^{-1/2}$, which is about 0.607, and a suitably-scaled heat loss rate $\tilde{L} = e^{-1}$ at the state of extinction, where ε is the reciprocal of the nondimensional activation energy to be defined later. The same result was shown to also hold [3] for a general $O(\varepsilon)$ volumetric heat loss function.

Recently, Sibulkin and co-workers [4–6] reported numerical solutions of transient planar and outwardly-propagating lean methane air flame, allowing for radiative heat loss but with constant transport properties and one-step overall reaction. It was shown that at the limit of propagation $\tilde{s}_f$ again assumed a value around 0.6. Lakshmisha *et al.* [7], and Law and Egolfopoulos [8] extended these calculations to include variable properties and detailed chemistry, and further demonstrated the near-constancy of this value. Compared to previous analytical studies, these computational results are significant because they indicate the possibility that at the extinction limit the flame speed is always reduced to about 60% of its adiabatic value, being very insensitive both to the reaction mechanism, whether it is one-step or detailed, and to the loss mechanism, whether it is conductive or radiative, as long as it is $O(\varepsilon)$ and volumetric in nature.

The objective of the present study is to provide a fairly general proof of the above possibility based on activation energy asymptotics. Recognizing that previous analytical studies mostly involve a one-step large activation energy reaction, which obviously cannot capture the inherently-important chain branching and termination nature of realistic reaction schemes, we shall employ the Zel'dovich–Liñán two-step mechanism [9, 10], which consists of a branching reaction and a competing recombination (termination) reaction. This is believed to be the simplest representation of the chain nature of realistic reaction mechanisms. A general, $O(\varepsilon)$ volumetric heat loss function will be used in the analysis.

The system to be analyzed is formulated in the next section. It will be shown that there are two situations of interest, which respectively involve fast and intermediate recombination reaction rates. These two situations are separately analyzed in Sections 3 and 4.

NOMENCLATURE

a, b, c	integration constants
B	pre-exponential factor
c_p	specific heat at constant pressure
D	mass diffusion coefficient
Da	Damköhler number
E	activation energy
f	mass flux through the flame or the flame propagation rate
f	flame propagation rate in the adiabatic limit
F	rate controlling reactant (fuel)
H	temperature-dependent volumetric heat loss function
H_ν	Heaviside function defined after equation (A24)
L	heat loss coefficient
L_C	conductive heat loss coefficient
L_R	radiative heat loss coefficient
Le	Lewis number
M	third body of collision needed for recombination
P	combustion product
p	pressure
q_F	heat of combustion per unit mass of fuel
R	radical species
R	universal gas constant
s_l	flame speed
s_l^0	adiabatic, laminar flame speed
T	temperature
T_{ad}	adiabatic flame temperature
T_f	leading order flame temperature
W	molecular weight
x	spatial coordinate attached to the flame front
Y	mass fraction.

Greek symbols

Γ	parameter defined after equation (A20)
γ	Euler's constant
δ	small parameter representing the relative thickness of the recombination region to the preheat region
ε	small parameter of expansion, defined as $\tilde{T}_{ad}^2/\tilde{E}$
η	compressed coordinate defined as $\varepsilon\tilde{x}$
Θ	temperature perturbation in the recombination region
θ	temperature perturbation in the branching region
Λ	burning rate eigenvalue
λ	thermal conductivity
ξ	stretched coordinate defined as $\tilde{x}/\varepsilon$
ρ	density
ϕ	fuel concentration perturbation in the branching region
Ψ	radical concentration in the recombination region
ψ	radical concentration in the branching region
ω	reaction rate function.

Subscripts

ex	the extinction state
F	fuel
M	third body of collision needed for recombination
R	radical species
$-\infty$	quantities at the upstream ambiance.

Superscripts

$-, +$	quantities in the upstream and downstream of the branching region
n	pressure exponent
$\sim$	dimensionless quantities.

2. FORMULATION

The two-step branching–recombination reaction mechanism adopted in this study is given by

$$F + R \rightarrow 2R \tag{1}$$

$$R + R + M \rightarrow P + M \tag{2}$$

where F, R, P and M respectively denote the rate controlling reactant (say the fuel), a radical species, the combustion product, and a third body of collision needed for recombination. In this mechanism, reaction (1) represents the two-body, high activation energy, branching reaction that has a small heat of combustion and produces more radicals than it consumes when reacted with the fuel. Equation (2) is the three-body, low activation energy, highly exothermic, termination reaction that combines the radicals to form combustion products and generate heat. For simplicity we shall therefore assume that the branching reaction is thermally neutral while the termination reaction has zero activation energy. If we further assume that the rates of these two reaction steps, ω_j, vary with the first order of each reactant, then they can be respectively expressed for reactions (1) and (2) as

$$\omega_1 = B_1 p^{n_1} \frac{Y_F}{W_F} \frac{Y_R}{W_R} \exp(-E/R^0 T), \tag{3}$$

$$\omega_2 = B_2 p^{n_2} \left(\frac{Y_R}{W_R}\right)^2 \frac{Y_M}{W_M}, \tag{4}$$

where T is the temperature, Y_i and W_i the mass fraction and molecular weight of species i, p the pressure,

B_j and n_j the pre-exponential factor and pressure exponent of reaction j, E the activation energy of the branching reaction, and R the universal gas constant. The mass fraction of the third body, Y_M, can be considered to be a constant.

The physical problem under study is the steady propagation of the one-dimensional premixed flame in the doubly-infinite domain with an arbitrary temperature-dependent volumetric heat loss function $H(T)$. The governing equations and boundary conditions are given by

$$f c_p \frac{dT}{dx} - \frac{d}{dx}\left(\lambda \frac{dT}{dx}\right) = q_F W_F \omega_2 - \varepsilon H(T), \quad (5)$$

$$f \frac{dY_F}{dx} - \frac{d}{dx}\left(\rho D_F \frac{dY_F}{dx}\right) = -W_F \omega_1, \quad (6)$$

$$f \frac{dY_R}{dx} - \frac{d}{dx}\left(\rho D_R \frac{dY_R}{dx}\right) = W_R(\omega_1 - 2\omega_2), \quad (7)$$

$$x \to -\infty: \quad T \to T_{-\infty}, \quad Y_F \to Y_{F,-\infty}, \quad Y_R \to 0. \quad (8a)$$

$$x \to \infty: \quad \frac{dT}{dx} \to 0, \quad \frac{dY_F}{dx} \to 0, \quad \frac{dY_R}{dx} \to 0. \quad (8b)$$

where x is the spatial coordinate attached to the flame front, f the mass flux through the flame, ρ the density, c_p the specific heat at constant pressure, q_F the heat of combustion per unit mass of fuel consumed, λ the thermal conductivity, and D_i the mass diffusion coefficient of species i. The quantities λ, c_p and ρD_i are assumed to be constants. It is appropriate to concentrate on only $O(\varepsilon)$ heat loss because it represents the limiting situations of the extinction of weakly-burning flames. Clearly a flame will extinguish with $O(1)$ heat loss if it extinguishes with $O(\varepsilon)$ heat loss.

It is worth noting that equation (8b) implies $T \to T_\infty$, $Y_F \to 0$, and $Y_R \to 0$ at $x \to \infty$, for which T_∞ is the adiabatic flame temperature if the system is adiabatic and $T_\infty = T_{-\infty}$ in the presence of heat loss. Thus both of these conditions are applicable and yield the same result. Equations (8b) are adopted because they are more general. For the case of moderate (i.e. $O(1)$) heat loss in the downstream of the branching region, equations (8b) are still valid except $Y_F \neq 0$ at $x \to \infty$.

Introducing the nondimensional quantities

$$\tilde{T} = \frac{2T}{q_F Y_{F,-\infty} c_p}, \quad \tilde{Y}_F = \frac{Y_F}{Y_{F,-\infty}},$$

$$\tilde{Y}_R = \frac{Y_R W_R}{Y_{F,-\infty} W_F}, \quad \tilde{f} = \frac{f}{f}, \quad \tilde{x} = \frac{x}{\lambda (f c_p)},$$

$$\tilde{E} = \frac{2E R}{q_F Y_{F,-\infty} c_p}, \quad \tilde{H} = \frac{2H\lambda}{(f)^2 c_p q_F Y_{F,-\infty}},$$

$$Le_i = \frac{\lambda c_p}{\rho D_i}, \quad \varepsilon = \frac{\tilde{T}_\infty^2}{\tilde{E}},$$

$$Da_1 = \frac{B_1 \lambda p^{n_1} Y_{F,-\infty}}{(f)^2 c_p W_F},$$

$$Da_2 = \frac{2B_2 \lambda p^{n_2} Y_{F,-\infty} Y_M}{(f)^2 c_p W_F W_M},$$

where Le_i is the Lewis number of species i, Da_j the Damköhler number of the jth reaction, $f(Le_F)$ the flame propagation rate in the adiabatic limit, and $\tilde{T}_{ad} = 1 + \tilde{T}_{-\infty}$ the adiabatic flame temperature, the governing equations are nondimensionalized to

$$\tilde{f} \frac{d\tilde{T}}{d\tilde{x}} - \frac{d^2\tilde{T}}{d\tilde{x}^2} = Da_2 \tilde{Y}_R^2 - \varepsilon \tilde{H}(\tilde{T}), \quad (9)$$

$$\tilde{f} \frac{d\tilde{Y}_F}{d\tilde{x}} - \frac{1}{Le_F} \frac{d^2\tilde{Y}_F}{d\tilde{x}^2} = -Da_1 \tilde{Y}_F \tilde{Y}_R \exp(-\tilde{E}/\tilde{T}), \quad (10)$$

$$\tilde{f} \frac{d\tilde{Y}_R}{d\tilde{x}} - \frac{1}{Le_R} \frac{d^2\tilde{Y}_R}{d\tilde{x}^2} = Da_1 \tilde{Y}_F \tilde{Y}_R \exp(-\tilde{E}/\tilde{T}) - Da_2 \tilde{Y}_R^2, \quad (11)$$

$$\tilde{x} \to -\infty: \quad \tilde{T} \to \tilde{T}_{-\infty}, \quad \tilde{Y}_F \to 1, \quad \tilde{Y}_R \to 0, \quad \tilde{H} \to 0, \quad (12a)$$

$$\tilde{x} \to \infty: \quad \frac{d\tilde{T}}{d\tilde{x}} \to 0, \quad \frac{d\tilde{Y}_F}{d\tilde{x}} \to 0, \quad \frac{d\tilde{Y}_R}{d\tilde{x}} \to 0, \quad \tilde{H} \to 0. \quad (12b)$$

This system will be solved by activation energy asymptotics.

Depending on the rate of the recombination reaction relative to that of the branching reaction, three flame propagation regimes can be identified. In a fast recombination regime both reaction rates are of the same order so that the reactions occur in the same thin reaction region. In an intermediate recombination regime the recombination rate is much slower than the branching rate but is much faster than the diffusion rate. Consequently the recombination region is much thicker than the branching region but much thinner than the preheat region. Finally, in a slow recombination regime the recombination rate is either comparable to or slower than the diffusion rate such that the thickness of the recombination region is either of the same order of or larger than that of the preheat region.

In the next two sections, the fast and intermediate recombination regimes will be analyzed sequentially. The slow recombination regime will not be analyzed because it represents very weak chemical systems which are not likely to be of interest to combustion.

3. FAST RECOMBINATION REGIME

In this regime, the rates of the recombination and branching reactions are of the same order so that both reactions occur in the same thin reaction region. Thus the radicals are consumed to produce heat almost immediately after they are generated. This implies that the concentration of the radicals is basically independent of time and is very small, and hence the steady

state approximation, $d\tilde{Y}_R/d\tilde{t} \to 0$, is applicable. Figure 1 shows the species and temperature profiles of such a flame.

With the application of the steady state approximation, setting equation (11) to zero readily yields

$$\tilde{Y}_R = \frac{Da_1}{Da_2}\tilde{Y}_F^2 \exp(-\tilde{E}/\tilde{T}). \tag{13}$$

The vanishing of the LHS of equation (11) is justified by the small radical concentration. Substituting $\tilde{Y}_R$ into the reaction rate terms of equations (9) and (10), the problem is then reduced to a one-step reaction with a rate

$$\frac{Da_1^2}{Da_2}\tilde{Y}_F^2 \exp(-2\tilde{E}/\tilde{T}),$$

which is second order with respect to $\tilde{Y}_F$, and has an effective Damköhler number Da_1^2/Da_2 and an effective activation energy $2\tilde{E}$. Compared with previous asymptotic studies (see, for example, refs. [2, 3]) which adopted a one-step first-order overall reaction, the difference in the mathematical aspect of the two problems is only the reaction order. It is therefore of interest to study that, apart from the obvious difference in the physical interpretation of these two problems, in terms of the chain branching and termination reactions through modifications of the effective Damköhler number and activation energy, what additional effect a simple change in the reaction order can produce. Due to the similar nature of the asymptotic derivation with previous studies, only the key steps will be shown below.

In the outer, chemically inert regions, there is no branching reaction in the upstream region because the flow temperature is low and the reaction has a high activation energy. In the downstream region branching is terminated because of complete fuel consumption. The recombination reaction does not exist in the outer regions due to complete radical consumption. Thus the outer solutions for $\tilde{Y}_F$ are

$$\tilde{Y}_F^- = 1 - (b_0 + \varepsilon b_1 + \cdots)\exp(Le_F \tilde{f}\tilde{x}), \tag{14}$$

$$\tilde{Y}_F^+ = 0. \tag{15}$$

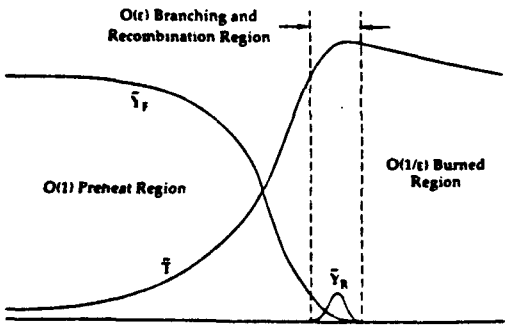

FIG. 1. Schematic of the flame structure for the fast recombination regime. $\tilde{Y}_R$ has been magnified for clarity.

while $\tilde{T}$ can be expanded as $\tilde{T}^{\pm} = \tilde{T}_0^{\pm} + \varepsilon\tilde{T}_1^{\pm} + \cdots$. This yields

$$\tilde{T}_0^- = \tilde{T}_{-\infty} + a_0 \exp(\tilde{f}\tilde{x}), \tag{16a}$$

$$\tilde{f}\tilde{T}_1^- - \frac{d\tilde{T}_1^-}{d\tilde{x}} = -\int_{-\infty}^{\tilde{x}} \tilde{H}(\tilde{T}_0^-)\,d\tilde{x}, \tag{16b}$$

$$\tilde{f}\frac{d\tilde{T}_0^+}{d\eta} = -\tilde{H}(\tilde{T}_0^+). \tag{17}$$

In the above the superscripts $-$ and $+$ respectively denote quantities in the upstream preheat region and downstream burned region, while a_i and b_i the integration constants to be determined. Note that in the downstream region, a compressed coordinate $\eta = \varepsilon\tilde{x}$ is used because the temperature decreases gradually from the flame temperature to the ambient temperature due to the heat loss.

In the inner, chemically reactive region, the coordinate is stretched as $\zeta = \tilde{x}/\varepsilon$ while $\tilde{T}$ and $\tilde{Y}_F$ are expanded as

$$\tilde{T} = \tilde{T}_f - \varepsilon\theta_1 - \varepsilon^2\theta_2 + \cdots, \tag{18}$$

$$\tilde{Y}_F = \varepsilon\phi_1 + \varepsilon^2\phi_2 + \cdots. \tag{19}$$

Substituting equations (18) and (19) into equations (9), (10) and (13), and expanding, we obtain the inner equations

$$\frac{d^2\phi_1}{d\zeta^2} = \Lambda\phi_1^2 \exp\left[-2\left(\frac{\tilde{T}_{ad}}{\tilde{T}_f}\right)^2\theta_1\right], \tag{20}$$

$$\frac{d^2\theta_1}{d\zeta^2} - \frac{1}{Le_F}\frac{d^2\phi_1}{d\zeta^2} = 0, \tag{21}$$

$$\frac{d^2\theta_2}{d\zeta^2} - \frac{1}{Le_F}\frac{d^2\phi_2}{d\zeta^2} - \tilde{f}\left(\frac{d\theta_1}{d\zeta} - \frac{d\phi_1}{d\zeta}\right) = 0, \tag{22}$$

where

$$\Lambda = \varepsilon^3 Le_F \frac{Da_1^2}{Da_2}\exp\left(-2\frac{\tilde{E}}{\tilde{T}_f}\right). \tag{23}$$

Matching the inner and outer solutions yields the relations

$$a_0 = \tilde{T}_f - \tilde{T}_{-\infty}, \quad \tilde{T}_0^+(\eta = 0) = \tilde{T}_f, \quad b_0 = 1, \tag{24}$$

and the matching conditions to solve equations (20) to (22),

$$\theta_1(\zeta \to -\infty) = -\tilde{T}_1^-(\tilde{x} = 0) - \tilde{f}(\tilde{T}_f - \tilde{T}_{-\infty})\zeta, \tag{25a}$$

$$\theta_1(\zeta \to \infty) = -\tilde{T}_1^+(\eta = 0), \tag{25b}$$

$$\left(\frac{d\theta_2}{d\zeta} - \tilde{f}\theta_1\right)_{\zeta\to-\infty} = \left(\tilde{f}\tilde{T}_1^- - \frac{d\tilde{T}_1^-}{d\tilde{x}}\right)_{\tilde{x}\to 0} = -\int_{-\infty}^{0} \tilde{H}(\tilde{T}_0^-)\,d\tilde{x}, \tag{26a}$$

$$\frac{d\theta_2}{d\zeta}(\zeta \to \infty) = -\frac{d\tilde{T}_0^-}{d\eta}(\eta \to 0) = \frac{\tilde{H}(\tilde{T}_f)}{\tilde{f}}, \tag{26b}$$

$$\phi_1(\zeta \to -\infty) = -b_1 - Le_F\tilde{f}\zeta. \tag{27a}$$

$$\phi_1(\xi \to \infty) = 0. \tag{27b}$$

$$\left(\frac{1}{Le_F}\frac{d\phi_2}{d\xi} - \tilde{f}\phi_1\right)_{\xi=-\infty} = 0. \tag{28a}$$

$$\frac{d\phi_2}{d\xi}(\xi \to \infty) = 0. \tag{28b}$$

where equations (27a, b) also imply

$$\frac{d\phi_1}{d\xi}(\xi \to -\infty) = -Le_F\tilde{f}. \tag{29a}$$

$$\frac{d\phi_1}{d\xi}(\xi \to \infty) = 0. \tag{29b}$$

Equations (16b) and (17) have been applied in obtaining the second relation of equations (26a, b).

Integrating equations (21) twice and (22) once subject to the matching conditions in equations (25)–(28) yields

$$\tilde{T}_1 = 1 + \tilde{T}_{-\infty} = \tilde{T}_{ad}. \tag{30}$$

$$\theta_1 = \frac{\phi_1}{Le_F} - \frac{\tilde{L}}{2\tilde{f}^2}. \tag{31}$$

where

$$\tilde{L} = 2\left[\tilde{H}(\tilde{T}_{ad}) + \tilde{f}\int_{-\infty}^{0}\tilde{H}(\tilde{T}_0)\,d\tilde{x}\right]. \tag{32}$$

It can be readily demonstrated, by re-defining $\hat{x} = \tilde{f}\tilde{x} = x/[\lambda/(\rho c_p)]$, that $\tilde{L}$ is independent of $\tilde{f}$.

Equation (30) shows that the leading order flame temperature is the adiabatic flame temperature, which is reasonable because the heat loss is assumed to be $O(\varepsilon)$. Substituting equation (31) into equation (20) and integrating the resulting equation once subject to the boundary conditions in equations (27a, b) and (29a, b), we obtain an expression which determines the flame propagation rate.

$$\tilde{f}^2\exp\left(\frac{\tilde{L}}{\tilde{f}^2}\right) = \frac{Le_F}{2}\Lambda. \tag{33}$$

In the adiabatic limit, $\tilde{H} \equiv 0$ and $\tilde{f} = 1$. We then have $(Le_F\Lambda/2) = 1$ for the laminar flame propagation rate f^0. Equation (33) then becomes

$$\tilde{f}^2\exp\left(\frac{\tilde{L}}{\tilde{f}^2}\right) = 1. \tag{34}$$

The quantities $\tilde{T}_1$ and b_1 are not of interest and hence will not be solved.

Equation (34), of course, is exactly the same as that of, say, Joulin and Clavin [2] who considered conductive heat loss and a first-order reaction. Reproducing equation (34) in Fig. 2, it is seen that there exists a maximum value of $\tilde{L}$, $\tilde{L}_{ex}$, above which no solution exists. For $\tilde{L} < \tilde{L}_{ex}$, there are two solutions for each $\tilde{L}$, although it is well established that only the upper branch gives the stable solution. This critical state is then defined as that of extinction, being characterized by

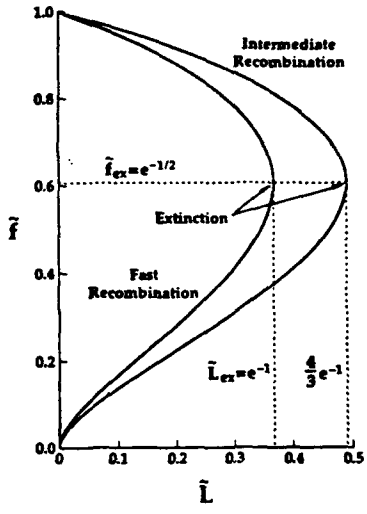

FIG. 2. Normalized flame propagation rate $\tilde{f}$ as a function of the heat loss parameter $\tilde{L}$ for the fast and intermediate recombination regimes.

$$\tilde{L}_{ex} = e^{-1} \quad \text{and} \quad \tilde{f}_{ex} = e^{-1/2}. \tag{35}$$

4. INTERMEDIATE RECOMBINATION REGIME

In this regime the rate of the recombination reaction is much slower than that of the branching reaction but much faster than the diffusive–convective transport rate. Consequently the recombination region is much thicker than the branching region but much thinner than the transport region. By defining a second small parameter δ to describe the characteristic thickness of the recombination region, where $\varepsilon \ll \delta \ll 1$, the flame structure then includes an $O(\varepsilon)$ branching region sandwiched by $O(\delta)$ recombination regions, which in turn are embedded within an $O(1)$ upstream preheat region and an $O(1/\varepsilon)$ downstream burned region. Since the exothermic recombination reaction continues subsequent to completion of the branching reaction, temperature will also continuously increase until heat loss becomes dominant. The species and temperature profiles are shown in Fig. 3.

By separately analyzing the five regions and performing the requisite matching, which is presented in the Appendix, the flame speed response is now given by

$$\tilde{f}^{4/3}\exp\left(\frac{\tilde{L}}{2\tilde{f}^2}\right) = 1. \tag{36}$$

Comparing equations (36) and (34), we can see that

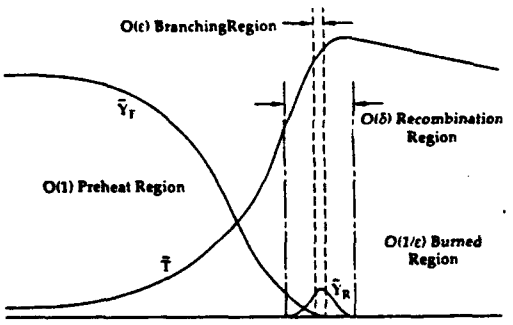

FIG. 3. Schematic of the flame structure for the intermediate recombination regime.

their functional expressions are similar although the branching and recombination reactions occur at different length scales. Thus the behavior of $\tilde{f}$ as a function of $\tilde{L}$ is qualitatively similar to that of the fast recombination regime, as shown in Fig. 2. The flame extinction limit is now described by

$$\tilde{f}_{ex} = e^{-1/2}, \quad \tilde{L}_{ex} = (4\sqrt{3})e^{-1}. \tag{37}$$

It is interesting to note that although the reaction kinetics adopted in this regime are different from those of Section 3, the flame still extinguishes at $\tilde{f} = e^{-1/2}$, albeit at a different $\tilde{L}_{ex}$. Combining this result with those obtained from the analysis by adopting a one-step overall reaction [2] and the numerical studies [4–8], it may be suggested that extinction is achieved when the inherent nonadiabaticity of the system reduces the flame propagation rate to about $e^{-1/2}$ or 0.607 of its adiabatic value. The fact that a large heat loss is needed to extinguish the flame in the intermediate recombination regime as compared to that in the fast recombination regime is also reasonable because the overall reaction rate is less temperature sensitive for the slower recombination rate.

5. CONCLUDING REMARKS

In this study, we have analyzed the extinction limit of the planar premixed flame with $O(\varepsilon)$ volumetric heat loss by adopting a two-step, branching and termination kinetics. Based on the relative rates of these two reactions, the fast and intermediate combination situations are studied. The results show that the flame always extinguishes when the flame propagation rate is reduced to $e^{-1/2}$ of its adiabatic value, which is consistent with previous analytical results with one-step reaction and numerical results with detailed chemistry.

The above analysis is based on a general heat loss function H. Two loss mechanisms that are usually specified are conduction and radiation. For a linear heat loss function, $H = L_C(T - T_{-\infty})$ where L_C is the heat loss coefficient. We then have $\tilde{L} = (4\lambda L_C)/(f c_p)^2$. For radiative loss, $H = L_R(T^4 - T_{-\infty}^4)$ and we have

$$\tilde{L} = \frac{2\lambda L_R}{(f c_p)^2}\left(\frac{q_F Y_{F,-\infty}}{2c_p}\right)^3\left(\frac{5}{4} + \frac{16}{3}\tilde{T}_{-\infty} + 9\tilde{T}_{-\infty}^2 + 8\tilde{T}_{-\infty}^3\right).$$

Finally, we note that the influence of the reactant concentration on flame extinction is primarily through the factor $(f^2)^2$ in the definition of $\tilde{H}$. Thus as the fuel concentration becomes either leaner or richer, the decrease in f^2 would lead to a corresponding increase in $\tilde{H}$. It is therefore clear that the present result also predicts the existence of concentration limits at the heat loss rate $\tilde{L}_{ex}$, beyond which steady flame propagation is not possible. Such limits have been identified as the flammability limits [1, 4, 5, 7, 8].

Acknowledgements—This study was supported by the Air Force Office of Scientific Research and the Office of Basic Energy Sciences of the Department of Energy. We thank Dr John K. Bechtold for stimulating discussions.

REFERENCES

1. D. B. Spalding, A theory of inflammability limits and flame-quenching. *Proc. R. Soc. Lond.* **A240**, 83–100 (1957).
2. G. Joulin and P. Clavin, Linear stability analysis of nonadiabatic flames: a thermal–diffusional model, *Combust. Flame* **35**, 139–153 (1979).
3. J. D. Buckmaster, The quenching of deflagration waves, *Combust. Flame* **26**, 151–162 (1976).
4. M. Sibulkin and A. Frendi, Lean flammability limit for methane at zero gravity, Paper No. 90, *Eastern Section, Combustion Institute Meeting*, Clearwater, FL (1988).
5. M. Sibulkin and A. Frendi, Prediction of flammability limit of an unconfined premixed gases in the absence of gravity, *Combust. Flame* **82**, 334–345 (1990).
6. A. Frendi and M. Sibulkin, Extinction of methane–oxygen mixtures by nitrogen dilution, *Combust. Flame* **86**, 185–186 (1991).
7. K. N. Lakshmisha, P. J. Paul and H. S. Mukunda, On the flammability limit and heat loss in flames with detailed chemistry, *Twenty-Third Symp. (Int.) on Combustion*, pp. 433–440 (1991).
8. C. K. Law and F. N. Egolfopoulos, A unified chain-thermal theory of fundamental flammability limits, *Twenty-Fourth Symp. (Int.) on Combustion*, pp. 137–144 (1992).
9. G. Joulin, A. Liñán, G. S. S. Ludford, N. Peters and C. Schmidt-Laine, Flames with chain-branching/chain-breaking kinetics, *SIAM J. Appl. Math.* **45**, 420–434 (1985).
10. M. A. Birkan and C. K. Law, Asymptotic structure and extinction of diffusion flame with chain mechanism, *Combust. Flame* **73**, 127–140 (1988).

APPENDIX: DERIVATION FOR THE INTERMEDIATE RECOMBINATION REGIME

All the solutions are expanded with respect to the two small parameters ε and δ. Thus in the outer, transport regions away from the recombination region, $\tilde{Y}_{\tilde{R}} = 0$, while $\tilde{Y}_{\tilde{F}}$ is given by equation (15) and

$$\tilde{Y}_{\tilde{F}} = 1 - \{[b_0 + O(\delta)] + \varepsilon[b_1 + O(\delta)] + O(\varepsilon^2)\}\exp(Le_F\tilde{f}\tilde{x}). \tag{A1}$$

The solution of $\hat{T}^{=}$ can be obtained by first expanding it in the form

$$\hat{T}^{=} = [\hat{T}^{=}_{0} + \delta\hat{T}^{=}_{1} + O(\delta^2)] + \varepsilon[\hat{T}^{=}_{\xi} + O(\delta)] + O(\varepsilon^2). \quad \text{(A2)}$$

which is then substituted into equation (9) to yield equations (16a), (17), and

$$\hat{T}^{-}_{1} = a_1 \exp(\hat{f}\tilde{x}). \quad \text{(A3)}$$

$$\hat{f}\hat{T}^{-}_{\xi} - \frac{d\hat{T}^{-}_{\xi}}{d\tilde{x}} = -\int_{-\infty}^{\tilde{x}} \hat{H}(\hat{T}^{-}_{0})\,d\tilde{x}. \quad \text{(A4)}$$

The compressed coordinate $\eta = \varepsilon\tilde{x}$ is again used in the burned region such that all the terms in $\hat{T}^{+}$ are functions of η.

In the $O(\delta)$ recombination region, the coordinate is stretched as $\zeta = \tilde{x}/\delta$. There is no branching reaction in this region because of its high activation energy. Thus the outer solution of $\hat{Y}_F$ is still applicable. Moreover, only $O(\delta)$ variations are possible for $\hat{T}^{=}$ and $\hat{Y}^{=}_{R}$ so that their expansions are

$$\hat{T}^{=} = [\hat{T}_{f,0} - \delta\Theta^{-}_{1} - \delta^2\Theta^{-}_{2} + O(\delta^3)] - \varepsilon[\Theta^{-}_{\xi} + \delta\Theta^{-}_{\delta} + O(\delta^2)] + O(\varepsilon^2). \quad \text{(A5)}$$

$$\hat{Y}^{=}_{R} = [\delta\Psi^{-}_{1} + \delta^2\Psi^{-}_{2} + O(\delta^3)] + \varepsilon[\Psi^{-}_{\xi} + \delta\Psi^{-}_{\delta} + O(\delta^2)] + O(\varepsilon^2). \quad \text{(A6)}$$

Substituting equations (A5) and (A6) into equations (9) and (11), but with the branching reaction frozen, and expanding, we obtain for $\hat{Y}^{=}_{R}$,

$$\frac{1}{Le_R}\frac{d^2\Psi^{=}_{i}}{d\zeta^2} = 2^{i-1}\Lambda_2\Psi^{=}_{1}\Psi^{=}_{i}, \quad i = 1, 2. \quad \text{(A7)}$$

$$\frac{1}{Le_R}\frac{d^2\Psi^{=}_{i+2}}{d\zeta^2} - \hat{f}\frac{d\Psi^{=}_{i}}{d\zeta} = 2\Lambda_2[\Psi^{=}_{1}\Psi^{=}_{i+2} + (i-1)\Psi^{=}_{i}\Psi^{=}_{i+1}], \quad i = 1, 2. \quad \text{(A8)}$$

where $\Lambda_2 = \delta^3 Da_2$ is the reduced Damköhler number for the termination reaction. The local coupling functions are given by

$$\frac{d^2}{d\zeta^2}\left(\Theta^{=}_{i} - \frac{\Psi^{=}_{i}}{Le_R}\right) = 0, \quad i = 1, 2. \quad \text{(A9)}$$

$$\frac{d^2}{d\zeta^2}\left(\Theta^{=}_{i+2} - \frac{\Psi^{=}_{i+2}}{Le_R}\right) - \hat{f}\frac{d}{d\zeta}(\Theta^{=}_{i} - \Psi^{=}_{i}) = 0, \quad i = 1, 2. \quad \text{(A10)}$$

The volumetric heat loss is not important in the above equations because the recombination regions are still very thin, of $O(\delta)$. Each of the above equations needs to be solved separately in the upstream and downstream of the branching region.

Matching the solutions in the recombination region with the outer diffusive–convective regions yield $a_0 = \hat{T}_{f,0} - \hat{T}_{-\infty}$, $\hat{T}^{-}_{0}(\eta = 0) = \hat{T}_{f,0}$, and the conditions to solve equations (A7)–(A10).

$$\Psi^{=}_{i}(\zeta \to \pm\infty) = 0, \quad i = 1, 2, 3, 4. \quad \text{(A11)}$$

$$\Theta^{-}_{i}(\zeta \to \infty) = -\hat{T}^{+}_{i}(\eta = 0), \quad i = 1, 2. \quad \text{(A12)}$$

$$\frac{d\Theta^{-}_{i}}{d\zeta}(\zeta \to \infty) = -\frac{d\hat{T}^{+}_{0}}{d\eta}(\eta = 0) = \frac{\hat{H}(\hat{T}_{f,0})}{\hat{f}}, \quad \text{(A13)}$$

$$\Theta^{-}_{1}(\zeta \to -\infty) = -a_1 - \hat{f}(\hat{T}_{f,0} - \hat{T}_{-\infty})\zeta, \quad \text{(A14)}$$

$$\Theta^{-}_{2}(\zeta \to -\infty) = -\hat{T}^{-}_{\xi}(\tilde{x} = 0). \quad \text{(A15)}$$

$$\left(\frac{d\Theta^{-}_{i}}{d\zeta} - \hat{f}\Theta^{-}_{i}\right)_{-\infty} = \left(\hat{f}\hat{T}^{-}_{\xi} - \frac{d\hat{T}^{-}_{\xi}}{d\tilde{x}}\right)_{\tilde{x}=0} = -\int_{-\infty}^{0} \hat{H}(\hat{T}^{-}_{0})\,d\tilde{x}. \quad \text{(A16)}$$

Equations (17) and (A4) have respectively been used in deriving the second relation of equations (A13) and (A16).

Solving equations (A7) and (A8) subject to the matching conditions in equation (A11), we obtain

$$\Psi^{-}_{1} = 4(\Gamma\zeta + c^{-}_{1})^2, \quad \text{(A17)}$$

$$\Psi^{-}_{2} = \Gamma c^{-}_{2}/(\Gamma\zeta + c^{-}_{1})^3, \quad \text{(A18)}$$

$$\Psi^{-}_{3} = \frac{1}{\Gamma\zeta + c^{-}_{1}}\left[\frac{c^{-}_{3}}{(\Gamma\zeta + c^{-}_{1})^2} + \frac{4}{5}\frac{Le_R\hat{f}}{\Gamma}\right], \quad \text{(A19)}$$

$$\frac{d\Psi^{-}_{4}}{d\zeta} = \frac{\Gamma}{(\Gamma\zeta + c^{-}_{1})^3}\left[\frac{c^{-}_{4}}{\Gamma\zeta + c^{-}_{1}} - \frac{3}{2}\frac{c^{-}_{2}c^{-}_{3}\Gamma}{(\Gamma\zeta + c^{-}_{1})^2} - \frac{1}{5}c^{-}_{2}Le_R\hat{f}\right], \quad \text{(A20)}$$

where c^{-}_{i} are the integration constants to be determined and $\Gamma = (2Le_R\Lambda_2/3)^{1/2}$.

Applying equations (A17)–(A20) to equations (A9) and (A10), then solving the resulting equations subject to the matching conditions (A12)–(A16), we obtain

$$\Theta^{-}_{1} = \frac{1}{Le_R}\frac{4}{(\Gamma\zeta + c^{-}_{1})^2} - [\hat{f}(\hat{T}_{f,0} - \hat{T}_{-\infty})\zeta - a_1]H_{-1}(-\zeta) - \hat{T}^{+}_{1}(\eta = 0)H_{-1}(\zeta), \quad \text{(A21)}$$

$$\Theta^{-}_{2} = \frac{1}{Le_R}\frac{\Gamma c^{-}_{2}}{(\Gamma\zeta + c^{-}_{1})^3} - \hat{T}^{-}_{2}(\tilde{x} = 0)H_{-1}(-\zeta) - \hat{T}^{+}_{2}(\eta = 0)H_{-1}(\zeta), \quad \text{(A22)}$$

$$\frac{d^2\Theta^{-}_{3}}{d\zeta^2} = \frac{8}{(\Gamma\zeta + c^{-}_{1})^3}\left[\frac{c^{-}_{3}\Lambda_2}{(\Gamma\zeta + c^{-}_{1})^2} + \Gamma\hat{f}\left(\frac{6}{5} - \frac{1}{Le_R}\right)\right] - \hat{f}^2(\hat{T}_{f,0} - \hat{T}_{-\infty})H_{-1}(-\zeta), \quad \text{(A23)}$$

$$\frac{d\Theta^{-}_{4}}{d\zeta} = \frac{1}{(\Gamma\zeta + c^{-}_{1})^3}\left[\frac{\Gamma}{Le_R}\frac{c^{-}_{4}}{\Gamma\zeta + c^{-}_{1}} - \Gamma\hat{f}c^{-}_{2}\left(\frac{6}{5} - \frac{1}{Le_R}\right) - \frac{c^{-}_{2}c^{-}_{3}\Lambda_2}{(\Gamma\zeta + c^{-}_{1})^2}\right] + \frac{\hat{H}(\hat{T}_{f,0})}{\hat{f}}H_{-1}(\zeta) - \left[\hat{f}\hat{T}^{-}_{2}(\tilde{x} = 0) + \int_{-\infty}^{0} \hat{H}(\hat{T}^{-}_{0})\,d\tilde{x}\right]H_{-1}(-\zeta), \quad \text{(A24)}$$

where H_{-1} is the Heaviside function with $H_{-1}(\zeta) = 1$ for $\zeta > 0$ and 0 for $\zeta < 0$. In the above only the solutions required for matching with those in the branching region are presented. Because $(d\Psi^{-}_{1}/d\zeta)_0 \geq 0$ and $(d\Psi^{+}_{1}/d\zeta)_0 \leq 0$, we must have $c^{-}_{1} < 0$ and $c^{+}_{1} > 0$.

In the thin branching region, the coordinate is stretched as $\xi = \tilde{x}/\varepsilon$ while $\hat{Y}_F$ and $\hat{Y}_R$ are expanded as

$$\hat{Y}_F = \varepsilon(\phi_1 + \cdots) + \varepsilon^2(\phi_2 + \cdots) + O(\varepsilon^3), \quad \text{(A25)}$$

$$\hat{Y}_R = (\delta\psi_1 + \delta^2\psi_3 + \cdots) + \varepsilon(\psi_2 + \cdots) + \varepsilon^2(\psi_4 + \cdots) + O(\varepsilon^3). \quad \text{(A26)}$$

Because the activation energy for the branching reaction is high, variation of temperature can only be $O(\varepsilon)$. Thus $\hat{T}$ is expanded as

$$\hat{T} = (\hat{T}_{f,0} - \delta\hat{T}_{f,1} + \cdots) - \varepsilon\left(\theta_1 + \frac{\varepsilon}{\delta}\theta_2 + \cdots\right) - \varepsilon^2(\theta_3 + \cdots) + \cdots. \quad \text{(A27)}$$

Although the activation energy is large, it is not extremely high such that the branching reaction can occur in a temperature range smaller than its maximum value by an $O(\delta)$ amount. Substituting equations (A25)–(A27) to equations (9)–(11) and expanding, we obtain the following equations that describe the branching region.

$$\frac{d^2\psi_i}{d\xi^2} = 0, \quad i = 1, 3. \quad \text{(A28)}$$

$$\frac{d^2\theta_1}{d\xi^2} = 0. \quad \text{(A29)}$$

$$\frac{d^2\theta_2}{d\xi^2} = \Lambda_2\psi^{+}_{1}. \quad \text{(A30)}$$

$$\frac{d^2\theta_2}{d\xi^2} - \bar{f}\frac{d\theta_1}{d\xi} = 2\Lambda_2\psi_1\psi_1. \tag{A31}$$

$$\frac{d^2}{d\xi^2}\left(\frac{\phi_1}{Le_F} + \frac{\psi_2}{Le_R}\right) = 0. \tag{A32}$$

$$\frac{1}{Le_F}\frac{d^2\phi_2}{d\xi^2} - \bar{f}\frac{d\phi_1}{d\xi} + \frac{1}{Le_R}\frac{d^2\psi_2}{d\xi^2} - \bar{f}\frac{d\psi_2}{d\xi} = 2\Lambda_2\psi_1\psi_1. \tag{A33}$$

$$\frac{1}{Le_F}\frac{d^2\phi_1}{d\xi^2} = \Lambda_1\phi_1\psi_1\exp\left[-\left(\frac{\bar{T}_{ad}}{\bar{T}_{f,0}}\right)\theta_1\right]. \tag{A34}$$

where

$$\Lambda_1 = \varepsilon^2\delta Da_1\exp\left(-\frac{\bar{E}}{\bar{T}_{f,0} - \delta\bar{T}_{f,1} + \cdots}\right) \tag{A35}$$

is the reduced Damköhler number for the branching reaction.

Matching is performed first by expressing the outer solutions of $\bar{T}_{\bar{F}}$ in terms of $\xi = \bar{x}\,\varepsilon$, expanding, and then equating the resulting expression with the solution in the branching region. This gives $b_0 = 1$ and equations (27)–(29). Next, the solutions of $\bar{T}^2$ and $\bar{T}_{\bar{R}}$ in the recombination region are expressed in terms of $\xi = (\varepsilon\ \delta)\zeta$ and expanded to yield

$$\bar{T}_{f,1} = \frac{4}{Le_R(c_1^+)^2} - \bar{T}_1^+(\eta = 0), \tag{A36}$$

and the matching conditions

$$\psi_1(\xi \to \pm\infty) = 4\ (c_1^+)^2, \tag{A37}$$

$$\psi_2(\xi \to \pm\infty) = \Gamma(c_2^+ - 8\xi)\ (c_1^+)^3, \tag{A38}$$

$$\psi_{\bar{F}}(\xi \to \pm\infty) = \frac{1}{c_1^+}\left[\frac{c_2^+}{(c_1^+)^2} + \frac{4}{5}\frac{Le_R\bar{f}}{\Gamma}\right]. \tag{A39}$$

$$\frac{d\psi_2}{d\xi}(\xi \to \pm\infty) = \frac{\Gamma}{(c_1^+)^3}\left\{\frac{c_2^+}{c_1^+} - \left[\frac{3}{2}\frac{c_2^+\Gamma}{(c_1^+)^2} + \frac{1}{5}Le_R\bar{f}\right](c_2^+ - 8\xi)\right\}. \tag{A40}$$

$$\theta_1(\xi \to \pm\infty) = \frac{\Gamma}{Le_R(c_1^+)^3}(c_2^+ - 8\xi) - [\bar{T}_2^+(\bar{x} = 0) + \bar{f}(\bar{T}_{f,0} - \bar{T}_{-\infty})\xi]H_1(-\xi) - \bar{T}_2^+(\eta = 0)H_1(\xi). \tag{A41}$$

$$\theta_2(\xi \to \pm\infty) = 2\Lambda_2(4\xi - c_2^+\xi)\ (c_1^+)^4. \tag{A42}$$

$$\frac{d\theta_2}{d\xi}(\xi \to \pm\infty) = \frac{1}{(c_1^+)^3}\left\{\frac{c_2^+\Gamma}{c_1^+Le_R} - \left[\frac{c_2^+\Lambda_2}{(c_1^+)^2} + \Gamma\bar{f}\left(\frac{6}{5} - \frac{1}{Le_R}\right)\right](c_2^+ - 8\xi)\right\} + \frac{\bar{R}(\bar{T}_{f,0})}{\bar{f}}H_1(\zeta) - \left[\bar{f}^2(\bar{T}_{f,0} - \bar{T}_{-\infty})\xi + \bar{f}\bar{T}_2^+(\bar{x} = 0) + \int_{-\infty}^{\infty}\bar{R}(\bar{T}_0)\,d\bar{x}\right]H_1(-\zeta). \tag{A43}$$

In analyzing the branching region, first equations (A28) for ψ_1 and (A32) are solved subject to equations (27), (A37) and (A38) to yield

$$c_1^+ = -c_1^- = 2\left(\frac{8\Lambda_2}{3Le_R\bar{f}^2}\right)^{1/6}. \tag{A44}$$

$$\psi_1 = \left(\frac{3Le_R\bar{f}^2}{8\Lambda_2}\right)^{1/3}. \tag{A45}$$

Substituting equations (A44) into equation (A36), $\bar{T}_{f,1}$ can be determined if $\bar{T}_1^+(\eta = 0)$ is known. Because $\bar{T}_{f,1}$ represents the temperature at which branching reaction occurs, it is only a function of activation energy and chemical reactivity but does not depend on the heat loss. Thus by knowing that $\bar{T}_1^+(\eta = 0) = 0$ and $\bar{f} = 1$ in the adiabatic limit, we obtain

$$\bar{T}_{f,1} = \left(\frac{3}{8Le_R^2\Lambda_2}\right)^{1/3}, \tag{A46}$$

and hence $\bar{T}_1^+(\eta = 0) = \bar{T}_{f,1}(\bar{f}^{2/3} - 1)$.

Next, by sequentially integrating equations (A28) and (A29) twice, and equations (A30), (A31) and (A33) once, subject to equation (A44) and the proper boundary conditions of (A39)–(A43), we obtain $\bar{T}_{f,0} = 1 + \bar{T}_{-\infty} = \bar{T}_{ad}$, $c_2^- = c_2^+$, $c_4^- = c_4^+$, $b_1 = -Le_F\bar{f}c_2^+/8$, as well as

$$\theta_1 = -\frac{\bar{f}}{2}\left(\xi - \frac{c_2^+}{8}\right) + \frac{\bar{L}}{2\bar{f}^{2/3}}, \tag{A47}$$

where $\bar{L}$ is defined in equation (32).

Finally, substituting equations (A45) and (A47) into equation (A34), and defining the new variables

$$\bar{\phi} = \frac{\phi_1}{2Le_F},$$

$$\bar{\xi} = \left[2(2Le_F\Lambda_1)^{1/2}\left(\frac{3Le_R}{\Lambda_2}\right)^{1/6}\right]\left[\bar{f}^{2/3}\exp\left(\frac{\bar{L}}{4\bar{f}^{2/3}}\right)\right]^{-1} \times \exp\left[\frac{\bar{f}}{4}\left(\xi - \frac{c_2^+}{8}\right)\right], \tag{A48}$$

the structure equation is obtained,

$$\bar{\xi}^2\frac{d^2\bar{\phi}}{d\bar{\xi}^2} + \bar{\xi}\frac{d\bar{\phi}}{d\bar{\xi}} - \bar{\xi}^2\bar{\phi} = 0. \tag{A49}$$

$$\bar{\phi}(\bar{\xi} = 0) = \ln\left\{\left[2Le_F\Lambda_1\left(\frac{3Le_R}{\Lambda_2}\right)^{1/3}\right] \times \left[\bar{f}^{4/3}\exp\left(\frac{\bar{L}}{2\bar{f}^{2/3}}\right)\right]^{-1}\right\} - 2\ln(\bar{\xi}/2), \tag{A50}$$

$$\bar{\phi}(\bar{\xi} \to \infty) = 0. \tag{A51}$$

This is a modified Bessel function of order zero whose solution is $\bar{\phi} = cK_0(\bar{\xi})$, where c is the integration constant, after equation (A51) is applied. Because $K_0(\bar{\xi} = 0) = -\ln(\bar{\xi}/2) - \gamma$, where $\gamma = 0.5772$ is the Euler's constant, upon applying equation (A50) we obtain

$$\left[2Le_F\Lambda_1\left(\frac{3Le_R}{\Lambda_2}\right)^{1/3}\right]\left[\bar{f}^{4/3}\exp\left(\frac{\bar{L}}{2\bar{f}^{2/3}}\right)\right]^{-1} = \exp(-2\gamma). \tag{A52}$$

In the adiabatic limit, $\bar{L} = 0$ and $\bar{f} = 1$, we have

$$\left[2Le_F\Lambda_1\left(\frac{3Le_R}{\Lambda_2}\right)^{1/3}\right] = \exp(-2\gamma). \tag{A53}$$

Substituting equation (A53) in equation (A52), we obtain the flame response given by equation (36).

Appendix B

COMBUSTION AND FLAME 97: 317–338 (1994)

The Structure of Premixed Methane–Air Flames with Large Activation Energy

J. K. BECHTOLD* and C. K. LAW

Department of Mechanical and Aerospace Engineering Princeton University, Princeton, NJ 08544

We examine the structure of both lean and stoichiometric premixed methane–air flames with a reduced reaction mechanism. Our starting point is a four-step, C_1-chain mechanism that has been derived previously using a series of steady-state and partial equilibrium assumptions. This same mechanism has been adopted in several recent asymptotic studies that have used the ratio of the branching to propagating reactions as the perturbation parameter to analyze the fuel consumption zone within the flame structure. In the present study, we assume that the activation energy of the intermediate reactions in the fuel consumption zone are sufficiently large to employ the method of large activation energy asymptotics. We obtain temperature and species profiles, as well as a structure problem whose solution determines the burning rate eigenvalue in terms of a parameter that represents the ratio of branching to terminating reactions. When this parameter is set to zero, the results of previous rate–ratio analyses are recovered. In the opposite limit that this parameter becomes large, the structure reduces to that of Liñán's premixed burning regime. In both limiting cases, we determine the parametric dependence of the burning rate on equivalence ratio, pressure, and the ratio of competing rates of branching and termination reactions. The trends are found to be largely in agreement with experimental observations. One advantage of the present approach is that the exponentially nonlinear reaction rate terms are retained, thus permitting the study of the response of methane–air flames to small perturbations.

NOMENCLATURE

A	parameter defined in Eq. 4.9
A_1, A_{11}	scaled preexponential factors defined after Eq. 4.5
$\hat{A}_1$, $\hat{A}_{11}$	preexponential factors in reaction 1, 11
a_n	integration constants
b_n	integration constants
c_p	specific heat
D	Damköhler number defined in Eq. 4.10
$\hat{D}$	scaled Damköhler number defined in Eq. 6.21
D_i	mass diffusivity of species i
E_1, E_{11}	activation energy of reactions 1, 11
F	fuel
K_i	equilibrium constants
k_i	elementary rate constants
Le_i	Lewis number of species i
m	parameter defined in Eq. (6.21)
p	pressure
Q_k	non-dimensional heat release of global reaction k, defined in Eq. 2.4
q	parameter defined in Eq. 5.5
q_k	heat release per mole of fuel consumed
q_F, q_H, q_{H_2}, q_{CO}	parameters defined after Eq. 4.10
R^0	universal gas constant
$\hat{T}$	temperature
t	temperature perturbation in oxidation layer defined in Eq. 5.2
v	velocity
W	variable defined in Eq. 4.18
W_i	molecular weight of species i
w_k	overall reactions defined in Eq. 2.1
X_i	species variable related to mole fraction normalized by mole fraction of fuel
x	spatial variable
Y	scaled variable defined in Eq. 6.14

* Corresponding author.

Published by Elsevier Science Inc.

0010-2180/94/$7.00

Y_i	mass fraction of species i
y_i	mole fraction in fuel consumption layer, defined in Eq. 4.4
Z_i	mole fraction in oxidation layer, defined in Eqs. 5.2, 5.3

Greek Symbols

α	parameter defined in Eq. 2.3
γ	parameter defined in Eq. 6.2
δ	thickness of fuel consumption layer, defined in Eq. 4.3
ϵ	thickness of oxidation layer, defined in Eqs. 5.10, 5.21
ζ	stretched spatial coordinate in fuel consumption layer
η	stretched spatial coordinate in oxidation layer
η_i	Chaperon efficiency of species i
θ	temperature perturbation in fuel consumption layer
λ	thermal conductivity
μ	thickness of radical consumption layer, defined in Eq. 4.21
ξ	scaled spatial coordinate defined in Eq. 6.14
ρ	density
σ	stretched spatial coordinate in radical consumption layer
τ	nondimensional temperature
ϕ	equivalence ratio
ω_k	nondimensional overall reaction rates

Subscripts and Superscripts

b	burned value
i	species, $i = F, CO, CO_2, H, H_2, H_2O, O_2$
k	global reaction step
0	value at radical consumption zone
u	unburned value

1. INTRODUCTION

The theory of flame propagation has been greatly advanced during the past 20 years through the use of large activation energy asymptotics to simplify the nonlinear reaction rate terms in chemically reacting flows. By modeling the complex chemical kinetics to consist of a single overall reaction with large activation energy confined to a narrow region in the flow field, a mathematical treatment of the governing equations is often possible.

While the one-step chemistry model facilitates mathematical analysis, it is recognized that this simplification is incapable of providing a satisfactory explanation for phenomena that depend largely on reaction intermediaries and thus an accurate description requires a more detailed chemical kinetic scheme. Since full kinetic mechanisms are frequently too large to permit either mathematical or numerical analysis, there has been a great deal of recent work devoted to identifying the most important reactions for various fuel–air mixtures in order to reduce the number of steps to a point where the governing equations become amenable to analysis. For example, Miller, et al. [1] have derived a "short" mechanism for methane–air flames consisting of about 40 steps using only C_1-hydrocarbon species. The resulting system of equations has been solved numerically to compute burning velocities for lean and stoichiometric mixtures over a wide range of conditions [2].

Although these "short" mechanisms represent a significant simplification over the original full system, the number of equations is still much too large for a mathematical treatment. Furthermore, in analyses based solely on numerics, it is frequently difficult to identify the most important parameters that mostly influence the global properties. Thus, in order to bridge the gap between the one-step kinetics and the large multistep schemes, Peters [3] has systematically reduced the existing "short" mechanism down to a mechanism consisting of four overall reactions using a series of steady-state and partial equilibrium assumptions. The resulting four-step model involves just seven of the original species and includes kinetic data from only five elementary reactions. On the basis of this reduced mechanism the basic structure of methane–air flames has been studied asymptotically [4–7].

In many of these studies, the activation energies of the individual elementary reactions

are not considered to be large enough to employ large activation energy asymptotics. The reaction rates are assumed to have a power law dependence on temperature, rather than the conventional Arrhenius form, and the ratios of the individual reaction rates are used as small parameters in the asymptotic analysis. This type of approach has been used in two-, three-, and four-step models to calculate burning velocities over a wide range of equivalence ratio, pressure, and temperature. However, the power-law dependence on temperature does not exhibit the same kind of sensitivity to temperature variations as the Arrhenius approximation. Consequently, the response of the flame to various external perturbations is not very significant.

In contrast to previous works, the key termination reaction in these studies was found to be the propagating step, rather than the three-body recombination reaction. Furthermore, the leading order flame structure analysis yielded a value for the "Damköhler number", which was independent of the burning rate. The resulting expression was therefore used to calculate the temperature $\hat{T}^0$ at the leading edge of the flame zone. A solution for $\hat{T}^0$ was previously sought of the form $\hat{T}^0 \sim \hat{T}_b + O(\epsilon)$, where $\hat{T}_b$ is the known flame temperature and ϵ (assumed small) is a measure of the flame width, which in turn is proportional to the burning rate. Thus an expression for the burning rate was obtained by equating the first two terms in this asymptotic expansion and solving for ϵ.

In the present study, we adopt the four-step mechanism as a starting point to analyze the structure of premixed methane–air flames in the same manner as Peters and Williams [4]. That is, we assume that the H radical is in steady state and that, to first approximation, the water–gas shift is in partial equilibrium, effectively reducing the four-step mechanism to a two-step mechanism. However, as in [4], we shall incorporate nonequilibrium effects as a perturbation from the leading order partial equilibrium state. Our analysis differs from theirs in that we retain the Arrhenius form for the individual reactions and, except for the three-body recombination reaction with zero activation energy, we consider the effective activation temperatures to be sufficiently large such that activation energy asymptotics can provide reasonable and useful results. We remark that although activation temperatures have been estimated to be on the order of 7000 K, it is known that even modest values are sufficient to confine the reaction to narrow regions, thereby enabling the use of activation energy asymptotics to obtain remarkably accurate results [8].

In our study the flame structure remains identical to that analyzed by Peters and Williams [4] (Fig. 1). It consists of a chemically inert preheat zone where the temperature increases from its unburned value to a characteristic temperature at which reaction can take place. There is a very thin fuel consumption zone where the hydrogen reaction occurs, and the H radical is entirely consumed by the fuel in a yet thinner zone that defines the leading edge of the flame structure. Immediately downstream of the fuel consumption layer lies a relatively broad, but still asymptotically small, oxidation layer where H_2 and CO oxidize to form H_2O and CO_2. This entire structure is embedded in a flow field which is chemically inert due to the absence of radicals.

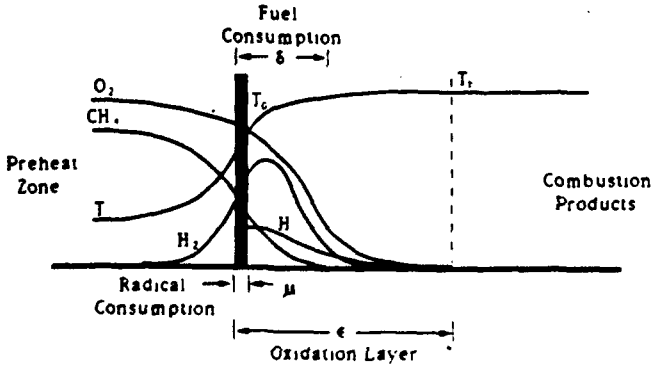

Fig. 1. Schematic of the flame structure, illustrating several species profiles and the temperature distribution.

The present analysis provides a complete description of the above flame structure, and the role of each of the overall reaction steps is determined. Our results include the evaluation of the burning rate in terms of pressure, equivalence ratio, and a parameter that represents the ratio of the competing rates of the branching and termination reactions. In particular, we find that when this rate-ratio is reduced, the burning rate eventually decreases to zero. For the opposite limit that the rate-ratio is large, we find that the burning rate asymptotes to a constant value. In this limit, the radical consumption zone retreats far upstream into the inert so that the fuel consumption region is governed solely by the concentration of the fuel. As a result, a coordinate transformation can be made which expresses the structure problem in a form identical to that found by Liñán [9] in the premixed burning regime of his diffusion flame analysis. Thus we are able to adopt his correlation curve as an approximate expression for the burning rate in this limit. We find that the role of the propagation step changes from retarding to enhancing reaction as this limit is approached.

In what follows, we present the analysis of the above structure to determine the characteristics of premixed methane–air flames. In the next section the mathematical formulation of the model problem will be discussed. The asymptotic analyses of all the sublayers in the flame structure are then performed in Sections 3–5. In Section 6 we analyze the resulting structure equation and in Section 7 we evaluate the burning rate over a range of parameter values. Finally, in Section 8 we summarize our results and add further discussion.

2. THE MATHEMATICAL MODEL

The reduced four-step mechanism derived in Ref. 3 consists of the following overall reaction steps:

$$CH_4 + 2H + H_2O \rightarrow CO + 4H_2, \quad \text{(I)}$$

$$CO + H_2O \rightleftharpoons CO_2 + H_2, \quad \text{(II)}$$

$$2H + M \rightarrow H_2 + M, \quad \text{(III)}$$

$$O_2 + 3H_2 \rightleftharpoons 2H_2O + 2H. \quad \text{(IV)}$$

which represent, respectively, fuel consumption, the water–gas shift, radical recombination, and a branching reaction. We employ the notation of Peters and Williams [4] to express the rates of these four steps as

$$w_I = k_{11}[CH_4][H], \quad \text{(2.1a)}$$

$$w_{II} = \frac{k_{10}[H]}{K_3[H_2]}([CO][H_2O] - [CO_2][H_2]/K_{II}), \quad \text{(2.1b)}$$

$$w_{III} = k_5[O_2][H][M] = k_{III}p[O_2][H], \quad \text{(2.1c)}$$

$$w_{IV} = k_1[H]\left([O_2] - \frac{[H]^2[H_2O]^2}{[H_2]^3 K_{IV}}\right), \quad \text{(2.1d)}$$

where p is the pressure, K_i are the equilibrium constants, and k_i are the elementary rate constants, which are given explicitly in Ref. 3. The concentration of the third body M in reaction III has been written in terms of the Chaperon efficiency η_i of species i in order to convert the three-body rate constant into a two-body form. In this model, reactions I, II, and IV have large activation energies while reaction III has zero activation energy [3]. This implies that the three-body radical recombination reaction is least sensitive to temperature variations and therefore takes place over a broader, but still asymptotically thin, region.

We start out by first assuming that the water–gas shift (reaction II) is in partial equilibrium, thereby reducing the four-step to a three-step mechanism. This assumption can be justified when the corresponding Damköhler number of reaction II is sufficiently large, a situation that can be achieved at sufficiently high pressure. We consider nonequilibrium effects as a perturbation, as was done in the studies of Peters and Williams [4] and Seshadri and Peters [5]. That is, we will account for the existence of a narrow zone immediately downstream of the fuel consumption layer, where the water–gas shift is not in equilibrium, followed by a layer where reaction II reaches equilibrium. In the first approximation, we set Eq. 2.1b to zero to obtain an expression for the concentration of CO.

The rate constants in the three remaining global reactions govern the intermediate reac-

tions

$$CH_4 + H \xrightarrow{k_{II}} CH_3 + H_2,$$

$$H + O_2 \xrightarrow{k_I} OH + O,$$

$$H + O_2 + M \xrightarrow{k_{\delta}} HO_2 + M,$$

which represent chain-propagating, chain-branching and chain-terminating steps respectively. Many previous studies have used the rate-ratio k_1/k_{11}, which describes the competition of oxygen and fuel for the H radical, as the small perturbation parameter to describe the fuel consumption zone thickness. Those studies have found that k_{11} ultimately has a chain-breaking effect, producing the more stable methyl radical, CH_3, at the expense of the very active H radical. In the present study, we demonstrate that k_{11} can play an intermediate role to that of the chain-branching and chain-breaking reactions k_1 and k_{III}, respectively. Specifically, we find that when a particular lumped parameter containing these rates is large, the chain-propagating reaction further enhances burning. On the other hand, when this lumped parameter is small, the flame burns weaker and reaction k_{11} is found to inhibit propagation.

We consider steady, planar deflagrations with constant burning rate ρv such that the nondimensional conservation equations for the remaining six species, as well as the temperature equation, can be written in the form

$$L_F(X_F) = -\omega_I, \tag{2.2a}$$

$$L_H(X_H) = -2\omega_I - 2\omega_{III} + 2\omega_{IV}, \tag{2.2b}$$

$$L_{H_2}(X_{H_2}) + \alpha L_{CO}(X_{H_2}) = 5\omega_I + \omega_{III} - 3\omega_{IV}, \tag{2.2c}$$

$$L_{O_2}(X_{O_2}) = -\omega_{II} - \omega_{IV}, \tag{2.2d}$$

$$L_{H_2O}(X_{H_2O}) - \alpha L_{CO}(X_{H_2}) = -2\omega_I + 2\omega_{II} - \omega_{IV}, \tag{2.2e}$$

$$L_{CO_2}(X_{CO_2}) + \alpha L_{CO}(X_{H_2}) = \omega_I, \tag{2.2f}$$

$$L(\tau) + Q_{II}\alpha L_{CO}(X_{H_2}) = (Q_I + Q_{II})\omega_I + Q_{III}\omega_{III} + Q_{IV}\omega_{IV}. \tag{2.2g}$$

In addition, the partial equilibrium assumption for reaction II yields the relation

$$X_{CO} = \alpha X_{H_2},$$

where

$$\alpha = \frac{Le_{H_2} Le_{CO_2} X_{CO_2}}{Le_{H_2O} Le_{CO} X_{H_2O} K_{II}}. \tag{2.3}$$

Peters and Williams [4] argue that the ratio X_{CO_2}/X_{H_2O} varies very little throughout the flame structure. Consistent with their study, we treat α as a constant in order to facilitate our analysis. Here the differential operators are defined as

$$L(\cdot) \equiv \left(\frac{d}{dx} - \frac{d^2}{dx^2}\right)(\cdot),$$

$$L_i(\cdot) \equiv \left(Le_i \frac{d}{dx} - \frac{d^2}{dx^2}\right)(\cdot),$$

where the Lewis number of each species $Le_i = \lambda/\rho D_i c_p$ has been assumed constant.

The nondimensional quantities in our system are given in terms of dimensional variables (with hats) by

$$x = \int_0^{\hat{x}} \frac{\rho v c_p}{\lambda}\, d\hat{x}, \qquad \tau = \frac{\hat{T} - \hat{T}_u}{\hat{T}^0 - \hat{T}_u},$$

$$X_i = \frac{Y_i W_F}{Le_i Y_{F,u} W_i},$$

and the reaction terms now have the form

$$\omega_k = \frac{\lambda W_F}{\rho^2 v^2 c_p Y_{F,u}} w_k, \qquad k = I, \ldots, IV.$$

In the above equations λ is the thermal conductivity, c_p the specific heat, and ρD_i the density-weighted mass diffusivities. The quantities Y_i and W_i are, respectively, the mass fraction and the molecular weight of species i so that each X_i is related to the mole fraction normalized with respect to the mole fraction of fuel in the fresh mixture. The subscript u denotes values in the fresh unburned mixture and $\hat{T}^0$ is the temperature of the leading edge

of the flame zone where fuel reacts with the H radical. The parameter Q_k appearing in the energy equation (2.2g) is given by

$$Q_k = \frac{Y_{F,u} q_k}{c_p W_F (\hat{T}^0 - \hat{T}_u)}, \tag{2.4}$$

where q_k is the heat release per mole of fuel consumed.

The above equations are to be solved subject to the boundary conditions

$$\left.\begin{aligned} &X_F = \mathrm{Le}_F^{-1},\ X_{O_2} = 2\mathrm{Le}_{O_2}^{-1}\phi^{-1},\ \tau = 0,\\ &X_H = X_{CO_2} = X_{H_2O} = X_{H_2} = X_{CO} = 0, \end{aligned}\right\} \quad x \to -\infty, \tag{2.5}$$

$$\left.\begin{aligned} &X_{H_2O} = X_{H_2O,b},\ X_{CO_2} = X_{CO_2,b},\\ &X_{O_2} = 2\mathrm{Le}_{O_2}^{-1}(\phi^{-1} - 1),\ \tau = \tau_b,\\ &X_H = X_F = X_{H_2} = X_{CO} = 0, \end{aligned}\right\} \quad x \to \infty, \tag{2.6}$$

where $\phi = 2Y_{F,u}W_{O_2}/(Y_{O_2,u}W_F)$ is the equivalence ratio, such that $\phi = 1$ for stoichiometric mixtures. Our analysis can only be considered valid for $\phi \le 1$ since the reduced mechanism and the corresponding flame structure are only appropriate for stoichiometric and fuel-lean mixtures. An analysis of fuel-rich mixtures will require the use of a different reaction mechanism and flame structure.

It is convenient to work with the reaction-free coupling functions

$$\begin{aligned} L(\tau) &+ (Q_I + Q_{II} + Q_{III} + 2Q_{IV})L_F(X_F)\\ &+ \frac{(3Q_{III} + Q_{IV})}{4}L_H(X_H)\\ &+ \frac{(Q_{III} + Q_{IV})}{2}L_{H_2}(X_{H_2})\\ &+ \left\{Q_{II} + \frac{(Q_{III} + Q_{IV})}{2}\right\}\alpha L_{CO}(X_{H_2}) = 0, \end{aligned} \tag{2.7}$$

$$L_F(X_F) + \tfrac{1}{4}L_H(X_H) + \tfrac{1}{2}L_{H_2}(X_{H_2}) + \tfrac{1}{2}L_{H_2O}(X_{H_2O}) = 0, \tag{2.8}$$

$$L_F(X_F) + \tfrac{1}{6}L_H(X_H) + \tfrac{1}{3}L_{H_2}(X_{H_2}) - \tfrac{2}{3}L_{O_2}(X_{O_2}) - \tfrac{1}{3}L_{CO_2}(X_{CO_2}) = 0, \tag{2.9}$$

which replace Eqs. (2.2e, f, g). These equations can be integrated across the entire flow field to yield the following leading order expressions for the burned temperature τ_b and the downstream product concentrations $X_{H_2O,b}$ and $X_{CO_2,b}$,

$$\tau_b = Q_I + Q_{II} + Q_{III} + 2Q_{IV}, \tag{2.10}$$

$$X_{H_2O,b} = 2\mathrm{Le}_{H_2O}^{-1}, \qquad X_{CO_2,b} = \mathrm{Le}_{CO_2}^{-1}. \tag{2.11}$$

Before analyzing the system 2.2, we first invoke an additional assumption in order to simplify matters. As discussed in Ref. 4, when the H radical is consumed much more rapidly than it is produced, its concentration remains very small and it is said to be in steady state. Under these conditions, the above system of equations is simplified and the three-step mechanism is further reduced to a two-step mechanism. By making this assumption we can set the right-hand side of Eq. 2.2b to zero to obtain

$$\omega_{IV} = \omega_I + \omega_{III}, \tag{2.12}$$

from which the radical concentration is found to be

$$X_H = \sqrt{K_{IV}X_{O_2}\mathrm{Le}_{O_2}}\,\frac{(\mathrm{Le}_{H_2}X_{H_2})^{3/2}}{\mathrm{Le}_H\mathrm{Le}_{H_2O}X_{H_2O}} \times \left\{1 - \frac{k_{11}\mathrm{Le}_F X_F}{k_1\mathrm{Le}_{O_2}X_{O_2}} + \frac{k_{III}}{k_1}p\right\}^{1/2}. \tag{2.13}$$

In Section 4 we will see that this steady state approximation for the H radical holds throughout the entire flame structure with the exception of a very narrow region at the leading edge where the fuel attacks the radical and totally depletes the concentration of H.

Equation 2.12 is used to eliminate ω_{IV} so that our system now can be written

$$L_F(X_F) = -\omega_I, \tag{2.14a}$$

$$(L_{H_2} + \alpha L_{CO})(X_{H_2}) = 2(\omega_I - \omega_{III}), \tag{2.14b}$$

$$L_{O_2}(X_{O_2}) = -\omega_I - \omega_{III}, \tag{2.14c}$$

$$L_{H_2O}(X_{H_2O}) - \alpha L_{CO}(X_{H_2}) = 2\omega_{III}, \tag{2.14d}$$

$$L_{CO_2}(X_{CO_2}) + \alpha L_{CO}(X_{H_2}) = \omega_I, \qquad (2.14e)$$

$$L(\tau) - Q_{II}L_{H_2}(X_{H_2}) = (Q_I - Q_{II} + Q_{IV})\omega_I + (2Q_{II} + Q_{III} + Q_{IV})\omega_{III}. \qquad (2.14f)$$

The remainder of this study is concerned with obtaining solutions to Eqs. 2.14 in order to gain a description of the methane–air flame structure sketched in Fig. 1; we begin with an analysis of the chemically inert outer regions.

3. THE CHEMICALLY INERT REGIONS

All of the chemistry is confined to a very narrow region located near $x = 0$, on either side of which the flow field is chemically inert. The H radicals are entirely produced and consumed within the flame so that the H-atom concentration is zero on either side of the flame zone. For the remaining species a balance is maintained between convection and diffusion. Solutions are readily found to be

$$X_F = \begin{cases} \mathrm{Le}_F^{-1}[1 - \exp(\mathrm{Le}_F x)] & x < 0, \\ 0 & x > 0, \end{cases} \qquad (3.1)$$

$$X_{O_2} = \begin{cases} 2\mathrm{Le}_{O_2}^{-1}\phi^{-1} - b_1 \exp(\mathrm{Le}_{O_2} x) & x < 0, \\ 2\mathrm{Le}_{O_2}^{-1}(\phi^{-1} - 1) & x > 0, \end{cases}$$

$$X_{H_2} = \begin{cases} b_2 \exp(\mathrm{Le}_{H_2} x) & x < 0, \\ 0 & x > 0, \end{cases} \qquad (3.2)$$

$$X_{H_2O} = \begin{cases} b_3 \exp(\mathrm{Le}_{H_2O} x) & x < 0, \\ X_{H_2O,b} & x > 0, \end{cases}$$

$$X_{CO_2} = \begin{cases} b_4 \exp(\mathrm{Le}_{CO_2} x) & x < 0, \\ X_{CO_2,b} & x > 0, \end{cases} \qquad (3.3)$$

$$\tau = \begin{cases} a_1 e^x + \delta a_3 e^x + \cdots, & x < 0, \\ \tau_b + \delta a_2 + \cdots, & x > 0, \end{cases} \qquad (3.4)$$

where the unknown constants a_i, b_i will be determined by matching to solutions in the inner flame region. In general, all constants are to be expanded in terms of the two parameters, δ and ϵ, which are assumed small relative to the thermal thickness of the flame. These parameters represent the thickness of the fuel consumption zone and the oxidation layer, respectively, and they will be defined in the next two sections.

We note that the fuel is entirely consumed by the flame so that no leakage to the downstream region occurs. Furthermore, we will impose continuity of X_F across the fuel consumption zone up to $O(\delta)$, which is the needed order of accuracy for the present problem. When continuity is applied, the concentration of fuel outside the flame structure is given entirely by Eq. 3.1 to all orders in ϵ and δ.

4. THE FUEL AND RADICAL CONSUMPTION LAYERS

In seeking solutions to the system 2.14 we assume that the nonzero activation energies are sufficiently large so as to confine reaction of fuel to a narrow region in the flow field, thus permitting the use of activation energy asymptotics. Of the reaction rates remaining in our system, k_{III} has zero activation energy while k_{11} and k_1 have the form

$$k_{11} = \tilde{A}_{11,\mathrm{eff}} \exp\left(-E_{11}/R^0\hat{T}\right),$$
$$k_1 = \tilde{A}_1 \exp\left(-E_1/R^0\hat{T}\right), \qquad (4.1)$$

where the E_is are the activation energies and R^0 is the gas constant. The preexponentials $\tilde{A}_i$ are generally quite large and so it is appropriate to rescale them as

$$\tilde{A}_i = \hat{A}_i \exp\left(E_i/R^0\hat{T}^0\right), \qquad (4.2)$$

where $\hat{T}^0$ was defined earlier as the characteristic temperature at which fuel reacts with the radical. It follows from Eq. 2.14a that fuel is consumed by the reaction with the rate k_{11} which suggests that an appropriate small parameter to define the thickness of the fuel consumption layer is given by

$$\delta = \frac{R^0(\hat{T}^0)^2}{E\left(\hat{T}^0 - \hat{T}_u\right)}. \qquad (4.3)$$

Thus, fuel consumption will be restricted to a narrow region of width $O(\delta)$ where the temperature is close to $\hat{T}^0$, that is, where $\tau - 1 = O(\delta)$. We note that, although the temperature will continue to increase downstream of this layer, reaction is terminated by the depletion of fuel.

4.1. The Fuel Consumption Layer

In terms of the outer variable, the flame resides at the location $x = 0$. To investigate the fuel consumption region we introduce the stretched coordinate $x = \delta\zeta$ and seek solutions of the form

$$\tau = 1 + \delta\theta + \cdots, \qquad X_F = \delta y_F + \cdots,$$
$$X_i = X_i^0 + \delta y_i + \cdots, \qquad (i \neq F). \tag{4.4}$$

The H-radical concentration is readily determined from Eq. 2.13 as

$$X_H = \sqrt{K_{IV} X_{O_2}^0 \mathrm{Le}_{O_2}} \frac{\left(\mathrm{Le}_{H_2} X_{H_2}^0\right)^{3/2}}{\mathrm{Le}_H \mathrm{Le}_{H_2O} X_{H_2O}^0} \times \left\{1 - \frac{\delta k_{11} \mathrm{Le}_F y_F}{k_1 \mathrm{Le}_{O_2} X_{O_2}^0} + \frac{k_{III}}{k_1} p\right\}^{1/2}. \tag{4.5}$$

Gradients are large in this region so that diffusion dominates over convection and thus we expect the diffusion and reaction terms to balance in our equations. In order that such a balance is maintained in the equation for the temperature perturbation, we require that $k_{11} = O(\delta^{-2})$ so that $\hat{A}_{11} = \delta^{-2} A_{11}$. We also want to retain the variation of H radical with fuel concentration and by balancing the first two terms on the right-hand side of Eq. 4.5 it is necessary to introduce the additional scaling $\hat{A}_1 = \delta^{-1} A_1$. Furthermore, the ratio k_1/k_{11} has a weak temperature dependence [4]. Thus we simplify matters by assuming the activation energies of these two rates are equal, that is, $E_{11} = E_1 \equiv E$. The above scalings imply that the last term in Eq. 4.5 is smaller in magnitude than the remaining terms throughout this region (i.e., $k_{III}/k_1 \ll 1$), and that the ratio $k_1/k_{11} = \delta A_1/A_{11}$ is a small parameter. Indeed, as discussed earlier, many previous studies have used the rate-ratio k_1/k_{11}, which describes the competition of oxygen and fuel for the H radical, as the small perturbation parameter to describe the fuel consumption zone thickness.

To leading order in δ, reaction ω_{III} is negligible and the relevant equations governing the fuel consumption zone (2.14a, b) and (2.7) can be expressed as

$$\frac{d^2 y_F}{d\zeta^2} = D y_F \sqrt{1 - A y_F} \exp(\theta), \tag{4.6}$$

$$\frac{d^2}{d\zeta^2}\left[\theta + q_F y_F + q_H y_H + (q_{H_2} + \alpha q_{CO}) y_{H_2}\right] = 0, \tag{4.7}$$

$$\frac{d^2(1+\alpha) y_{H_2}}{d\zeta^2} = -2\frac{d^2 y_F}{d\zeta^2}, \tag{4.8}$$

where we have defined the parameters

$$A = A_{11} \mathrm{Le}_F / \left(A_1 \mathrm{Le}_{O_2} X_{O_2}^0\right), \tag{4.9}$$

$$D = \frac{\mathrm{Le}_F \lambda Y_{F,u} \rho_0^2}{\rho^2 v^2 c_p W_F} \sqrt{K_{IV} X_{O_2}^0 \mathrm{Le}_{O_2}} \times \frac{\left(\mathrm{Le}_{H_2} X_{H_2}^0\right)^{3/2}}{\mathrm{Le}_{H_2O} X_{H_2O}^0} A_{11}, \tag{4.10}$$

$$q_F = Q_I + Q_{II} + Q_{III} + 2Q_{IV},$$
$$q_H = (3Q_{III} + Q_{IV})/4,$$
$$q_{H_2} = (Q_{III} + Q_{IV})/2,$$
$$q_{CO} = Q_{II} + (Q_{III} + Q_{IV})/2.$$

These equations are to be solved subject to appropriate boundary conditions which are obtained through matching with the upstream inert region and the downstream oxidation layer. We have avoided writing equations for the O_2, H_2O, and CO_2 perturbations since the system 4.6–4.8 is independent of these quantities.

As we mentioned earlier, the steady-state approximation implies that the H-radical concentration is small so that y_H can be neglected in Eq. 4.7. However, it is easily seen that Eq. 4.6 breaks down as $y_F \to 1/A$, suggesting that our steady-state assumption for H becomes invalid. Thus we expect a boundary layer to develop near $y_F = 1/A$, where the fuel depletes the radical concentration. Peters and Williams [4] have analyzed this boundary layer and have demonstrated the smooth transition to a zero H-atom concentration. For completeness, we briefly summarize that analysis.

4.2. The Radical Consumption Layer

We first need to determine the local behavior of X_F. Since the region preceding the radical consumption layer is chemically inert (due to the absence of the H-radical), the solution 3.1 for X_F is valid everywhere upstream of the boundary layer at $\zeta = -1/A$. Thus by expanding Eq. 3.1 in terms of the inner variable $x = \delta\zeta$ we find

$$X_F \sim -\delta\zeta + \cdots, \tag{4.11}$$

from which it follows

$$y_F \equiv -\zeta \quad \text{for } \zeta < -1/A. \tag{4.12}$$

In the remainder of the structure, i.e., $\zeta > -1/A$, y_F is determined by solving Eq. 4.6, and continuity of y_F and $dy_F/d\zeta$ at $\zeta = -1/A$ provides the boundary conditions

$$y_F = -\zeta \quad \text{at } \zeta = -1/A. \tag{4.13}$$

The equation governing the radical concentration in the flame structure (where ω_{III} is negligible) (Eq. 2.2b) can be written as

$$\frac{d^2X_H^0}{d\zeta^2} = 2\delta^2(\omega_I - \omega_{IV}) = \delta^2\frac{2\mathrm{Le}_{O_2}\mathrm{Le}_H\lambda Y_{F,u}\rho_0^2}{\rho^2 T^2 c_p W_F}k_1 X_{O_2}^0 X_H^0 \times\left[-1 + \frac{k_{11}\mathrm{Le}_F X_F}{k_1\mathrm{Le}_{O_2}X_{O_2}^0} + \frac{\left(\mathrm{Le}_H\mathrm{Le}_{H_2O}X_{H_2O}^0X_H^0\right)^2}{\left(\mathrm{Le}_{H_2}X_{H_2}^0\right)^3\mathrm{Le}_{O_2}X_{O_2}^0K_{IV}}\right]. \tag{4.14}$$

In the much thinner radical consumption layer temperature variations are negligible, so that $\theta \approx 0$, and we introduce the stretched variable σ as

$$\zeta = -1/A + \mu\sigma/A, \tag{4.15}$$

where the small parameter μ will be appropriately chosen shortly. It follows from Eq. 4.13 that the fuel concentration in this layer has the form $y_F \sim 1/A - \mu\sigma/A$. We insert this into the steady-state expression for X_H (4.5) to obtain the following matching condition for X_H^0

$$X_H^0 \sim \frac{\sqrt{K_{IV}\mathrm{Le}_{O_2}X_{O_2}^0}\left(\mathrm{Le}_{H_2}X_{H_2}^0\right)^{3/2}}{\mathrm{Le}_H\mathrm{Le}_{H_2O}X_{H_2O}^0}\sqrt{\mu\sigma}, \qquad \sigma \to \infty. \tag{4.16}$$

At the opposite end of this region the radical is attacked and consumed by the fuel, yielding the additional boundary condition

$$X_H^0 \sim 0, \qquad \sigma \to -\infty. \tag{4.17}$$

The matching condition (4.16) suggests the magnitude of X_H^0 to be $O(\sqrt{\mu})$ in this region and it is convenient to introduce the new variable W as

$$X_H^0 = \sqrt{\mu}W\frac{\sqrt{K_{IV}\mathrm{Le}_{O_2}X_{O_2}^0}\left(\mathrm{Le}_{H_2}X_{H_2}^0\right)^{3/2}}{\mathrm{Le}_H\mathrm{Le}_{H_2O}X_{H_2O}^0}, \tag{4.18}$$

so that our system governing the radical consumption layer takes the simple form

$$\frac{d^2W}{d\sigma^2} = W[W^2 - \sigma], \tag{4.19}$$

$$W = 0 \quad \text{as } \sigma \to -\infty, \qquad W = \sqrt{\sigma} \text{ as } \sigma \to \infty. \tag{4.20}$$

Here μ is chosen as

$$\mu = \left\{\frac{A^3}{2\delta D}\frac{\sqrt{K_{IV}\mathrm{Le}_{O_2}X_{O_2}^0}\left(\mathrm{Le}_{H_2}X_{H_2}^0\right)^{3/2}}{\mathrm{Le}_H\mathrm{Le}_{H_2O}X_{H_2O}^0}\right\}^{1/3} \ll 1, \tag{4.21}$$

where we have made use of definition 4.10. The system 4.19–4.20 can be solved numerically [4] and the resulting profiles for W illustrate the smooth transition to zero of the H-atom concentration in the radical consumption zone.

We remark that the analysis of this region is based on the assumption that μ is a small parameter and it follows from Eq. 4.21 that

$$\frac{\sqrt{K_{IV}\mathrm{Le}_{O_2}X_{O_2}^0}\left(\mathrm{Le}_{H_2}X_{H_2}^0\right)^{3/2}}{\mathrm{Le}_H\mathrm{Le}_{H_2O}X_{H_2O}^0} \ll \delta. \tag{4.22}$$

By comparing this expression to Eq. 4.5 we conclude that the radical concentration must be smaller in magnitude than the width of the fuel consumption zone, which is in agreement with our earlier comments regarding the validity of the steady-state approximation.

As discussed in Ref. 4, the existence of this radical consumption layer indicates that it is the consumption of H atoms by the fuel that terminates the reaction in the upstream preheat zone. This differs from standard analyses with one-step kinetics where reaction is frozen in the preheat zone by a drop in temperature.

Based on the above boundary layer analysis we can neglect the perturbation y_H in Eq. 4.7. Furthermore, we can use Eq. 4.8 to replace y_{H_2} and thus reduce the structure of the fuel consumption layer to the two equations

$$\frac{d^2 y_F}{d\zeta^2} = D y_F \sqrt{1 - A y_F}\exp(\theta), \tag{4.23}$$

$$\frac{d^2}{d\zeta^2}\left[\theta + q_F y_F - 2\frac{(q_{H_2} + \alpha q_{CO})}{1+\alpha} y_F\right] = 0. \tag{4.24}$$

Upstream boundary conditions for this system are obtained by matching to the solutions in the preheat zone, where in particular we have obtained Eq. 4.13 for y_F, and the expansion of the outer solution 3.4 in terms of $x = \delta\zeta$ provides the necessary conditions for θ. The fuel is entirely consumed downstream, which implies that

$$y_F = 0 \text{ as } \zeta \to \infty, \tag{4.25}$$

and boundary conditions for θ are obtained by matching to the solution in the oxidation layer immediately adjacent to the fuel consumption zone. An analysis of this oxidation layer, which we now present, also provides us with the needed expression for $X^0_{H_2}$ appearing in D, as shown in Eq. 4.10.

5. THE H_2 AND CO OXIDATION LAYER

Immediately downstream of the fuel consumption region lies a somewhat broader layer where H_2 and CO oxidize to form H_2O and CO_2. The width of this layer is characterized by ϵ which will be chosen shortly such that $\delta \ll \epsilon \ll 1$. For this reason the present flame structure resembles that of the Zel'dovich–Liñán mechanism [10, 11], which consists of a very thin branching reaction zone, characterized by a large activation energy, embedded within a somewhat broader recombination zone with zero activation energy.

Our governing equations simplify in this region since $X_F = 0$ and $\omega_I = 0$. The molar concentrations for H and CO are obtained directly from Eqs. 2.13 and 2.3. In order to determine the remaining species concentrations we introduce the stretched coordinate, η, as

$$x = \epsilon\eta/2q, \tag{5.1}$$

and seek solutions of the form

$$\begin{aligned} \tau &= \tau_b - \epsilon t + \cdots, \\ q(1+\alpha)X_{H_2} &= \epsilon Z + \cdots, \\ X_{O_2} &= X_{O_2,b} + \epsilon Z_{O_2} + \cdots, \qquad (5.2) \\ X_{H_2O} &= X_{H_2O,b} - \epsilon Z_{H_2O} + \cdots, \\ X_{CO_2} &= X_{CO_2,b} - \epsilon Z_{CO_2} + \cdots. \qquad (5.3) \end{aligned}$$

At leading order, the equations governing this region can now be written in the form

$$\begin{aligned} &\frac{d^2 Z}{d\eta^2} = \frac{\epsilon}{2q}\omega_{III}, \qquad \frac{d^2}{d\eta^2}[Z - 2qZ_{O_2}] = 0, \\ &\frac{d^2}{d\eta^2}[Z - t] = 0, \\ &\frac{d^2}{d\eta^2}\left[Z - q(1+\alpha)Z_{H_2O}\right] = 0, \\ &\frac{d^2}{d\eta^2}\left[Z - q\frac{(1+\alpha)}{\alpha}Z_{CO_2}\right] = 0, \end{aligned} \tag{5.4}$$

where we have employed the notation

$$q = q_{H_2} = q_{CO} = (Q_{III} + Q_{IV})/2. \tag{5.5}$$

Peters and Williams [4] have computed the values of Q_k and found that Q_{II} is sufficiently small, thus enabling us to write the second equality in Eq. 5.5. By integrating these equa-

tions and matching to the outer inert solutions 3.1–3.4 at $\eta \to \infty$ we obtain the relations

$$t = Z - \frac{\delta}{\epsilon} a_2, \qquad Z_{O_2} = \frac{Z + a}{2q},$$

$$Z_{H_2O} = \frac{Z}{q(1+\alpha)}, \qquad Z_{CO_2} = \frac{\alpha Z}{q(1+\alpha)}, \tag{5.6}$$

where $a = 4q(1-\phi)/(\epsilon \mathrm{Le}_{O_2})$ for near-stoichiometric flames. These are all expressed in terms of the H_2 concentration, Z, which in turn is found by solving Eq. 5.4a. The nature of this structure equation changes depending on whether the mixture is near-stoichiometric or if there is an abundance of oxygen. The analysis of this region for stoichiometric flames has been performed by Peters and Williams [4], and a similar analysis for near-stoichiometric flames can be found in the analysis of Seshadri and Göttgens [6].

5.1. The Oxidation Layer for Near-Stoichiometric Mixtures

When $1 - \phi = O(\epsilon)$, the oxygen is nearly entirely consumed by the flame, so that the oxygen concentration is at most $O(\epsilon)$ in the oxidation layer. We use Eq. 2.1c to write the equation for Z in the form

$$\frac{d^2Z}{d\eta^2} = \frac{\epsilon}{2q} \frac{\mathrm{Le}_{O_2}\mathrm{Le}_H \lambda Y_{F,u} \rho_0^2}{\rho^2 v^2 c_p W_F} pk_{III} X_H X_{O_2}, \tag{5.7}$$

and the H-radical concentration obtained from Eq. 2.13 is given by

$$X_H = \frac{\sqrt{K_{IV}\mathrm{Le}_{O_2}}\mathrm{Le}_{H_2}^{3/2}}{\mathrm{Le}_H \mathrm{Le}_{H_2O} X_{H_2O} X_{H_2O,b}} X_{O_2}^{1/2} X_{H_2}^{3/2} = \frac{\sqrt{K_{IV}\mathrm{Le}_{O_2}}\mathrm{Le}_{H_2}^{3/2}}{\mathrm{Le}_H \mathrm{Le}_{H_2O} X_{H_2O,b}} \frac{\epsilon^2 Z^{3/2}(Z+a)^{1/2}}{\sqrt{2}q^2(1+\alpha)^{3/2}}. \tag{5.8}$$

This is now inserted into Eq. 5.7 to obtain the equation

$$\frac{d^2Z}{d\eta^2} = Z^{3/2}(Z+a)^{3/2}, \tag{5.9}$$

where ϵ has been chosen to be

$$\epsilon = \left\{ \frac{\lambda Y_{F,u} \rho_0^2 (\mathrm{Le}_{O_2}\mathrm{Le}_{H_2})^{3/2} \sqrt{K_{IV}}}{\rho^2 v^2 c_p W_F \mathrm{Le}_{H_2O} X_{H_2O,b}} \times \frac{pk_{III}}{4\sqrt{2}q^4(1+\alpha)^{3/2}} \right\}^{-1/4} \ll 1. \tag{5.10}$$

Alternatively, we can use Eq. 4.10 to express ϵ in terms of $O(1)$ quantities, which yields

$$\epsilon = \left\{ \frac{\mathrm{Le}_F A_{11}}{D\mathrm{Le}_{O_2}} \frac{4\sqrt{2}q^2}{pk_{III}} \right\}^{1/2}. \tag{5.11}$$

Since ϵ must be a small parameter, it follows that pk_{III} must be sufficiently large. We remark, however, that it must not be so large as to violate our previous assumption that $k_{III} \ll k_1 = O(\delta^{-1})$.

Boundary conditions for Eq. 5.9 are obtained by matching to solutions in the outer inert region at $\eta \to \infty$, and to the solutions in the fuel consumption layer at $\eta = 0$. This matching procedure yields

$$\frac{dZ}{d\eta} = -1 \quad \text{at } \eta = 0, \tag{5.12}$$

$$\frac{dZ}{d\eta} = Z = 0 \quad \text{as } \eta \to \infty, \tag{5.13}$$

where the first of these is obtained by a single integration of Eq. 4.8 across the entire fuel consumption region. For the stoichiometric flame, $a = 0$, the solution of Eq. 5.9 subject to these boundary conditions is readily found to be

$$Z = \frac{\sqrt{2}}{\eta + 2^{1/4}}, \tag{5.14}$$

from which the H_2 concentration in the fuel consumption zone is determined from $Z(0) = 2^{1/4}$. For nonzero values of a, a single integration of the above system determines $Z(0)$ as $Z(0) = a(s-1)/2$, where s is the root of the equation

$$s\sqrt{s^2-1} + \tfrac{3}{2}\ln\left[s + \sqrt{s^2-1}\right] = 32/a^4.$$

Solutions for the remaining quantities follow immediately from Eqs. 5.6, and their evalua-

tion at $\eta = 0$ provides the necessary matching conditions for variables in the fuel consumption layer.

The above analysis assumes partial equilibrium of the water–gas shift. However, as discussed in Ref. 4, assuming this reaction to be infinitely fast overestimates the amount of H_2 produced. A correction due to nonequilibrium effects can be obtained by considering an additional layer of $O(\nu)$, $\nu \ll \epsilon \ll 1$, on the downstream side of the fuel consumption zone where reaction II is not in equilibrium. Peters and Williams [4] have performed that analysis so the details will not be presented here. To examine this boundary layer one first perturbs the mass fractions of H_2 and CO, which are the relevant quantities in this zone, about their value at $\eta = 0$. The resulting equations for the perturbed quantities are linear and can easily be integrated subject to appropriate matching conditions [4]. This procedure is straightforward and, when the solution is combined with that of the partial equilibrium layer, the concentration of H_2 at the fuel consumption zone is found to be

$$X^0_{H_2}(0) = \frac{\epsilon Z(0)}{q(1+\alpha)} - \nu, \tag{5.15}$$

where

$$\nu = \frac{1-\alpha}{(1+\alpha)^{3/2}\sqrt{D_{II}}} = \frac{1-\alpha}{(1+\alpha)^2}\left(\frac{\epsilon}{q}\right)^{3/2} \times \left\{\frac{\mathrm{Le}_{O_2}\mathrm{Le}_{H_2} p k_{III} K_3}{8\mathrm{Le}_{CO} k_{10}\sqrt{Z(0)[Z(0)+a]}}\right\}^{1/2}.$$

The expression 5.15 provides the matching condition for the variables in the fuel consumption layer and will be applied in Section 6, but we first reexamine the oxidation layer for the case when the mixture contains an abundance of oxygen.

5.2. The Oxidation Layer for Fuel-Lean Mixtures

When $\phi < 1$ there is a surplus of oxygen in the mixture so that a portion of it passes through the flame unreacted. The resulting flame structure has not been considered in previous asymptotic studies that have employed rate-ratio techniques. In this case, the structure equation 5.9 is modified since, to a first approximation, the molar concentration X_{O_2} takes on the value $X_{O_2,b} = O(1)$, shown in Eq. 3.2.

All the relations in Eqs. 5.6 remain unchanged, but now the leading order expression for the radical concentration is given by

$$X_H = \frac{\sqrt{K_{IV}\mathrm{Le}_{O_2}}\,\mathrm{Le}_{H_2}^{3/2}}{\mathrm{Le}_H \mathrm{Le}_{H_2O} X_{H_2O,b}} (X_{O_2,b})^{1/2} \times \left(\frac{\epsilon Z}{q(1+\alpha)}\right)^{3/2}, \tag{5.16}$$

and when this is inserted into Eq. 5.7 we obtain

$$\frac{d^2Z}{d\eta^2} = \frac{\epsilon}{2q}\frac{\mathrm{Le}_{O_2}^{3/2}\lambda Y_{F,u}\rho_0^2}{\rho^2 v^2 c_p W_F}\frac{\sqrt{K_{IV}}\,\mathrm{Le}_{H_2}^{3/2}}{\mathrm{Le}_{H_2O} X_{H_2O,b}} \times p k_{III}(X_{O_2,b})^{3/2}\left(\frac{\epsilon Z}{q(1+\alpha)}\right)^{3/2} \tag{5.17}$$

The boundary conditions 5.12–5.13 are unchanged so that our system takes the simple form

$$\frac{d^2Z}{d\eta^2} = Z^{3/2}, \tag{5.18}$$

$$\frac{dZ}{d\eta} = -1 \quad \text{at } \eta = 0, \tag{5.19}$$

$$\frac{dZ}{d\eta} = Z = 0 \quad \text{as } \eta \to \infty, \tag{5.20}$$

where ϵ is now given by

$$\epsilon = \left\{\frac{\lambda Y_{F,u}\rho_0^2(\mathrm{Le}_{O_2}\mathrm{Le}_{H_2})^{3/2}\sqrt{K_{IV}}}{\rho^2 v^2 c_p W_F \mathrm{Le}_{H_2O} X_{H_2O,b}} \times \frac{p k_{III}}{2q^{5/2}(1+\alpha)^{3/2}}(X_{O_2,b})^{3/2}\right\}^{-2/5} \ll 1, \tag{5.21}$$

or alternatively

$$\epsilon = \frac{\mathrm{Le}_F A_{11}(5/4)^{3/5}}{D\mathrm{Le}_{O_2} X_{O_2,b}} \frac{2q}{pk_{III}}. \tag{5.22}$$

As in the case of the stoichiometric mixture, the requirement that ϵ be small implies that the three-body reaction rate pk_{III} is large, since all other quantities in Eq. 5.22 are known to be $O(1)$.

The system 5.18–5.20 possesses the solution

$$Z = \left[\frac{\eta}{2\sqrt{5}} + \left(\frac{2}{\sqrt{5}}\right)^{1/5}\right]^{-4}, \tag{5.23}$$

from which we obtain the needed information at $\eta = 0$, $Z(0) = (\sqrt{5}/2)^{4/5}$.

As in the preceding subsection, we can consider nonequilibrium effects of reaction II as a perturbation to the above leading order result. Again Eq. 5.15 is obtained for the H_2 concentration at the fuel consumption zone where now

$$\nu = \frac{1-\alpha}{(1+\alpha)^{3/2}\sqrt{D_{II}}} = \frac{1-\alpha}{(1+\alpha)^{3/2}} \frac{\epsilon}{q} \times \left\{\frac{\mathrm{Le}_{O_2}\mathrm{Le}_{H_2} pk_{III} K_3 X_{O_2}^0}{4(1+\alpha)\mathrm{Le}_{CO} k_{10}\sqrt{Z(0)}}\right\}^{1/2}.$$

We now have the necessary matching conditions to complete the analysis of the fuel consumption region that was begun in Section 4.

6. THE FINAL STRUCTURE EQUATION

In Sections 3 and 5 we obtained solutions for each species as well as the temperature distribution in both the inert regions and the H_2–CO oxidation layer. These solutions provide the matching conditions needed to solve the structure equations 4.23 and 4.24. For our purpose, we only need to consider the expressions for τ, X_F and X_{H_2}. Upstream of the fuel consumption layer, solutions for these quantities are given entirely by Eqs. 3.1–3.4. Downstream of the fuel consumption layer, the solutions in the inert region and the oxidation layer can be combined to construct composite solutions that are valid in the entire flow field. We now discuss these composite solutions, as well as the resulting matching conditions, for both stoichiometric and fuel-lean mixtures.

6.1. Structure Equation for Near-Stoichiometric Mixtures

For near-stoichiometric mixtures, the solutions downstream of the fuel consumption layer are given by Eqs. 3.1–3.4, 5.6, and 5.14. Appropriate composite solutions for τ^+, X_F^+ and $X_{H_2}^+$ are given by

$$X_F^+ \equiv 0, \tag{6.1}$$

$$\tau^+ \sim \tau_b + \delta a_2 - \epsilon Z + \cdots, \tag{6.2}$$

$$X_{H_2}^+ \sim \epsilon \frac{Z}{q(1+\alpha)} + \cdots. \tag{6.3}$$

To leading order in δ we impose continuity at $x = 0$, and the nondimensionalization further requires that $\tau(0^+) = \tau(0^-) = 1$, which yields

$$a_1 = 1, \qquad b_2 = \epsilon \frac{Z(0)}{q(1+\alpha)},$$

$$\tau_b = 1 + \epsilon Z(0) + o(\epsilon). \tag{6.4}$$

The last of these relations, together with Eq. 2.10, provides the two equations necessary to determine the dimensional temperatures $\hat{T}_b$ and $\hat{T}^0$.

The matching conditions needed for Eqs. 4.23–4.24 are now obtained by expanding the outer solutions in terms of the inner variable $x = \delta\zeta$. At this stage of the analysis, we have not explicitly related the two independent small parameters, ϵ and δ, although we have chosen them such that $\delta \ll \epsilon$. The matching procedure requires that we retain solutions up to $O(\delta^2)$, and thus we will now assume that the solutions 5.6 are valid to all orders in ϵ. We neglect all terms of $o(\delta^2)$ so that the matching

conditions are

$$X_F^- \sim -\delta\zeta - \delta^2\zeta^2 \mathrm{Le}_F/2 + \cdots, \tag{6.5}$$

$$X_{H_2}^- \sim \epsilon\frac{Z(0)}{q(1+\alpha)}\left(1 + \delta\zeta\,\mathrm{Le}_{H_2} + \delta^2\zeta^2\mathrm{Le}_{H_2}^2/2 + \cdots\right), \tag{6.6}$$

$$\tau^- \sim 1 + \delta(\zeta + a_3) + \delta^2\left[\frac{\zeta^2}{2} + a_3\zeta\right] + \cdots, \tag{6.7}$$

$$X_F^+ \sim 0 \tag{6.8}$$

$$X_{H_2}^+ \sim \frac{1}{q(1+\alpha)}\left(\epsilon Z(0) - 2\delta\zeta q + \delta^2\zeta^2 q^2 2Z_{\eta\eta}(0)/\epsilon + \cdots\right), \tag{6.9}$$

$$\tau^+ \sim 1 + \delta[a_2 + 2q\zeta] - 2\delta^2\zeta^2 q^2 Z_{\eta\eta}(0)/\epsilon] + \cdots. \tag{6.10}$$

Integration of Eqs. 4.23 and 4.24 subject to the above matching conditions now yields the leading order result

$$\theta = -y_F(q_F - 2q) + 2q\zeta, \tag{6.11}$$

where $a_2 = a_3 = 0$. We insert Eq. 6.11 into Eq. 4.23 to obtain the following boundary value problem for the fuel concentration in the fuel consumption layer

$$\frac{d^2y_F}{d\zeta^2} = Dy_F\sqrt{1 - Ay_F} \times \exp[-y_F(q_F - 2q) + 2q\zeta], \tag{6.12}$$

$$y_F = -\zeta \quad \text{at } \zeta = -1/A,$$

$$y_F = 0 \quad \text{as } \zeta \to \infty. \tag{6.13}$$

The burning rate ρv appears as an eigenvalue of this system. In particular, for stoichiometric mixtures we note from Eq. 5.10 the relation $\epsilon \sim \sqrt{\rho v}$, and it follows from Eqs. 4.9 and 5.11 that the rate-ratio parameters A and D depend on the burning rate as

$$A \sim 1/\sqrt{\rho v}, \qquad D \sim 1/\rho v.$$

In general, Eqs. 6.12 and 6.13 (which includes the evaluation of the burning rate in terms of all remaining parameters) must be solved numerically. However, we will first discuss several limiting cases for which explicit expressions for the burning rate can be obtained. Computed values of the burning rate as a function of various parameters will be given in Section 7.

We first consider the limit $A \ll 1$. This can be achieved for example when the chain-branching reaction becomes comparable to the chain-propagating step such that $A_1 \gg A_{11}$. We should mention that such small values of A are unlikely for the methane–air flames of interest here, and the steady-state assumption for the H radical becomes questionable. However, it is possible to achieve smaller values of A by using a different inert or by considering a different hydrocarbon, for which the basic flame structure remains the same (cf. the analysis of propane–air flames in Ref. 12). In any case, it is instructive to examine this limit in order to determine the explicit dependence of the burning rate on various parameters. In this limit, the radical consumption layer moves far upstream into the preheat zone; the radical concentration assumes the value unity (i.e., $\sqrt{1 - Ay_F} \sim 1$); and the fuel consumption layer is limited by a single reactant namely the fuel. In fact, we can make the coordinate transformations

$$y_F = Y/(q_F - 2q),$$

$$\zeta = \frac{\xi}{q_F - 2q} + \frac{1}{2q}\ln\left[\frac{(q_F - 2q)^2}{2D}\right], \tag{6.14}$$

and introduce the parameter $m = 2q/(2q - q_F)$ to write our system in the form

$$2\frac{d^2Y}{d\xi^2} = Y\exp[-Y - m\xi], \tag{6.15}$$

$$Y = -\xi + \frac{1}{m}\ln\left[\frac{2q^2}{m^2D}\right] \text{ as } \xi \to -\infty,$$

$$Y = 0 \quad \text{as } \xi \to \infty, \tag{6.16}$$

which is identical to the structure problem obtained by Liñán [9] in the premixed burning regime of his diffusion flame analysis. The latter boundary condition implies there can be no leakage of fuel through the flame. Liñán has demonstrated that solutions to the above

system only exist when $-\infty < m < 0$. In methane–air flames, the value of m can be taken as $m \sim -2$ [4], and thus we are in the range of physically meaningful solutions. Liñán [9] has also provided a correlation function for the limiting value $\lim_{\xi \to -\infty}(Y + \xi)$ which we use to obtain the following expression for D

$$D = \frac{2q^2}{m^2}[0.6307m^2 - 1.344m + 1]. \quad (6.17)$$

Now the definition of D, Eq. 4.10, can be used in this equation to obtain an expression for the burning rate, ρv, for small values of A. We note that since $m < 0$, the solutions of the above system do not exhibit turning point behavior, and thus no extinction is predicted.

In the opposite limit that $A \to \infty$, radical production is extremely weak, and thus we expect the flame to slow down and possibly "extinguish." To analyze this limit it is convenient to remove the parameters from the boundary conditions by introducing the scaled variables

$$\zeta = \hat{\zeta}/A, \qquad y_F = \hat{y}/A. \quad (6.18)$$

Our system can then be written

$$\frac{d^2\hat{y}}{d\hat{\zeta}^2} = \hat{D}\hat{y}\sqrt{1-\hat{y}}\exp\left[-\gamma(\hat{y} + m\hat{\zeta})\right], \quad (6.19)$$

$$\hat{y} = -\hat{\zeta} \quad \text{at } \hat{\zeta} = -1, \qquad \hat{y} = 0 \quad \text{as } \hat{\zeta} \to \infty, \quad (6.20)$$

where we have defined the parameters

$$\gamma \equiv \frac{q_F - 2q}{A}, \qquad m \equiv \frac{2q}{2q - q_F},$$

$$\hat{D} \equiv D/A^2. \quad (6.21)$$

We can now exploit the limit of small γ. When γ is set to zero in the above system we recover the structure problem of Peters and Williams [4]. The resulting equation can be integrated once subject to the boundary conditions to yield $\hat{D} = 15/8$. A correction for small values of γ is readily found to be

$$\hat{D} \sim 15/8 + \gamma\hat{D}_1, \quad (6.22)$$

where

$$\hat{D}_1 = \tfrac{15}{8}\{4/7 - m + 2mI\},$$

$$I \equiv \int_0^1 w(1-w)\left\{1 + 2w + 3w^2 + \tfrac{3}{2}w^3\right\}^{1/2} dw$$

$$= 0.291\ldots.$$

From the definitions of D and A, we find that the rate-ratio parameter $\hat{D}$ has the explicit form

$$\hat{D} = \frac{A_1^2 \mathrm{Le}_{O_2}}{A_{11}\mathrm{Le}_F}\frac{Z(0)^{3/2}(Z(0)+a)^{5/2}}{pk_{III}} \times\left[1 - \frac{\nu q(1+\alpha)}{\epsilon Z(0)}\right]^{3/2}. \quad (6.23)$$

If we consider stoichiometric flames ($a = 0$) and invoke the partial equilibrium assumption ($\nu = 0$), then the leading order result $\hat{D} = 15/8$ does not provide an expression for the burning rate. Therefore Peters and Williams [4] used this leading order result to determine $\hat{T}^0$, and then equated the first two terms in the expansion for τ_b, shown in Eq. 6.4, to evaluate the burning velocity. In our model, this value of $\hat{D}$ is approached in the limit that $\gamma \to 0$. Since γ is proportional to the square root of the burning rate (see Eq. 6.21), $\hat{D} = 15/8$ represents the critical point at which ρv decreases to zero. In this limit $\epsilon \to 0$, the oxidation layer collapses down to the fuel consumption layer, and the burned temperature, τ_b, decreases to unity.

In Fig. 2 we have plotted γ, which represents the burning rate for the stoichiometric

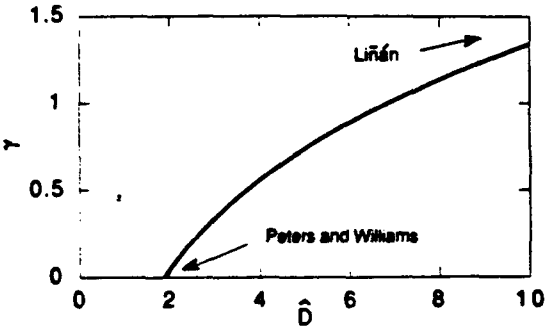

Fig. 2. Plot of γ, representing the burning rate for stoichiometric flames, versus the rate-ratio, $\hat{D}$. Curve is generated by solving equations 6.19 and 6.20.

flame, as a function of $\hat{D}$ for the fixed value $m = -2$. It is clear from Eq. 6.23 that the parameter $\hat{D}$ represents the ratio of the chain-branching reaction, k_1, to the chain-propagating and chain-breaking reactions, k_{11} and k_{111}. As previously discussed, when $\hat{D}$ is sufficiently large the flame has a structure similar to the premixed flame regime of Liñán's [9] diffusion flame. The limiting value of the burning rate is obtained from Eq. (6.17), which can be expressed in terms of the parameters γ and $\hat{D}$ as

$$\gamma^2 = 2\hat{D}[0.6307m^2 - 1.344m + 1]^{-1} = \frac{2\hat{D}}{M}.$$

For the stoichiometric flame with $\nu = 0$ we can also make use of Eqs. 4.9, 4.10, and 6.21 to obtain the following explicit expression for ρv in terms of original system parameters

$$\rho v = \frac{2^{1/4} A_{11} \mathrm{Le}_F m^2}{q^2[0.6307m^2 - 1.344m + 1]} \times \left\{ \frac{\lambda Y_{F,u} \rho_0^2 \sqrt{K_{IV}} \times (\mathrm{Le}_{H_2}\mathrm{Le}_{O_2})^{3/2}}{pk_{III} c_p W_F \mathrm{Le}_{H_2O} \times X_{H_2O,b}(1+\alpha)^{3/2}} \right\}^{1/2}. \tag{6.24}$$

This represents the maximum value of the burning rate that is achieved when the rate of radical production is large. It is interesting to note that k_{11} and k_{111} have opposite effects on the burning rate. Since Eq. 6.24 is obtained in the limit $A_1 \to \infty$, there are many radicals present in the flame structure. The present theory predicts that the flame will propagate more rapidly when the fuel consumes these radicals at a faster rate than they recombine.

When $\hat{D}$ is decreased, for example by increasing the pressure, the flame speed also decreases monotonically, as shown in Fig. 2. Eventually, the chain-breaking reaction becomes dominant, the burning rate decreases to zero, and the flame ceases to propagate. Since $m \sim -2$ for the methane–air flames considered here, the correction term in Eq. 6.22 is always positive, indicating that the response curve is monotonic and no turning point behavior is predicted. This is in agreement with previous numerical results [13] which have shown that, in the absence of heat loss, the flame speed will decrease to zero monotonically and a distinct extinction state does not exist.

For the two limiting cases discussed above we are able to determine the explicit dependence of the stoichiometric burning rate on pressure. In particular, when $\hat{D} \to \infty$ we note from Eq. 6.24 that ρv varies with the square root of pressure. Thus while the burning rate increases with pressure, the burning velocity is seen to decrease. For the other limiting case, Eq. 6.22 for which the velocity approaches zero, ρv has the explicit form (with $\nu = 0$)

$$\rho v = \frac{2^{1/4} A_{11}^2 \mathrm{Le}_F^2}{A_1^2 \mathrm{Le}_{O_2}^2 \hat{D}_1^2} \times \left\{ \frac{\lambda Y_{F,u} \rho_0^2 pk_{III} \sqrt{K_{IV}} (\mathrm{Le}_{H_2}\mathrm{Le}_{O_2})^{3/2}}{c_p W_F \mathrm{Le}_{H_2O} X_{H_2O,b}(1+\alpha)^{3/2}} \right\}^{1/2} \times \left[\frac{2A_1^2 \mathrm{Le}_{O_2}}{A_{11} \mathrm{Le}_F pk_{III}} - \frac{15}{8} \right]^2. \tag{6.25}$$

In this case, both burning rate and velocity decrease as pressure is increased. We also observe from the above expression that an increase in A_{11} results in a decrease in ρv. This is in contrast to the strongly burning limit, Eq. 6.24, for which the chain-propagating reaction was found to further enhance burning.

6.2. Structure Equation for Fuel-Lean Mixtures

The analysis for the fuel-lean mixture is nearly identical to the stoichiometric case discussed above, so we omit most of the details. The form of the structure equations remains the same as in Eqs. 6.12–6.13 and 6.19–6.20. However, to leading order we now have $(X_{O_2})^0 = X_{O_2,b} = 2\mathrm{Le}_{O_2}^{-1}(\phi^{-1} - 1)$. Thus the parameters A and γ, given by Eqs. 4.9 and 6.21, respectively, are independent of the burning rate. An expression for D is obtained by inserting Eq. 5.21 into Eq. 5.22 which yields the dependence $D \sim (\rho v)^{-4/5}$. It follows from Eq. 6.21 that the rate-ratio parameter $\hat{D}$ also exhibits this dependence on burning rate.

In the limit $A \to 0$ we again obtain Eq. 6.17 as the expression that determines the burning

rate. When $\nu = 0$ we can use Eqs. 5.21 and 5.22 to write the following explicit expression for ρv in terms of all other system parameters

$$\rho v = \frac{(5/4)^{3/4}(A_{11}\mathrm{Le}_F m^2)^{5/4}}{(\mathrm{Le}_{O_2} X_{O_2,b})^{1/2}(pk_{III})^{3/4} q^{5/2} M^{5/4}} \times \left\{ \frac{\lambda Y_{F,u} \rho_0^2 \sqrt{K_{IV}} (\mathrm{Le}_{H_2})^{3/2}}{2c_p W_F \mathrm{Le}_{H_2O} X_{H_2O,b} (1+\alpha)^{3/2}} \right\}^{1/2}. \tag{6.26}$$

The burning rate is seen to increase with pressure as $\rho v \sim p^{1/4}$ and thus burning velocity decreases with pressure. We also note the direct dependence on equivalence ratio $\rho v \sim (\phi^{-1} - 1)^{-1/2}$. In addition, ρv is proportional to $A_{11}^{5/4}$ with $A_{11} \sim \exp(-E_{11}/R^0 \hat{T}^0)$, where $\hat{T}^0$ decreases with equivalence ratio. Thus the burning rate decreases as we move further away from stoichiometry (for $1 - \phi = O(\epsilon)$ the analysis of the preceding subsection is appropriate). Reactions k_{11} and k_{III} are seen to have opposite effects on the burning rate, in agreement with the stoichiometric situation for this limit. Again we find that the flame propagates faster when the rate of fuel consumption exceeds the rate of radical recombination.

In the limit that radical production is very slow, that is, $A_1 \to 0$, we again obtain Eq. 6.22. For the present case, however, $\hat{D}$ depends explicitly on ρv so that the leading order value $\hat{D} = 15/8$ does provide an expression for the burning rate. In particular, this equation can be written in the form

$$\rho v = \frac{8(\mathrm{Le}_{O_2} X_{O_2,b})^2 A_1^{1/2}}{(3A_{11}\mathrm{Le}_F)^{5/4}(pk_{III})^{3/4}} \times \left\{ \frac{\lambda Y_{F,u} \rho_0^2 \sqrt{K_{IV}} (\mathrm{Le}_{H_2})^{3/2}}{5c_p W_F \mathrm{Le}_{H_2O} X_{H_2O,b} (1+\alpha)^{3/2}} \right\}^{1/2}, \tag{6.27}$$

so that $\rho v \sim A_1^{5/2}$ when $A_1 \to 0$. Again we find the dependence on pressure to be $\rho v \sim p^{1/4}$. As before, although $\rho v \sim (X_{O_2,b})^2 \sim (\phi^{-1} - 1)^2$, the Arrhenius dependence of ρv on $\hat{T}^0$ will cause the burning rate to decrease as the mixture is made more lean, so long as ϕ is bounded away from unity. From definition 5.21 ϵ is found to decrease as the lean limit is approached, resulting in a lower reaction zone temperature (as determined by solving Eqs. 2.10 and 6.4 simultaneously) and consequently a lower burning rate. We remark that the burning rate is small in this limit, and the flame will probably have been extinguished by the presence of unavoidable heat loss before the limiting value 6.27 can be reached. This point is currently being investigated.

When $\nu = 0$ the only place the burning rate appears in the structure equation is in the form $D^{-5/4}$, or $(\hat{D}/\gamma^2)^{-5/4}$, which is plotted as a function of γ in Fig. 3. This curve can be interpreted as showing the velocity of fuel-lean flames as a function of the ratio of branching to propagating reactions. The response is seen to be monotonic, and the burning rate approaches the limiting values Eqs. 6.26 and 6.27 as $\gamma \to \infty$ and 0, respectively.

7. RESULTS AND DISCUSSION

Equations 6.19 and 6.20 were solved numerically to compute the burning velocity as a function of pressure and equivalence ratio for both stoichiometric and lean mixtures. Appropriate values for all parameters were the same as those used by Peters and Williams [4], and Seshadri and Peters [5]. In particular, the value of λ/c_p was taken to be $\lambda/c_p = 2.58 \times 10^{-4}(\hat{T}/\hat{T}_u)^{0.7}$ g/cm s, and the Lewis numbers

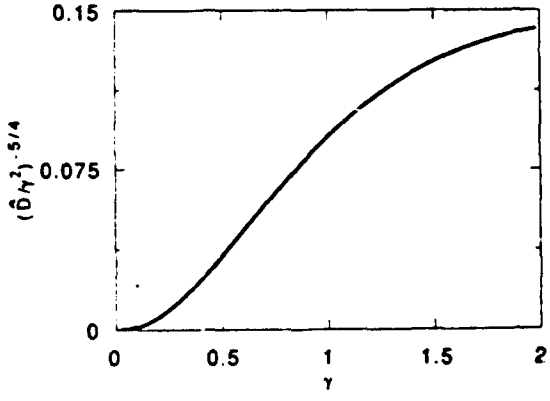

Fig. 3. Plot of $(\hat{D}/\gamma^2)^{-5/4}$, representing burning rate for fuel-lean flames, versus the parameter γ. Curve is generated by solving equations 6.19 and 6.20.

were assigned the values $Le_F = 0.97$, $Le_{O_2} = 1.1$, $Le_{H_2O} = 0.83$, $Le_{CO_2} = 1.39$, $Le_{H_2} = 0.3$, $Le_H = 0.18$, and $Le_{CO} = 1.11$. The average molecular weight was assumed constant equal to 27.62 kg/kmol, and the ambient temperature was taken to be $\hat{T}_u = 300$ K. The kinetic data, given in [4] and [5], is $\bar{A}_1 = 2.0 \times 10^{14}$ cm^3/mol · s, $\bar{A}_{11} = 2.2 \times 10^4$ cm^3/mol · s, $E_1 = 16800$ cal/mol, $E_{11} = 8750$ cal/mol. The reaction rate k_{11} has the form $k_{11} = \bar{A}_{11}\hat{T}^3 \exp(-E_{11}/R^0\hat{T})$ where $R^0 = 1.987$ cal/mol K ($R = 82.05$ atm cm^3/mol K) is the gas constant. Since k_1/k_{11} has a weak temperature dependence, we have approximated this reaction rate by $k_{11} = \bar{A}_{11,\text{eff}} \exp(-E_1/R^0\hat{T})$. Consistent with this approximation, we have defined an effective pre-exponential term $\bar{A}_{11,\text{eff}} = \bar{A}_{11}\hat{T}_{\text{ref}}^3 \exp[(E_1 - E_{11})/R^0\hat{T}_{\text{ref}}]$, where we have chosen $\hat{T}_{\text{ref}} = 1600$ K. The remaining reaction rates and equilibrium constants are given by $\sqrt{K_{IV}} = 1.22 \exp(3067/\hat{T})$, $\alpha = 3.86 \exp(-3652/\hat{T})$, $K_3 = 0.216 \exp(7658/\hat{T})$, $k_{10} = 1.51 \times \hat{T}^{1.3} \exp(758/R^0\hat{T})$.

The procedure we used to determine the burning velocity and the temperature $\hat{T}^0$ is as follows. For a given equivalence ratio, the unburned fuel mass fraction is given by $Y_{F,u} = (17.16 + \phi)$, and a thermochemical calculation yields the value of $\hat{T}_b$. Equations 6.19, 6.20, and 6.4, which can be expressed in terms of original variables as

$$\hat{T}_b - \hat{T}^0 = \epsilon Z(0)\left(\hat{T}^0 - \hat{T}_u\right), \tag{7.1}$$

are solved simultaneously to determine $\hat{T}^0$ and v as a function of p. It actually proved easier to solve for v and p in terms of $\hat{T}^0$, which was first assigned a value close to $\hat{T}_b$ and then gradually decreased. For a fixed value of $\hat{T}^0$, a value of ϵ is immediately obtained from Eq. 7.1. The solution of Eqs. 6.19 and 6.20 is used to determine the pressure p, and the velocity is then found using the appropriate definition of ϵ given in Section 5.

In Fig. 4 we have plotted v and $\hat{T}^0$ as a function of pressure for stoichiometric mixtures assuming partial equilibrium of the water–gas shift ($\nu = 0$). At $p = 1$ atm, our analysis yields a value for the burning velocity of $v = 36$ cm/s, in reasonable agreement with experimentally measured values [14, 15]. The

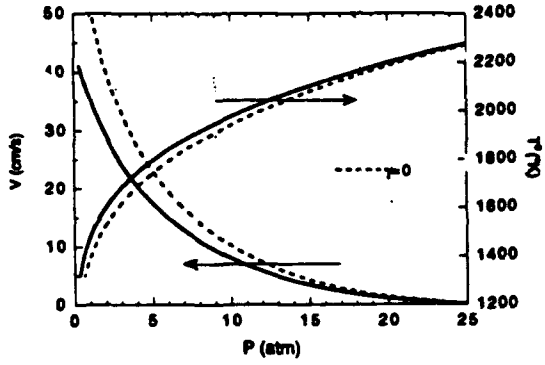

Fig. 4. Velocity and fuel consumption-zone temperature $\hat{T}^0$ as a function of pressure for stoichiometric flame with partial equilibrium of water–gas shift. Dashed line indicates results obtained using rate-ratio asymptotics.

velocity is seen to decrease as pressure is increased, again in agreement with observations. However, the predicted drop is much more rapid than experiments indicate, and the velocity approaches zero when the pressure approaches a critical value $p_c \sim 26$ atm. As pointed out in Ref. 4, this poor agreement at elevated pressures is due to deficiencies in the kinetic scheme. Better agreement can in fact be obtained by including more reactions from the starting mechanisms [4].

The dashed lines in Fig. 4 are the results obtained by setting $\gamma = 0$ in Eq. 6.19. Recall that in this limit the structure problem 6.19 and 6.20 reduces to the form found using rate-ratio techniques, and we will refer to this as the *rate-ratio limit*. The rate-ratio approach is seen to predict somewhat higher velocities than our theory, most notably at lower pressures. At $p = 1$ atm the rate-ratio analysis predicts a value for the burning velocity of $v = 51$ cm/s. The slight difference in this number and the value quoted in Refs. 4 and 6 is due to the way in which they chose to represent the reaction rate terms. As pressure is increased the difference in the two theories is seen to diminish, and the curves converge as $p \to p_c$, $v \to 0$. As discussed earlier, agreement between the two theories in this limit is not surprising since the value $\gamma = 0$ corresponds to $v \to 0$ in our theory.

Figure 5 shows the correction to the burning rates for stoichiometric mixtures when nonequilibrium effects are included. For both

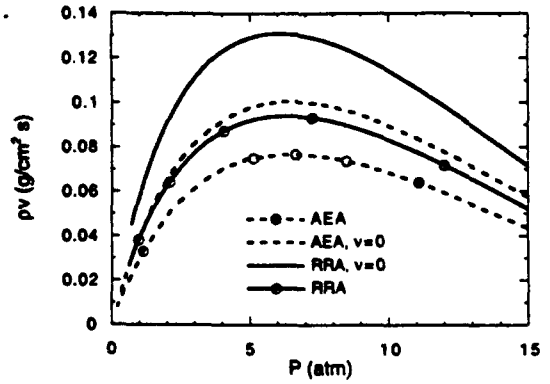

Fig. 5. Burning rate as a function of pressure for stoichiometric flame illustrating modification due to nonequilibrium of the water-gas shift. Solid line indicates results obtained using rate-ratio asymptotics.

theories, nonequilibrium effects are seen to cause a reduction in the burning rate. Again the difference in the curves is seen to be greatest at lower pressures. Partial equilibrium of reaction II becomes a better assumption as pressure is increased, and the curves converge as $p \to p_c$.

Overall, the agreement between the rate-ratio approach and the present theory is seen to be quite favorable for premixed methane-air flames. In both cases comparison with experimental observations is satisfactory, especially at lower pressures. The reason for the good agreement between the two theories is that the parameter γ appearing in our structure equation 6.19 is typically quite small. For the wide range of parameters considered in our computations, rarely did γ approach unity. However, the present analysis can be extended to other hydrocarbon-air mixtures with the same basic structure for which larger values of γ are possible. From the definitions of γ and A, Eqs. 6.21 and 4.9, respectively, any mixture change that results in a slower propagation reaction rate or an increased O_2 concentration will also yield larger values of γ. In those cases, the structure equations 6.19-6.20 may yield more accurate results than when rate-ratio techniques are used in the fuel consumption zone. An additional advantage of the present approach is the fact that we have retained the exponential nonlinearity of the reaction rate term in the fuel consumption layer. This should enable us to study the response of these flames to small perturbations such as heat loss and stretch. These points are currently being investigated.

The velocity and the burning rate as computed from the present theory with $\phi = 1$ are plotted in Fig. 6, where results from both partial equilibrium and nonequilibrium calculations are shown. Although the velocity decreases with an increase in pressure, the burning rate is seen to first increase before reaching a maximum value and then dropping off. This trend has been observed both numerically and experimentally for dilute mixtures [16], although preliminary data for nondilute mixtures does not conclusively show this trend. Measurements need to be made over a wider range of pressures to determine whether the trend predicted by the present theory can be realized for non-dilute mixtures.

In Fig. 7 we compare experimentally measured velocities and burning rates to values predicted by the present asymptotic theory and by numerical calculations with the detailed C_2-chain mechanism discussed in Ref. 17. The experimental measurements were made in our laboratory using the counterflow twin-flame technique. The numerics are seen to agree quite well with the experimental results for the entire range of pressures up to 8 atm. The asymptotic results show good agreement up to about 4 atm, after which velocity and burning rate drop off too quickly. As mentioned earlier, better agreement can be obtained by including more elementary reactions from the starting mechanism.

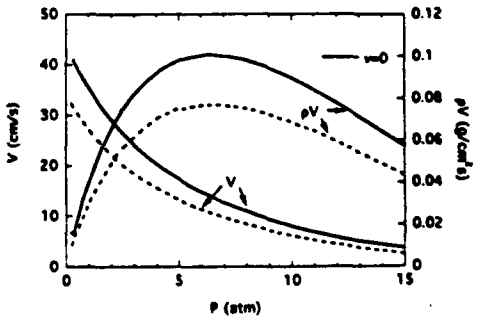

Fig. 6. Velocity and burning rate shown as a function of pressure for stoichiometric flame. Solid line denotes values obtained when partial equilibrium of the water-gas shift is assumed.

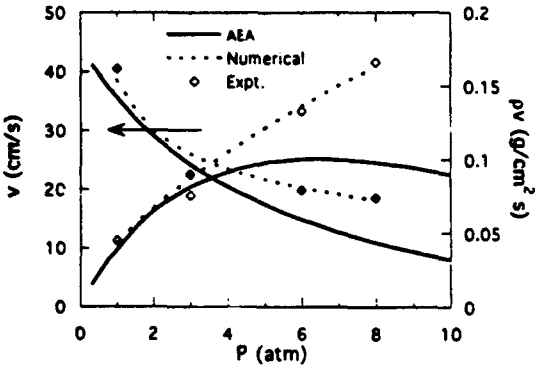

Fig. 7. Comparison of experimentally measured velocity and burning rate with values obtained numerically and with present asymptotic theory. Solid diamonds denote velocity.

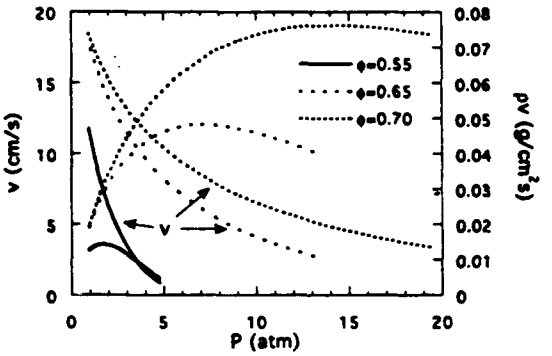

Fig. 8. Velocity and burning rate of lean flame as a function of pressure for three different values of equivalence ratio.

The temperature at the leading edge of the flame $\hat{T}^0$ and the burning velocity of near-stoichiometric flames were also computed for several values of equivalence ratio. As the mixture was made more lean, the characteristic temperature of the fuel consumption zone $\hat{T}^0$ was found to decrease, as expected. However, computed burning rate and velocity profiles first show a slight increase until $\phi \sim 0.85$, after which ρv decreases with further decreases in equivalence ratio. If we examine the explicit expression for ρv, found by using Eqs. 5.10 and 7.1,

$$(\rho v)^2 = \left[\frac{3(\hat{T}_b - \hat{T}^0)}{Z(0)(\hat{T}_b - \hat{T}_u)}\right]^4 \times \left\{\frac{\lambda Y_{F,u} p^2 \overline{W} (\mathrm{Le}_{O_2}\mathrm{Le}_{H_2})^{3/2}\sqrt{K_{IV}}}{R(\hat{T}^0)^2 c_p W_F \mathrm{Le}_{H_2O} X_{H_2O,b}} \times \frac{pk_{III}}{4\sqrt{2}(1+\alpha)^{3/2}}\right\}, \quad (7.2)$$

we see that although the difference between $\hat{T}_b$ and $\hat{T}_0$ decreases with decreasing $\hat{T}^0$, the other quantities in Eq. 7.2 increase. These factors lead to the increase in velocity as ϕ is decreased in the range (1.0, 0.85). We remark that the same incorrect trend is obtained if γ is set to zero in our structure equation 6.19, and therefore this erroneous prediction is not due to the activation-energy asymptotic techniques that we employed in the fuel consumption zone. Rather, the discrepancy is most likely due to deficiencies in the simplified kinetic scheme. The increase is very slight (roughly 10%), suggesting that higher-order terms that we neglected can reverse this trend. Indeed, Seshadri and Göttgens [6] and Bui-Pham et al. [7] have included many more intermediate reactions in their rate-ratio asymptotic analyses of lean methane–air flames, and they report good agreement with experiments, cf. Fig. 13 of Ref. 6. The inclusion of these additional reactions in our analysis will also yield the appropriate trend, although the additional parameters that enter into the analysis greatly complicate the details. It is clear that, if one desires to compute accurate values for burning velocities over a wide range of parameters, many intermediates need to be retained in the analysis.

As the mixture is made more lean such that $1 - \phi = O(1)$, an abundance of oxygen passes through the flame unreacted and the structure equation discussed in Section 6.2 becomes appropriate. As mentioned earlier, the system of equations 6.19 and 6.20 remain the same but the definitions of $\hat{D}$ and γ change. In Fig. 7 we show the velocity of these lean flames as a function of pressure as computed for several values of equivalence ratio. Now the flame is seen to burn weakest as the lean limit is approached and, near this limit, the velocity increases with ϕ. As ϕ is increased further such that $1 - \phi = O(\epsilon)$, the analysis of Section 5.2 is no longer valid, the structure of the oxidation layer changes, and the analysis of Section 5.1 is appropriate.

8. SUMMARY AND CONCLUSIONS

The structure of premixed methane–air flames with a detailed four-step kinetic mechanism has been studied theoretically. The basic flame structure, first identified by Peters and Williams [4], remains the same as in previous rate-ratio asymptotic analyses. However, in the present work the effective activation energies of the intermediate reactions describing the competition of fuel and oxidant for radicals are assumed to be sufficiently large such that activation energy asymptotics can be employed in the fuel consumption zone.

Our results include the evaluation of the burning rate in terms of pressure, equivalence ratio, and the ratio of the competing rates of the branching reaction to the termination reaction. Although limitations of the simplified kinetic scheme were noted in the analysis of near-stoichiometric flames, for the most part the trends are found to be in qualitative agreement with experimental observations, cf. [14, 15]. For the adiabatic conditions considered here, the burning velocity does not exhibit turning-point behavior (i.e., extinction), in agreement with numerical computations [13].

We remark that although the activation energies of the intermediate reactions are not significantly large, our results suggest that they are sufficiently large to permit the use of activation energy asymptotics. Our results agree quite well with those obtained using rate-ratio asymptotics, and in fact, the structure equation found with rate-ratio techniques can be recovered as a limiting case of the equation that we have derived. Specifically, by setting $\gamma = 0$ in Eq. 6.19, the equation first derived in Ref. 4 is obtained. For the premixed methane–air flames of primary interest here, the value of γ is typically quite small. However, it is possible to consider other hydrocarbons or to modify the mixture in such a way as to obtain larger values of γ without changing the basic flame structure. For such situations there will certainly be less quantitative agreement between the two theories. As discussed in Section 6, qualitative differences will also arise for larger values of γ. For example, the RRA theory predicts that k_{11} is always terminating, while the present theory indicates that its role is reversed for larger values of γ. One advantage of the method proposed here is that the nonlinear reaction rate term is retained in the fuel consumption zone. Experience with one-step chemistry suggests that such nonlinearities can realistically capture a variety of flame responses to perturbations. Although Damköhler number asymptotics and rate-ratio techniques are needed to analyze many of the layers within these complicated flame structures, by employing activation energy asymptotics in the fuel consumption layer, perhaps we can better study the response of these hydrocarbon flames to heat loss, stretch, etc.

To illustrate our method we have used the most basic kinetic mechanism, which represents a significant simplification from the original starting mechanism, and consequently there is a certain degree of error inherently present. However, more intermediate reactions can be retained, and in addition several assumptions regarding the relative thickness of the various zones can be relaxed in order to gain increased accuracy. Seshadri (cf. Refs. 5–7) has done a great deal of work in refining this mechanism to obtain much-improved results. The results of those studies agree favorably with the detailed numerical calculations of Smooke and Giovangigli [2] and Egolfopoulos et al. [15], as well as the experimental measurements reported in Ref. 15. The same improvements can be made in the present study to obtain better agreement with numerics and experiments.

As a final comment, we remark that the four global reactions used in the present study can also be used to investigate the structure of methane–air diffusion flames, as has been done using rate-ratio asymptotics (cf Refs. 18–20).

This work was supported by the National Science Foundation and the Air Force Office of Scientific Research, under the technical monitoring of Dr. M. K. King and Dr. J. M. Tishkoff, respectively. The authors would like to thank Mr. C. J. Sung and Mr. G. Yu for providing the numerical and experimental data, respectively, shown in Fig. 7.

REFERENCES

1. Miller, J. A., Kee, R. J., Smooke, M. D., and Grcar, J. F., Paper NO. WSS/CI 84-10, Western States Section of the Combustion Institute, Spring Meeting, 1984.

2. Smooke, M. D., and Giovangigli, V., *Lect. Notes Phys.* 384:1–47 (1991).
3. Peters, N., *Lect. Notes Phys.* 241:90–109 (1985).
4. Peters, N., and Williams, F. A., *Combust. Flame* 68:185–207 (1987).
5. Seshadri, K., and Peters, N., *Combust. Flame* 81:96–118 (1990).
6. Seshadri, K., and Göttgens, J., *Lect. Notes Phys.* 384:113–133 (1991).
7. Bui-Pham, M., Seshadri, K., and Williams, F. A., *Combust. Flame* 89:343–362 (1992).
8. Buckmaster, J. D., and Ludford, G. S. S., *Theory of Laminar Flames*, Cambridge University Press, Cambridge, 1982.
9. Liñán, A., *Acta Astronaut.* 1:1007–1039 (1974).
10. Zel'dovich, Y. B., *Zhur. Fiz. Khim.* 22:27–49 (1948).
11. Liñán, A., Tech. Rept. 1, AFOSR Contract No. E00AR68-0031, INTA, Madrid, 1971.
12. Kennel, C., Göttgens, J., and Peters, N., *Twenty-Third Symposium (International) on Combustion*, The Combustion Institute, Pittsburgh, 1990, pp. 479–485.
13. Law, C. K., and Egolfopoulos, F. N., *Twenty-Fourth Symposium (International) on Combustion*, The Combustion Institute, Pittsburgh, 1992, pp. 137–144.
14. Bradley, D., and Hundy, G. F., *Thirteenth Symposium (International) on Combustion*, The Combustion Institute, Pittsburgh, 1971, pp. 575–583.
15. Egolfopoulos, F. N., Cho, P., and Law, C. K., *Combust. Flame* 76:375–391 (1989).
16. Egolfopoulos, F. N., and Law, C. K., *Combust. Flame* 80:7–16 (1990).
17. Egolfopoulos, F. N., Du, D. X., and Law, C. K., *Combust. Sci. Technol.* 83:33–75 (1992).
18. Seshadri, K. and Peters, N., *Combust. Flame* 73:23–44 (1988).
19. Treviño, C., and Williams, F. A., *Prog. Astronaut. Aeronaut.* 113:129–165 (1988).
20. Chelliah, H. K., and Williams, F. A., *Combust. Flame* 80:17–48 (1990).

Received 2 February 1993; revised 20 January 1994

AIAA JOURNAL
Vol. 32, No. 2, February 1994

Appendix C

Analysis of Thermal Ignition in the Supersonic Mixing Layer

H. G. Im,* B. H. Chao,† J. K. Bechtold,‡ and C. K. Law§
Princeton University, Princeton, New Jersey 08544

Ignition in a laminar supersonic mixing layer between two parallel streams of initially separated reactants is studied both numerically and through the use of large activation energy asymptotics. The asymptotic analysis provides a description of ignition characteristics over the entire range of system parameters. In particular, it is demonstrated that, for small values of viscous heating, the ignition distance scales approximately linearly with the freestream Mach number, whereas for large viscous heating it decreases rapidly due to the temperature-sensitive nature of the reaction rate. This indicates the potential of using local flow retardation to enhance ignition rather than relying solely on external heating. The asymptotic analysis further identifies several distinct ignition situations, yielding results that compare well with those obtained from the full numerical calculation. The effects of flow nonsimilarity are also assessed and are found to be more prominent for the mixing layer flow in comparison to the flat-plate configuration studied previously.

Introduction

THE study of combustion within supersonic boundary-layer flows has generated much recent interest due to its relevance in the development of scramjet engines. The most essential feature of supersonic boundary-layer combustion, in contrast to the subsonic situation, is that the high-speed flow contains a considerable amount of kinetic energy that can be converted to thermal energy through viscous dissipation, thus facilitating ignition of the combustible mixture.

In a recent study[1] we investigated the effect of viscous heating on the ignition of a supersonic stream of premixed combustible over a flat plate, using full numerical computation and large activation energy asymptotics. Several distinct ignition regimes were identified, depending on the relative magnitude of the external heat transfer from the hot boundary and the internal heat generation due to viscous heating. The analysis of each regime was shown to properly capture the ignition characteristics.

Whereas the flat-plate configuration studied previously[1] provides a simple model problem, many applications of interest, most notably the scramjet engine, involve the compressible mixing layer between fuel and oxidizer supplies.[2] In contrast to the flat plate, the problem is nonpremixed in nature; therefore mixing of the reactants must occur to achieve ignition. Furthermore, the internal generation of heat in the presence of a shear layer will vary depending on the difference in velocities of the two parallel streams. Thus the ignition characteristics of the mixing layer are expected to be different from that of the supersonic flat-plate flow, for which the no-slip condition at the wall always results in large amounts of viscous heating. Therefore, in this paper we extend our previous work[1] and consider a mixing layer configuration to provide a comprehensive treatment on the subject of ignition within supersonic boundary-layer flows.

The effect of viscous heating on the ignition in a supersonic mixing layer was first considered asymptotically by Jackson and Hussaini,[3] in which nearly equal freestream temperatures and velocities were assumed. Ju and Niioka[4] allowed for an $O(1)$ temperature difference between the two freestreams, nonetheless restricting the analysis to small velocity differences. A pseudomultistep chemistry model was also used. A more thorough treatment of $O(1)$ viscous heating in the mixing layer was subsequently made by Grosch and Jackson,[5] in which Jackson's and Hussaini's previous analysis[3] was extended to render it valid over a wider range of parameters characterizing the strength of the ignition source. A numerical and asymptotic analysis of the evolution from a weakly reactive state to the fully developed laminar diffusion flame was also provided, yielding a more accurate description of the diffusion flame structure. It was further emphasized that, because combustion in the mixing layer can introduce additional flow instabilities,[6] which in turn enhances reactant mixing, it is of fundamental importance to investigate the effect of chemical reaction on the flowfield. Furthermore, a good understanding of ignition and flame propagation in an idealized laminar mixing layer provides useful information for more complicated studies involving chemically reacting flows.

The present study extends the work of Grosch and Jackson[5] by treating all possible weakly reactive regimes that can exist in supersonic mixing layers prior to the point of thermal runaway. This includes the case, not considered in Ref. 5, in which the heat for ignition generated by the hot stream and through viscous heating are comparable. Furthermore, for each ignition situation, we derive explicit expressions for the minimum ignition distance, which is then mapped out over the complete range of system parameters. The results compare well with numerical computations. The significance of flow nonsimilarity is discussed, and comparisons with the flate-plate case[1] are also made.

In the following section, the model problem is formulated and the distinct ignition situations are classified. Next, the numerical solutions for the full system of equations are presented. We then proceed with the asymptotic analysis, and the results are compared with numerical predictions. Finally, we add further discussions and concluding remarks.

Formulation

As shown in Fig. 1, we consider a stream of reactant 1 with reactant mass fraction $\hat{Y}_{1,\infty}$, density $\hat{\rho}_\infty$, velocity $\hat{u}_\infty$, and temperature $\hat{T}_\infty$, flowing parallel to a stream of reactant 2, with $\hat{Y}_{2,\infty}$, $\hat{\rho}_\infty$, $\hat{u}_\infty$, and $\hat{T}_\infty$. We assume a zero pressure gradient exists across the boundary layer such that the inert solution has a self-similar form. The two initially separated reactants diffuse into one another, thus permitting ignition to occur when the temperature is elevated to a sufficiently high value. Chemical reaction is weak near the leading edge of the mixing layer, and it evolves gradually in the downstream direction. Eventually an abrupt temperature rise,

Presented as Paper 93-0449 at the AIAA 31st Aerospace Sciences Meeting, Reno, NV, Jan. 11–14, 1993; received Feb. 3, 1993; revision received April 27, 1993; accepted for publication May 19, 1993.

*Graduate Student, Department of Mechanical and Aerospace Engineering.

†Research Staff Member, Department of Mechanical and Aerospace Engineering; currently Assistant Professor, Department of Mechanical Engineering, University of Hawaii, Honolulu, HI.

‡Research Staff Member, Department of Mechanical and Aerospace Engineering.

§Professor, Department of Mechanical and Aerospace Engineering. Fellow AIAA.

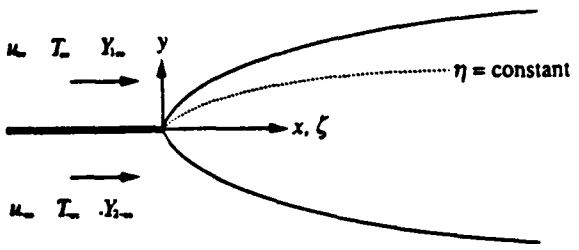

Fig. 1 Schematic of the flow configuration.

corresponding to thermal runaway, occurs at a certain location within the mixing layer. We are interested in analyzing the reaction zone structure up to the point of ignition to obtain explicit expressions for the minimum ignition distance as a function of all the system parameters. We assume that a one-step, overall reaction, with an Arrhenius temperature dependence, takes place between species 1 and 2 to form the product. We further assume constant properties such as specific heat c_p, density-weighted viscosity $\hat{\rho}\hat{\mu}$, and unity values for the Lewis and Prandtl numbers. The conservation equations for momentum, mass fraction of species i, and static energy in the supersonic mixing layer are then given by[7]

$$f''' + ff'' = 0 \tag{1}$$

$$\frac{\partial^2 Y_i}{\partial \eta^2} + \frac{\partial Y_i}{\partial \eta} - 2\zeta f' \frac{\partial Y_i}{\partial \zeta} = \zeta Y_1^p Y_2^q T^{r-p-q+1} \exp(-T_a/T) \tag{2}$$

$$\frac{\partial^2 T}{\partial \eta^2} + f\frac{\partial T}{\partial \eta} - 2\zeta f' \frac{\partial T}{\partial \zeta} = -\zeta Y_1^p Y_2^q T^{r-p-q+1} \exp(-T_a/T)$$

$$-2\mu [f''(\eta)]^2/(1-\lambda)^2 \tag{3}$$

where $(\,)'$ denotes $d/d\eta$, and the preceding equations are to be supplemented by the ideal-gas equation of state. The nondimensional temperature T and the mass fraction for species i, Y_i are defined in terms of the original variables by $T = c_p\hat{T}/\hat{q}\hat{Y}_{2,\infty}$ and $Y_i = \hat{Y}_i/\sigma_i\hat{Y}_{2,\infty}$, respectively. Here, $\hat{q}$ is the heat of reaction per unit mass of species 2, and σ_i is the stoichiometric mass ratio of each species relative to species 2, such that $\sigma_2 = 1$. Other parameters include the nondimensional activation temperature $T_a = c_p(E_a/R^0)/\hat{q}\hat{Y}_{2,\infty}$, and the viscous heating parameter $\mu = (1/2)(\gamma-1)M_\infty^2 T_\infty/(1-\lambda)^2$, where $\gamma = c_p/c_v$, $\lambda = \hat{u}_{-\infty}/\hat{u}_\infty$, and

$$M_\infty = \hat{u}_\infty/\sqrt{\gamma R^0 \hat{T}_\infty/W}$$

is the Mach number of the upper freestream. The variables ζ and η are the normalized Howarth-Dorodnitsyn variables defined as

$$\eta = \eta_0 + \left(\frac{\hat{u}_\infty}{2\hat{\rho}_\infty\hat{\mu}_\infty x}\right)^{1/2}\int_0^y \rho(x,\bar{y})\,d\bar{y} \tag{4}$$

$$\zeta = x\left(\frac{2B\nu_2 W_2}{\hat{u}_\infty W_1^p W_2^q}\right)\left(\frac{\hat{p}\bar{W}}{R^0}\right)^{p+q-1}\sigma_1^p\hat{Y}_{2,\infty}^{r}\left(\frac{\hat{q}}{c_p}\right)^{r-p-q+1} \tag{5}$$

and f is the stream function $\psi(x,y)$ normalized as

$$f(\eta) = \psi(x,y)/(2\hat{\rho}_\infty\hat{\mu}_\infty\hat{u}_\infty x)^{1/2} \tag{6}$$

Here p and q represent the reaction orders of species 1 and 2, respectively, and r is the temperature exponent of the pre-exponential reaction rate term. In Eq. (4), η_0 denotes a shift of the origin; it may remain indeterminate,[8] but we are free to translate the coordinate such that $\eta = 0$ at the origin. We note that the streamwise coordinate ζ is proportional to the frequency factor B and hence can be interpreted as a reduced Damköhler number, representing the ratio of a characteristic flow time to a characteristic reaction time. In these expressions, W_i is the molecular weight of species i, $\bar{W}$ the average molecular weight, and x and y the physical coordinates parallel and normal to the stream. The last term in the energy equation (3) represents the contribution due to viscous heating, i.e., the amount of kinetic energy that is converted to thermal energy within the mixing layer.

Equations (1–3) are to be solved subject to the boundary conditions

$$f'(\infty) = 1, \quad f(0) = 0, \quad f'(-\infty) = \lambda \tag{7}$$

$$Y_1(\infty,\zeta) = Y_{1,\infty}, \quad Y_1(-\infty,\zeta) = 0 \tag{8}$$

$$Y_2(\infty,\zeta) = 0, \quad Y_2(-\infty,\zeta) = 1 \tag{9}$$

$$T(\infty,\zeta) = T_\infty, \quad T(-\infty,\zeta) = T_{-\infty} = T_\infty - \beta \tag{10}$$

It may be noted that Eqs. (1) and (7), which govern the flowfield, are decoupled from the energy and species equations and can be solved independently to yield the self-similar Blasius profile for mixing layer flows.[9,10] Without loss of generality, we consider $0 \le \lambda \le 1$, so that the upper stream is always at a higher velocity. The case $\lambda = 1$, corresponding to a uniform parallel flow of initially separated reactants with no viscous heating, has been studied by Liñán and Crespo.[11] In the main text, we consider the upper stream to be the hotter of the two, i.e., $\beta > 0$. For the case $\beta < 0$, ignition can occur near the slower stream when $|\beta| \ge \mu$. The solution for this case can be obtained by redefining the coordinate system, as discussed in Appendix A for completeness.

Coupling functions that relate the mass fractions of species 1 and 2 to temperature are found by integrating appropriate chemistry-free linear combinations of Eqs. (2) and (3), yielding

$$Y_1 = T_\infty + Y_{1,\infty} - (\beta + Y_{1,\infty})\xi + \mu\xi(1-\xi) - T \tag{11}$$

$$Y_2 = T_\infty - (\beta - 1)\xi + \mu\xi(1-\xi) - T \tag{12}$$

where we have made the convection-free coordinate transformation

$$\xi = \begin{cases} (1-f')/(1-\lambda) & \text{for } \lambda \neq 1 \\ \operatorname{erfc}(\eta/\sqrt{2})/2 & \text{for } \lambda = 1 \end{cases} \qquad 0 \le \xi \le 1 \tag{13}$$

The relations (11) and (12), together with the previously determined flowfield, can now be inserted into Eq. (3) to reduce the problem to a single equation for T.

In the weakly reactive state, the reaction term in Eq. (3) is small and can be neglected in a first approximation. The frozen temperature T_f is governed by

$$\frac{\partial^2 T_f}{\partial \xi^2} = -2\mu \tag{14}$$

which, when solved subject to the boundary conditions (10), yields

$$T_f = T_\infty - \alpha\xi - \mu\xi^2 \tag{15}$$

where $\alpha = \beta - \mu$. The frozen solution (15) serves as the initial condition for the numerical solution and as the basic solution for the asymptotic analysis. As will be discussed later in the asymptotic analysis, the point of the maximum frozen temperature identifies the ignition location for systems with large activation energy and varies with the system parameter α, which indicates the relative

importance of either the external ignition source represented by β or the internal source represented by μ.

In the next section, we shall study the ignition dynamics for the preceding two cases through direct numerical integration of the energy equation (3) with the boundary conditions (10). We shall then proceed to an asymptotic analysis and derive explicit expressions for the ignition distance as functions of all relevant parameters.

Numerical Solutions

Equations (3) and (10) are solved numerically using a second-order finite-difference scheme with implicit determination in the η direction and marching along the streamwise coordinate ζ. The step size of ζ is readjusted as the solution approaches the ignition point to capture the abrupt temperature rise. In the present calculations we have set $p = q = r = 1$ for simplicity. The parameter values used are $\hat{q} = 1.0 \times 10^4$ kcal/kg, $c_p = 0.25$ kcal/kg-K, $E_a = 60$ kcal/mole, and $\gamma = 1.4$, which are typical numbers for hydrocarbon/air mixtures. Boundary conditions for species concentrations are taken to be $\hat{Y}_{2,\infty} = 0.5$, $\hat{Y}_{1,\infty} = 0.3$ with $\sigma_1 = 3$, which correspond to the scaled values $Y_{2,\infty} = 1$, $Y_{1,\infty} = 0.2$.

The streamwise evolution of the temperature profile within the mixing layer is illustrated in Figs. 2a and 2b. Figure 2a corresponds to the subsonic case in the absence of viscous heating ($M_\infty = 0$), with $\hat{T}_- = 1000$ K, $\hat{T}_{-\infty} = 500$ K, and $\lambda = 0$. This particular case is similar to the problem studied in several previous hot boundary ignition analyses.[10,11] It is seen that as ζ increases, the maximum temperature at first rises gradually, but then exhibits a dramatic increase, resulting in the thermal runaway behavior at $\zeta_i = 1.64 \times 10^{13}$. Solutions for the other extreme case, for which viscous heating is the only heat source, are shown in Fig. 2b, where we have set $\hat{T}_- = \hat{T}_{-\infty} = 500$ K, $\lambda = 0$, and $M_\infty = 4.472$ so that the

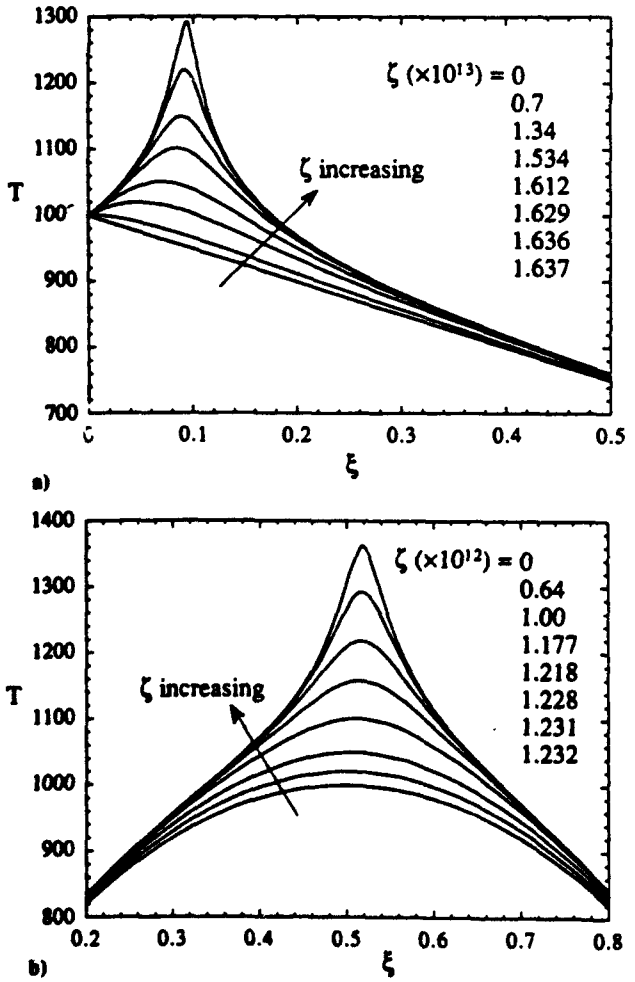

Fig. 2 Evolution of the temperature profiles as computed numerically for a) the hot-stream case with $\hat{T}_- = 1000$ K, $\hat{T}_{-\infty} = 500$ K, $M_\infty = 0$ and b) the viscous heating case with $\hat{T}_- = \hat{T}_{-\infty} = 500$ K, $M_\infty = 4.472$.

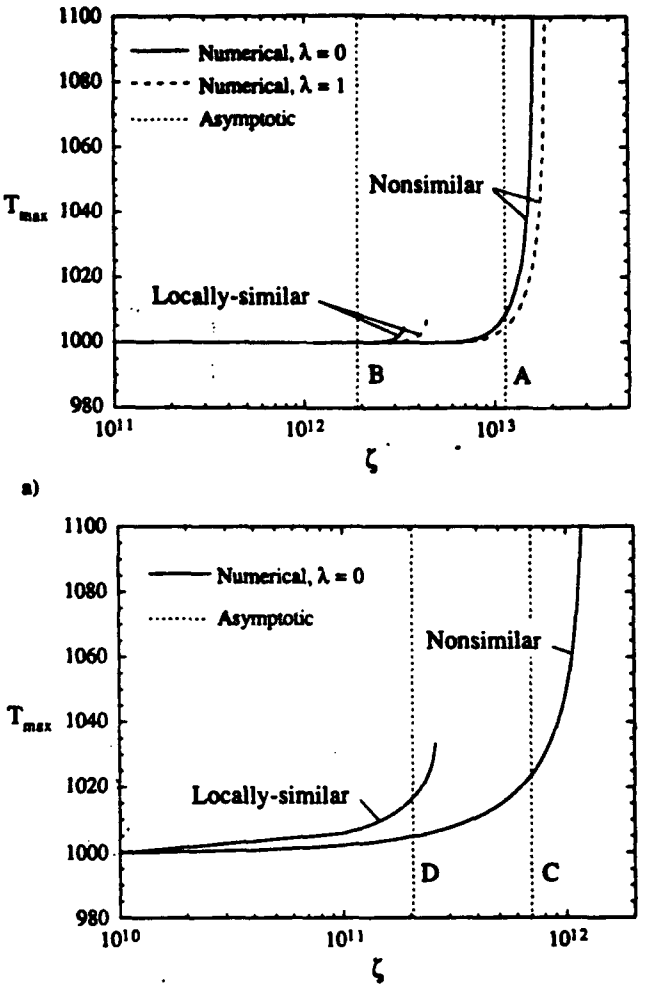

Fig. 3 Streamwise variation of the maximum temperature for a) the hot-stream case with same parameter values as in Fig. 2a: vertical lines represent asymptotic solution, Eq. (24), with A, leading-order result only and B, additional subdominant term retained; b) the viscous heating case with same parameter values as in Fig. 2b: vertical lines represent asymptotic results for C, fully nonsimilar solution, Eq. (33); and D, locally similar solution, using Eq. (34).

initial temperature profile becomes symmetric about $\xi = 1/2$ and the maximum temperature takes the same value as that in Fig. 2a. As a result, the most rapid temperature rise is seen to take place near $\xi = 1/2$, and thermal runaway occurs at $\zeta_i = 1.23 \times 10^{12}$.

The streamwise variation of the maximum temperature for the above two cases is plotted in Figs. 3a and 3b, respectively. The existence of a critical ignition distance ζ_i is clearly illustrated. Figure 3a represents solutions in the absence of viscous heating, and curves are drawn for two different values of λ, with all other parameters taken to be the same as in Fig. 2a. The two curves demonstrate that, for a given strength of the ignition source, i.e., for a fixed value of β, ζ_i increases as the flow velocity of the slower stream increases. This indicates that the ignition distance is proportional to the velocity at the ignition location. It should be pointed out, however, that the dependence of ζ_i on λ is quite weak. This is physically reasonable given that ignition occurs near the hot boundary, $\xi = 0$, which moves with velocity $\hat{u}_-$ (see Ref. 10). Thus an increase in $\hat{u}_{-\infty}$ results in only a slight increase in the velocity field near the opposite boundary at $\xi = 0$. The asymptotic analysis of the next section also reveals the weak dependence of ζ_i on λ for this particular ignition situation.

To assess the importance of retaining nonsimilar effects, we have also solved the problem by neglecting the $\partial/\partial\zeta$ term in Eq. (3). The results are plotted in Fig. 3a, where the curves terminate at a point where they approach an infinite slope. Thus for locally similar flows, ignition is identified as the turning point of

these curves, in contrast to the full evolutionary problem that exhibits thermal runaway. These locally similar solutions are seen to underestimate the ignition distance, consistent with previous results.[1] The present results, however, show a more significant deviation between the actual value of ζ_i and that obtained with the local-similarity approximation. This can be explained by comparing the relative magnitudes of the diffusion and convection terms for both flow configurations. In the mixing layer, the reaction zone is broader (in physical scale) than it is for the flat plate, thereby resulting in smaller transverse temperature gradients whereas the streamwise convection term is larger due to the greater flow velocity at the ignition location. We note that, in the flat-plate configuration,[1] the local streamwise velocity at the ignition point was found to be very small when ignition occurs near the hot plate. A more detailed discussion of nonsimilarity effects will be given in the next section.

Figure 3b shows a similar plot of the maximum temperature evolution for the case of ignition induced purely by viscous heating, where parameter values are the same as those used in Fig. 2b. When viscous heating is included, it is difficult to compare the dependence of ζ_i on λ in a straightforward manner as is done in Fig. 3a, since variations in λ affect the viscous heating term, which in turn shifts the maximum temperature location. The curves shown in Fig. 3b are for the case $\lambda = 0$ specifically, and it is clear that the local-similarity approximation substantially underestimates the actual ignition distance.

Asymptotic Analysis

In this section we study Eqs. (1–3) and (7–10) using large activation energy asymptotics. We consider the weakly reactive state and identify the ignition distance ζ_i as the point at which we observe either thermal runaway or turning point behavior.

As mentioned earlier, the flowfield is known.[9,10] Thus when Eqs. (11) and (12) are used we only have to consider a single equation for T, with appropriate boundary conditions. These can be expressed in terms of the ξ coordinate as

$$\left[\frac{f''(\eta)}{1-\lambda}\right]^2\frac{\partial^2 T}{\partial \xi^2} - 2\zeta\,[1-(1-\lambda)\,\xi]\,\frac{\partial T}{\partial \zeta}$$

$$= -\zeta Y_1^p Y_2^q T^{r-p-q+1}\exp(-T_a/T) - 2\mu\left[\frac{f''(\eta)}{1-\lambda}\right]^2 \qquad (16)$$

$$T(0,\zeta) = T_\infty, \quad T(1,\zeta) = T_{\infty_2}, \quad T(\xi,0) = T_f(\xi) \qquad (17)$$

Here the frozen profile T_f, given by Eq. (15), provides the initial condition at the leading edge ($\zeta = 0$) of the mixing layer. We use $\varepsilon = T_c^2/T_a$ as the small parameter in the analysis, where T_c is the maximum value of the frozen temperature.

The parabolic form of the frozen profile (15) and the numerical results shown in Fig. 2 suggest that three distinct regimes of ignition should be considered depending on the range of the parameter α, as shown schematically in Fig. 4. When $\alpha > 0$ (Fig. 4a), the frozen temperature has a maximum value of $T_c = T_\infty$ at $\xi = 0$. This is called the hot-stream case, since the dominant ignition source is the hot temperature of the freestream. Here the linear behavior of the frozen temperature near $\xi = 0$ implies that reaction is confined within the layer of $\mathcal{O}(\varepsilon)$ thickness provided the activation energy is sufficiently large. On the other hand, when $\alpha < 0$ (Fig. 4c), the maximum temperature $T_c = T_\infty + \alpha^2/4\mu$ is attained in the interior of the mixing layer at $\xi = (1 - \beta/\mu)/2 > 0$. In this viscous heating case, ignition is characterized by the internal viscous heating represented by the parameter μ. The structure of the mixing layer consists of two frozen outer zones of $\mathcal{O}(1)$ extent, $0 < \xi < \xi_*$ and $\xi_* < \xi < 1$, separated by a thin reaction zone. The parabolic form of T_f near its maximum suggests that the reaction zone has $\mathcal{O}(\sqrt{\varepsilon})$ thickness. Finally, as α approaches zero (Fig. 4b), i.e., when β and μ are comparable, neither of the analyses is valid and thus a different analytical treatment is required. In this intermediate case, the maximum frozen temperature occurs at $\xi = 0$, but now the reaction zone is of $\mathcal{O}(\sqrt{\varepsilon})$ near its maximum, which is broader than the case shown in Fig. 4a. We now proceed to analyze Eqs. (16) and (17) for these three different cases in sequence.

Hot Stream Case: $\alpha > 0$

As observed in Fig. 4a, in this case the reaction is confined to the thin layer of $\mathcal{O}(\varepsilon)$ near $\xi = 0$ at which the frozen temperature attains the maximum value of T_∞. To study the structure of this layer, we introduce the stretched coordinate $\chi = \alpha\xi/\varepsilon$ and seek an inner solution of the form

$$T_{in}(\chi,\zeta) = T_f(\chi) + \varepsilon\theta_0(\chi,\zeta) + \mathcal{O}(\varepsilon^2) \qquad (18)$$

After substituting these expansions into Eq. (16), and using the asymptotic behavior of the flowfield (see Appendix B)

$$\left(\frac{f''}{1-\lambda}\right)^2 \sim -\xi^2 \ell_n \xi^2 \quad \text{as } \xi \to 0 \qquad (19)$$

we can write the leading order structure equation as

$$\chi^2\frac{\partial^2\theta_0}{\partial\chi^2} = -\Delta\,(\chi - \alpha\theta_0)^q \exp(\theta_0 - \chi) \qquad (20)$$

where

$$\Delta = \frac{\zeta\varepsilon^{q-1}Y_{1_\infty}^p T_\infty^{r-p-q+1}}{\alpha^q \ell_n \varepsilon^{-2}}\exp(-T_a/T_\infty) \qquad (21)$$

Equation (20) is to be solved subject to the boundary conditions

$$\theta_0(0,\zeta) = 0, \quad \frac{\partial\theta_0}{\partial\chi}(\infty,\zeta) = 0 \qquad (22)$$

where the latter condition is obtained by matching to the outer solution, which is expanded as $T_{out}(\xi,\zeta) = T_f(\xi) + \varepsilon\Phi_0(\xi,\zeta) + \mathcal{O}(\varepsilon^2)$.

The previous system is identical to that found by Liñán and Crespo[11] for a uniform parallel flow of initially separated reactants. This implies that, when the hot boundary is the dominant en-

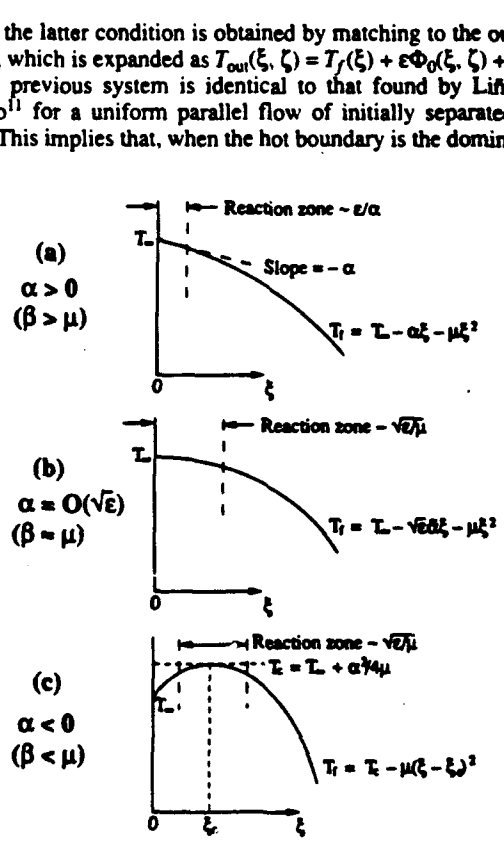

Fig. 4 Schematic of the frozen temperature profile in ξ coordinate for a) the hot-stream case, b) the intermediate case, and c) the viscous heating case.

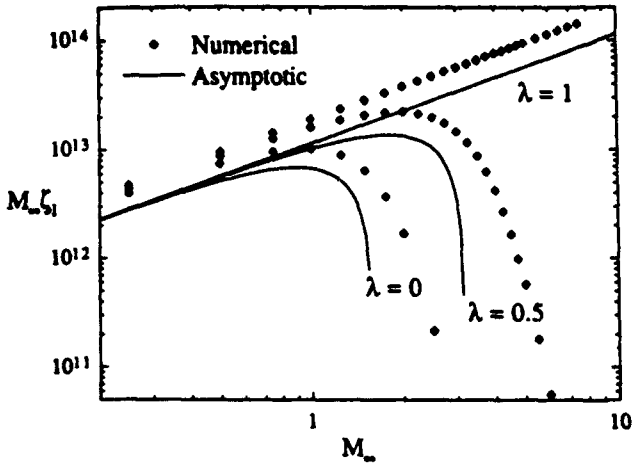

Fig. 5 Log-log plot of the predicted ignition distance as a function of the freestream Mach number for the hot-stream case.

ergy source, the ignition characteristics are minimally affected by the additional effects of viscous heating in the interior of the boundary layer. The only modification here is the parameter α, which represents the combined effects of the temperature difference of the two streams β and the viscous heating effect μ.[4,5]

Equations (20) and (22) are solved numerically, and the solution for θ_0 is found to have a turning point at a critical Damköhler number Δ_I beyond which no solution exists. The value of Δ_I can be evaluated numerically as a function of the parameter α, after which the minimum ignition distance can be obtained from the definition of Δ in Eq. (21), yielding

$$\zeta_I = \Delta_I(\alpha)\frac{\alpha^q \varepsilon^{1-q} f_\infty \varepsilon^{-2}}{Y_{1,\infty}^p T_\infty^{r-p-q+1}} \exp(T_a/T_\infty) \tag{23}$$

For $q = 1$, Liñán and Crespo[11] provided a useful correlation for the ignition Damköhler number as a function of the parameter α in the form

$$\Delta_I(\alpha) = 2e^{-2}(2-\alpha)/(1-\alpha)^2 \tag{24}$$

which is valid for $0 < \alpha < 1$. Substituting Eq. (24) into Eq. (23), we obtain an explicit formula for ζ_I.

Equation (23) reveals that the leading-order value for the nondimensional ignition distance ζ_I is a function of μ, which groups the two parameters M_∞ and λ. There is no additional dependence on λ so that, in the absence of viscous heating ($M_\infty = 0$), ζ_I is unaffected by changes in λ to leading order. This implies that variations in the flowfield at the cold boundary have only a secondary effect (see Appendix B), in agreement with the previous numerical results.

We also note that the structure equation (20) is locally similar. Furthermore, the matching condition (22) shows that there is no heat transfer between the inner structure and the outer frozen flow up to $\mathcal{O}(\varepsilon)$. Consequently, the effect of nonsimilarity is of higher order and does not appear in the leading-order analysis, as was true for the flat-plate flow.[1] However, the numerical result shown in Fig. 3a seems to suggest that there is a larger difference between the similar and nonsimilar solutions for the present study as compared to the "subadiabatic wall case" of the flat-plate analysis.[1] This can be explained by examining the relative order of magnitude of the diffusion and (nonsimilar) convection terms in the equations governing the structure for each flow configuration. It can be readily shown that the ratio of convective to diffusive terms in the structure equation is $\mathcal{O}(1/f_\infty\varepsilon^{-2})$ for the present problem, which is larger than the $\mathcal{O}(\varepsilon^3)$ ratio for the flat-plate problem. As discussed in the previous section, the physical implication is that the streamwise flow velocity at the ignition location is relatively larger for the present problem than for the flat-plate problem. Therefore, the nonsimilar terms can be expected to play a somewhat larger role in the mixing layer situation, although they still remain as a higher order effect.

In Fig. 3a the vertical dotted lines A and B represent the ignition distance for $M_\infty = 0$ obtained from Eq. (23). For the line denoted by A, only the leading-order term describing the behavior of the flowfield near the hot boundary is retained (see Appendix B), whereas for line B, a constant subdominant term is retained as well, as is done by Liñán and Crespo.[11] The latter case requires that $f_\infty\varepsilon$ be replaced by $f_\infty(2\pi\varepsilon/\alpha)$ in Eq. (23). Although both results are asymptotically equivalent, the resulting values for the ignition distances are seen to differ by a considerable amount. This is due to the fact that the value of α used in the calculation is quite small.

The predicted ignition distance for the hot-stream case as a function of the freestream Mach number is shown in Fig. 5 for several values of λ. We have chosen to plot the quantity $M_\infty\zeta_I$, since it is directly proportional to the actual ignition distance in physical length. The numerical and asymptotic results agree quite well, except for large M_∞ when viscous heating becomes important. When M_∞ is sufficiently large, the ignition point shifts to the interior of the boundary layer. The present analysis is therefore no longer valid, and the analysis of the next section becomes appropriate.

As a final comment for the hot-stream case, in a uniform parallel flowfield, i.e., $\lambda = 1$, an increase in M_∞ does not generate additional heat, and the ignition distance simply increases linearly, as shown in Fig. 5. In the presence of shear between the two streams, i.e., when $\lambda \neq 1$, $M_\infty\zeta_I$ is seen to achieve a maximum value, after which viscous heating causes it to decrease, thereby enhancing ignitibility.

Viscous Heating Case: $\alpha < 0$

We now consider the case when viscous heating exceeds the absolute value of the temperature difference between the two streams, i.e., $|\beta| < \mu$. In this case, the frozen temperature profile (15) achieves its maximum value of $T_c = T_\infty + \alpha^2/4\mu$ at the location $\xi_c = (1 - \beta/\mu)/2$, in the interior of the mixing layer. The structure of the mixing layer, shown in Fig. 4c, consists of two $\mathcal{O}(1)$ frozen outer zones separated by a narrow diffusive-reactive zone near $\xi = \xi_c$. The parabolic form of T_f near $\xi = \xi_c$ suggests that the appropriate stretched inner coordinate is $Z = \sqrt{\mu}\,(\xi - \xi_c)/\sqrt{\varepsilon}$, such that

$$f''(1-\lambda) = f''(\eta_c)/(1-\lambda) + o(1) \tag{25}$$

where $[1 - f'(\eta_c)]/(1-\lambda) = \xi_c$. We seek a solution for the temperature in the reaction zone of the form

$$T_{in}(Z,\zeta) = T_f(Z) + \varepsilon\theta_0(Z,\zeta) + \varepsilon^{3/2}\theta_1(Z,\zeta) + \mathcal{O}(\varepsilon^2) \tag{26}$$

To achieve proper balancing of the diffusion and reaction terms,[1] we introduce the rescaled Damköhler number as

$$\tilde{\Delta} = \frac{1}{\sqrt{\varepsilon}}\frac{\zeta(1-\xi_c)^p \xi_c^q Y_{1,\infty}^p T_c^{r-p-q+1}}{\mu\,[f''(\eta_c)/(1-\lambda)]^2}\exp(-T_a/T_c) \tag{27}$$

After substituting the expansions into Eq. (16), the structure equations at the first two orders become

$$\frac{\partial^2\theta_0}{\partial Z^2} = 0, \qquad \frac{\partial^2\theta_1}{\partial Z^2} = -\tilde{\Delta}\exp(\theta_0 - Z^2) \tag{28}$$

As discussed in the flat-plate study,[1] integration of the preceding equations provides boundary conditions and a jump condition for the outer temperature profile, which is expanded in each region as

$$T_{out}^{\pm}(\xi,\zeta) = T_f(\xi) + \varepsilon\Phi_0^{\pm}(\xi,\zeta) + \mathcal{O}(\varepsilon^{3/2}) \tag{29}$$

We substitute Eq. (29) into Eq. (16) and introduce the new streamwise coordinate $\tau = \ell_n(\sqrt{\pi\mu}\,\tilde{\Delta})$ to obtain an equation for the leading-order temperature perturbation of the form

$$\frac{\partial^2 \Phi_0^{\pm}}{\partial \xi^2} - \frac{2[1-(1-\lambda)\xi]}{[f''(\eta)/(1-\lambda)]^2}\frac{\partial \Phi_0^{\pm}}{\partial \tau} = 0, \qquad \xi \neq \xi_c \tag{30}$$

Matching solutions of Eq. (30) with the inner solutions (28) yields the conditions

$$\Phi_0^-(0,\tau) = \Phi_0^+(1,\tau) = \Phi_0^{\pm}(\xi,-\infty) = 0 \tag{31}$$

$$\left[\frac{\partial \Phi_0}{\partial \xi}\right]_-^+ = \frac{\partial \Phi_0^+}{\partial \xi}(\xi_c,\tau) - \frac{\partial \Phi_0^-}{\partial \xi}(\xi_c,\tau)$$

$$= -\exp[\Phi_0(\xi_c,\tau) + \tau] \tag{32}$$

The system (30–32), which has also been obtained independently by Grosch and Jackson,[5] has a similar form to that appearing in our previous study.[1] The solution of the present system exhibits thermal runaway at τ_I, which is determined as a function of the two parameters ξ_c and λ. The numerical solution of τ_I as a function of ξ_c for several values of λ is shown in Fig. 6. From the definition of τ_I, we can readily determine the ignition distance as

$$\zeta_I = \exp[\tau_I(\xi_c,\lambda)]$$

$$\times \sqrt{\frac{\mu\varepsilon}{\pi}}\frac{[f''(\eta_c)/(1-\lambda)]^2 \exp(T_a/T_c)}{(1-\xi_c)^p \xi_c^q Y_{1,\infty}^p T_c^{r-p-q+1}} \tag{33}$$

We remark that in the present analysis, nonsimilar effects have been accounted for in the outer, frozen regions, and thus the solution possesses evolutionary-type behavior similar to that of thermal explosion. If the nonsimilar term $\partial/\partial\tau$ in Eq. (30) is neglected, then the equation can be easily integrated to yield an explicit analytical solution which possesses a turning point at

$$\tau_I(\xi_c) = -1 - \ell_n[\xi_c(1-\xi_c)]. \tag{34}$$

This locally similar result, however, underestimates the ignition distance by a substantial amount as shown by the vertical dotted lines C and D in Fig. 3b.

Intermediate Case: $|\alpha| \ll 1$

Neither of the preceding analyses is valid when $|\alpha| \ll 1$, or more specifically $\alpha = \mathcal{O}(\sqrt{\varepsilon})$, which occurs when the two ignition sources generate comparable amounts of heat. We now consider this limiting case to provide a complete description of ignition in compressible mixing layers.

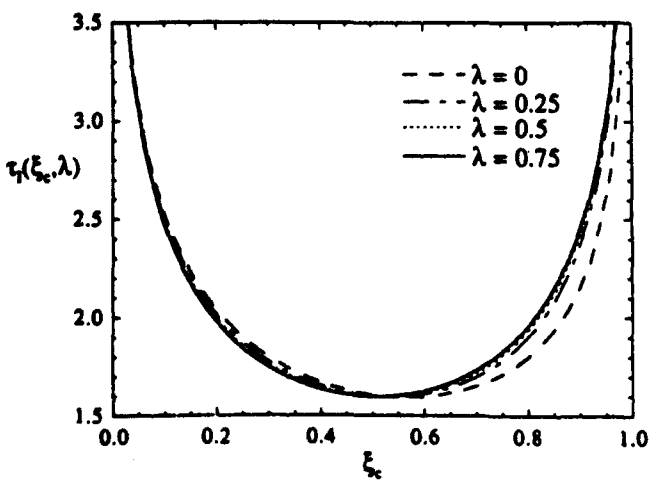

Fig. 6 Functional relation between the streamwise τ_I and transverse ξ_c location of ignition for the viscous heating case for various λ.

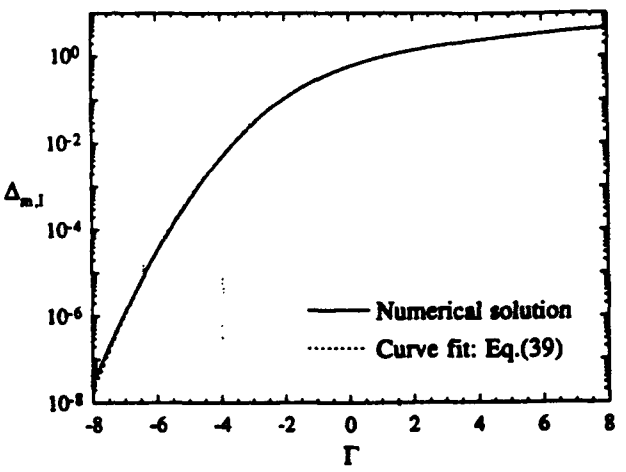

Fig. 7 Functional relation between the ignition Damköhler number $\Delta_{m,I}$ and Γ for the intermediate case for $q = 1$.

We rescale α as $\alpha = \sqrt{\varepsilon}\tilde{\alpha}$, introduce the stretched coordinate $X = \sqrt{\mu}\xi/\sqrt{\varepsilon}$, and seek solutions for the inner temperature profile as

$$T_{in}(X,\zeta) = T_f(X) + \varepsilon\theta_0(X,\zeta) + \mathcal{O}(\varepsilon^{3/2}) \tag{35}$$

To leading order, the inner structure equation is found to be

$$X^2\frac{\partial^2\theta_0}{\partial X^2} = -\Delta_m X^q \exp(\theta_0 - X^2 - \Gamma X) \tag{36}$$

where $\Gamma = \tilde{\alpha}/\sqrt{\mu}$, and

$$\Delta_m = \frac{\zeta\varepsilon^{q/2-1}}{\ell_n\varepsilon^{-1}\sqrt{\mu}} Y_{1,\infty}^p T_\infty^{r-p-q+1}\exp(-T_a/T_\infty) \tag{37}$$

The outer temperature profile is expanded as in the hot-stream case such that the boundary and matching conditions are given by

$$\theta_0(0,\zeta) = 0, \quad \frac{\partial\theta_0}{\partial X}(\infty,\zeta) = 0 \tag{38}$$

which are identical to those in Eq. (22). The inner structure problem for the present case is locally similar, consistent with the hot-stream case. Furthermore, all variations of ζ_I with λ and M_∞ are felt through the single lumped parameter μ. Numerical solution of Eqs. (36) and (38) shows that for a given value of Γ, no solution exists beyond a critical value $\Delta_{m,I}$, which is defined as the ignition Damköhler number. Solutions only exist for $q > 0$, and we choose $q = 1$ to be consistent with the other cases considered earlier. In Fig. 7, $\Delta_{m,I}$ is plotted as a function of the parameter Γ and is seen to increase monotonically with Γ. A useful correlation for this curve is given by

$$\Delta_{m,I}(\Gamma) = \ell_n\left[1 + \frac{1.141\exp(0.547\Gamma)}{1 + 0.433\exp(-0.756\Gamma - 0.017\Gamma^3)}\right] \tag{39}$$

Given the value of $\Delta_{m,I}$, the ignition distance for the intermediate case is determined from the definition of Δ_m in Eq. (37) as

$$\zeta_I = \Delta_{m,I}(\Gamma)\frac{\varepsilon^{1-q/2}\ell_n\varepsilon^{-1}\mu^{q/2}}{Y_{1,\infty}^p T_\infty^{r-p-q+1}}\exp(T_a/T_\infty) \tag{40}$$

in which $q = 1$ when the correlation (39) is used.

Summary of Asymptotic Analysis

Equations (23), (33), and (40) now provide a complete description of the ignition distance over a wide range of parameters. We remark that we have not treated the case of $\mathcal{O}(\epsilon)$ temperature and velocity differences as studied by Jackson and Hussaini.[3] For that limiting case, reaction occurs over the entire domain, and a full numerical approach must be employed. We also note that the present study can be extended to describe a three-step chain branching-termination mechanism proposed by Birkan and Law.[12] For such a case, in the limit of fast recombination in which the radicals are in steady state, the problem degenerates to that of the one-step model,[4,12] and thus the present analysis can be readily applied.

The predicted ignition distances obtained in the analyses for the previous three cases, together with the direct numerical results, are plotted in Fig. 8 as a function of M_∞. To avoid cluttering the graph, only the nonsimilar results are included. The curves demonstrate how the three different cases match together to provide a global picture for the ignition distance as a function of Mach number. The overall agreement with the numerical results is also seen to be quite good. For the case of $\lambda = 1$, which corresponds to a uniform parallel flow,[11] there is no viscous heating, and thus $M_\infty \zeta_I$ is determined by the result of the hot-stream case, Eq. (23), for all M_∞. As discussed earlier in Fig. 5, the ignition distance in this case varies linearly with the freestream velocity, as illustrated by the top curve in Fig. 8. For nonunity values of λ, however, $M_\infty \zeta_I$ passes through a maximum value and then decreases rapidly as a result of viscous heating. Since the amount of viscous heating is proportional to M_∞^2 and the reaction rate increases exponentially with the characteristic temperature of the reaction zone, we observe a drastic decrease of the ignition distance.

The maximum point $(M_\infty \zeta_I)_{max}$ of each curve in Fig. 8 may have practical importance in the design of the scramjet engine, as it represents the most difficult situation in which to achieve ignition. The value of $(M_\infty \zeta_I)_{max}$ can be used to evaluate the critical length of a flame holding region that is sufficient to ensure ignition for all Mach numbers. In holding regions of smaller dimension, it may be necessary to vary operating conditions to achieve shorter ignition distances. We will now discuss how the critical distance varies with each of the system parameters.

Since this maximum point is described by the hot-stream case, the critical ignition distance is determined from Eqs. (23) and (5). It is clear from Eq. (23) that the actual distance is most sensitive to variations in the hot-stream temperature T_∞. An increase in T_∞ will result in a substantial decrease in the critical ignition distance due to the Arrhenius dependence.

To assess the effect of the two remaining relevant parameters $T_{-\infty}$ and $M_{-\infty}$, we fix both T_∞ and $\lambda(< 1)$. Then it is convenient to work with the scaled variable

$$L_I = \sqrt{\mu}\,\zeta_I \frac{Y_{1,\infty}^{p} T_\infty^{r-p-q+1}}{\epsilon^{1-q} f_\infty \epsilon^{-2}} \exp(-T_a/T_\infty) \qquad (41)$$

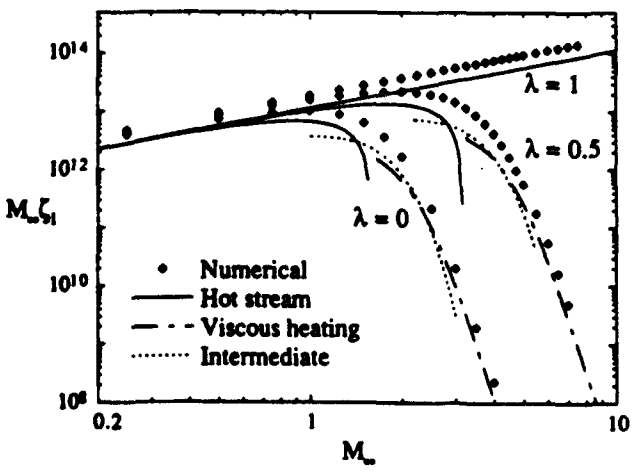

Fig. 8 Global log-log plot of the predicted ignition distance as a function of the freestream Mach number for various λ.

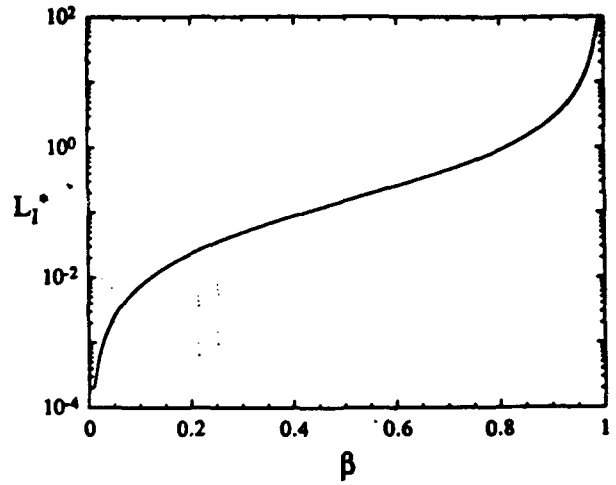

Fig. 9 Maximum ignition length in terms of the nondimensional quantity L_I^* defined in Eq. (41) as a function of β.

which corresponds to the properly normalized distance. It follows from Eq. (23) that L_I is a function of only two parameters, β and μ, representing $T_{-\infty}$ and $M_{-\infty}$, respectively. For $q = 1$, the correlation function (24) can be used to obtain an explicit expression for L_I as

$$L_I(\mu, \beta) = 2e^{-2}\sqrt{\mu}\,(\beta - \mu)(2 - \beta + \mu)/(1 - \beta + \mu)^2 \qquad (42)$$

When β is fixed, L_I attains a maximum at a critical value of μ, which represents the Mach number at the maximum point of each curve in Fig. 8.

In Fig. 9 we have plotted the maximum value, L_I^*, as a function of β. Since L_I^* and β both vary with $T_{-\infty}$, it is necessary to hold T_∞ fixed when interpreting Fig. 9. Therefore, an increase in β here implies a decrease in the cold boundary temperature $T_{-\infty}$, which leads to an increase in the heat loss from the hot boundary. Consequently, ignition is more difficult to achieve, and L_I^* is seen to increase with β.

Conclusions

The thermal ignition in a supersonic mixing layer between two streams of reactants, allowing for arbitrary differences in both velocities and temperatures, has been studied numerically and asymptotically. The asymptotic analysis has revealed that the reaction zone structure takes different forms, depending on whether the primary source for ignition is the hot freestream, the viscous heating generated within the shear layer, or a combination of the two.

Similar to the flat-plate case,[1] the ignition behavior in the mixing layer is characterized by the parameter α, which is a measure of the relative effects of the temperature difference of the two freestreams and the amount of viscous heating. In the present mixing layer situation, however, there is an additional parameter involved, namely, λ, which represents the velocity ratio of the slower to the faster freestreams. In the subsonic limit ($M_\infty = 0$), viscous heating is negligible and an increase in λ results in a small increase in the ignition distance. For finite values of M_∞, such that viscous heating is effective, a direct comparison of the results for various values of λ is difficult because the amount of viscous heating depends on both M_∞ and λ. As a result of the combined effect of the two parameters, the ignition distance exhibits several different types of behavior as M_∞ is varied. In particular, for the hot-stream case ($\alpha > 0$), variations in λ produce only higher order effects and the ignition characteristics are structurally similar to those of a uniform parallel flow.[11] For the case of $\alpha < 0$, viscous heating is the dominant energy source for ignition, and the point of maximum temperature shifts to the interior of the mixing layer. Consequently, variations in the flowfield at both boundaries have a significant influence on the ignition distance.

The effects of flow nonsimilarity have also been assessed by comparing solutions of the full system with those found by assum-

ing local similarity in the flowfield. Nonsimilar effects are most important when viscous heating is sufficiently large so as to cause a temperature bulge in the interior of the mixing layer. In general, the locally similar assumption has been found to underestimate the ignition distance, in agreement with the results of the flat-plate case.[1] It has also been demonstrated that nonsimilar effects are more important for the mixing layer than for the flat-plate flow, indicating the importance in retaining these terms in studies involving the ignition behavior of supersonic mixing layer flows.

Appendix A: Ignition at the Slow Boundary

When $\beta < 0$, ignition occurs near the slow boundary. However, it is possible to redefine certain quantities to obtain the same leading order structure problem as in Eqs. (20–22). It is convenient to first choose the transverse coordinate ξ to be

$$\xi = \frac{f' - \lambda}{1 - \lambda} \tag{A1}$$

so that ignition again occurs at $\xi = 0$. Following the same procedure as in the hot-stream case, the identical structure equation, Eq. (20), is obtained if we redefine the variables as

$$\varepsilon = T_{-\infty}^2/T_a, \qquad \alpha \equiv (T_{-\infty} - T_{-} - \mu)/Y_{1,-\infty} \tag{A2}$$

$$\Delta = \frac{\zeta \varepsilon^{p-1}}{\lambda \alpha^p \ell_n \varepsilon^{-2}} T_{-\infty}^{r-p-q+1} \exp(-T_a/T_{-\infty}) \tag{A3}$$

Thus if use is made of Eq. (24) in Eq. (A3), the ignition distance is found to be

$$\zeta_I = \lambda \Delta_I(\alpha) \frac{\alpha^p \varepsilon^{1-p} \ell_n \varepsilon^{-2}}{T_{-\infty}^{r-p-q+1}} \exp(T_a/T_{-\infty}) \tag{A4}$$

which depends on an additional factor λ.

For the intermediate case, $|\alpha| \ll 1$, we again use the coordinate in Eq. (A1), and by redefining the variables

$$\varepsilon = T_{-\infty}^2/T_a, \qquad \tilde{\alpha} = T_{-\infty} - T_{-} - \mu \tag{A5}$$

we obtain the same structure equations (36) and (38). Now the reduced Damköhler number is given by

$$\Delta_m = \frac{\zeta \varepsilon^{p/2-1} Y_{1,-\infty}^p T_{-\infty}^{r-p-q+1}}{\lambda \ell_n \varepsilon^{-1} \sqrt{\mu}} \exp(-T_a/T_{-\infty}) \tag{A6}$$

so that, when use is made of the correlation (39) for Δ_{mJ}, the expression for the ignition distance becomes

$$\zeta_I = \lambda \Delta_{m,I}(\Gamma) \frac{\varepsilon^{1-p/2} \ell_n \varepsilon^{-1} \mu^{p/2}}{Y_{1,-\infty}^p T_{-\infty}^{r-p-q+1}} \exp(T_a/T_{-\infty}) \tag{A7}$$

Appendix B: Asymptotic Behavior of $f''/(1-\lambda)$ as $\xi \to 0$

The analysis of the hot-stream case requires the asymptotic behavior of $f''/(1-\lambda)$ as $\xi \to 0$ which, from definition (13), corresponds to $\eta \to \infty$. By integrating Eqs. (1) and (7) near $\eta = \infty$, it can be shown that[9]

$$f - \eta + C_{-\infty} \equiv \sqrt{2}z, \qquad f' - 1 - \sqrt{2}D_{-\infty}\frac{\exp(-z^2)}{z}$$

$$f'' - D_{-\infty}\exp(-z^2) \tag{B1}$$

where the constants of integration, $C_{-\infty}$ and $D_{-\infty}$, are functions of λ.

Combining the preceding formulas yields

$$\frac{f''}{1-\lambda} - f\xi - \sqrt{2}z\xi \tag{B2}$$

where

$$\xi = \frac{1-f'}{1-\lambda} - \frac{\sqrt{2}D_{-\infty}}{(1-\lambda)}\frac{\exp(-z^2)}{z} \tag{B3}$$

It follows from Eq. (B3) that

$$\ell_n\xi \sim -z^2 - \ell_n z + \ell_n[\sqrt{2}D_{-\infty}/(1-\lambda)] \tag{B4}$$

which, to leading order, yields

$$z^2 \sim -\ell_n\xi \tag{B5}$$

Substituting Eq. (B5) into Eq. (B2) provides the result

$$\left(\frac{f''}{1-\lambda}\right)^2 \sim 2z^2\xi^2 \sim -\xi^2\ell_n\xi^2 \tag{B6}$$

that is used to derive Eq. (20). We note that the last term in Eq. (B4) is a subdominant term and thus was eliminated in the present leading order analysis. Consequently, the final structure equation (20) is independent of the parameter λ.

For the special case of a uniform flowfield, i.e., $\lambda = 1$, the solution for the flowfield is simply $f = \eta$ and the factor $[f''/(1-\lambda)]^2$ multiplying the diffusion term in Eq. (16) has the explicit form

$$\frac{1}{2\pi}\exp(-2\eta^2) \tag{B7}$$

It is convenient to work in terms of the original coordinate $\xi \equiv \text{erfc}(\eta/\sqrt{2})/2$ [see Eq. (13)] so that the asymptotic behavior of Eq. (B7) near the ignition point η_I is given by

$$\frac{1}{2\pi}\exp(-2\eta^2) \sim \xi^2\eta_I^2 \tag{B8}$$

where the large number η_I can be evaluated by taking the logarithm of Eq. (B8), yielding

$$\eta_I^2 \sim 2\ell_n(\alpha/2\varepsilon\chi\sqrt{\pi}) - 2\ell_n\eta_I \sim -\ell_n\varepsilon^2 + 2\ell_n(\alpha/2\sqrt{\pi})$$

$$- 2\ell_n\eta_I - 2\ell_n\chi \tag{B9}$$

in terms of the inner variable χ defined in the hot-stream case. When only the leading-order term on the right-hand side of Eq. (B9) is retained, namely, the first term, we obtain

$$\eta_I^2 \sim -\ell_n\varepsilon^2 \tag{B10}$$

which is consistent with our previous result Eq. (B6), whereas Liñán and Crespo[11] retained the second term on the right-hand side of Eq. (B9). Although the two expressions must be asymptotically the same in the limit $\varepsilon \to 0$, in practice they can result in quite a large difference in the predicted ignition distance as shown in Fig. 3a.

Acknowledgment

This research has been supported by the Air Force Office of Scientific Research under the technical monitoring of J. M. Tishkoff.

References

[1]Im, H. G., Bechtold, J. K., and Law, C. K., "Analysis of Thermal Ignition in Supersonic Flat-Plate Boundary Layers," *Journal of Fluid Mechanics*, Vol. 249, April 1993, pp. 99–120.

[2]Drummond, J. P., and Mukunda, H. S., "A Numerical Study of Mixing Enhancement in Supersonic Reacting Flow Field," *Numerical Combustion*, edited by A. Dervieux and B. Larrouturou, Lecture Notes in Physics, Vol. 351, May 1989, pp. 36–64.

[3]Jackson, T. L., and Hussaini, M. Y., "An Asymptotic Analysis of Supersonic Reacting Mixing Layers," *Combustion Science Technology*, Vol. 57, No. 4-6, 1988, pp. 129–140.

[4]Ju, Y., and Niioka, T., "Ignition Analysis of Unpremixed Reactants with Chain Mechanism in a Supersonic Mixing Layer," *AIAA Journal*, Vol. 31, No. 5, 1993, pp. 863–868.

[5]Grosch, C. E., and Jackson, T. L., "Ignition and Structure of a Laminar Diffusion Flame in a Compressible Mixing Layer with Finite Rate Chemistry," *Physics of Fluids A*, Vol. 3, No. 12, 1991, pp. 3087–3097.

[6]Jackson, T. L., and Grosch, C. E., "Inviscid Spatial Stability of a Compressible Mixing Layer. Pt. 2. The Flame Sheet Model," *Journal of Fluid Mechanics*, Vol. 217, Aug. 1990, pp. 391–420.

[7]Williams, F. A., *Combustion Theory*, 2nd ed., Benjamin Cummings, Menlo Park, CA, 1985, pp. 485–495.

[8]Klemp, J. B., and Acrivos, A., "A Note on the Laminar Mixing of Two Uniform Parallel Semi-infinite Streams," *Journal of Fluid Mechanics*, Vol. 55, Sept. 1972, pp. 25–30.

[9]Lock, R. C., "The Velocity Distribution in the Laminar Boundary Layer between Parallel Streams," *Quarterly Journal of Mechanics and Applied Mathematics*, Vol. 4, Pt. 1, 1951, pp. 42–63.

[10]Law, C. K., and Law, H. K., "A Theoretical Study of Ignition in the Laminar Mixing Layer," *Journal of Heat Transfer*, Vol. 104, May 1982, pp. 329–337.

[11]Liñán, A., and Crespo, A., "An Asymptotic Analysis of Unsteady Diffusion Flames for Large Activation Energies," *Combustion Science Technology*, Vol. 14, No. 1–3, 1976, pp. 95–117.

[12]Birkan, M. A., and Law, C. K., "Asymptotic Structure and Extinction of Diffusion Flames with Chain Mechanism," *Combustion and Flame*, Vol. 73, No. 2, 1988, pp. 127–146.